1968

Absorption spectrum and Zeeman effect of dysprosium ethylsulfate

William James Haas Jr.
Iowa State University

ABSORPTION SPECTRUM AND ZEEMAN EFFECT OF DYSPROSIUM ETHYLSULFATE

by

William James Haas Jr.

A Dissertation Submitted to the
Graduate Faculty in Partial Fulfillment of
The Requirements for the Degree of
DOCTOR OF PHILOSOPHY

Major Subject: Physical Chemistry

Approved:

Signature was redacted for privacy.

In Charge of Major Work

Signature was redacted for privacy.

Head of Major Department

Signature was redacted for privacy.

Dean of Graduate College

Iowa State University
Ames, Iowa

1968

TABLE OF CONTENTS

INTRODUCTION

The study of the spectra of substances has held the attention of scientists ever since the discovery of the refraction of light by Newton. This attention is well deserved because the spectrum of a substance can give considerable information concerning its detailed atomic or molecular structure. The spectrum gives information on the interactions of the constituent particles with each other and with externally applied fields, and provides perhaps the fastest method of identifying and determining the concentration of many elements in a mixture. Spectral studies provide such an abundance of high precision data on the relative energies and intensities of transitions between the numerous discrete energy levels of substances that regularities observed in one region of a spectrum frequently suggest theories which can then be thoroughly checked in other regions of the same spectrum. For this reason the results of spectra work were one of the big stimuli toward the development of the quantum theory, and the explanation of the spectra was among its most notable successes. It is the same today. There are many areas, particularly in the case of liquid and solid materials, where careful spectroscopic work can contribute substantially to the advancement and understanding of theories, or to the prediction or interpretation of thermodynamic and magnetic properties of materials. As we

shall see, rare earth compounds are well suited for this work because they have sharp line spectra in the liquid or solid state.

Dysprosium ethylsulfate, chemical formula $Dy(C_2H_5SO_4)_3 \cdot 9H_2O$, is one of a large class of crystalline rare earth compounds whose properties are particularly interesting to scientists because the rare earths form what is known as an inner shell transition series. In the case of the rare earth or lanthanide series this means that as we proceed through the elements in the periodic table from cerium through lutetium, the number of 4f electrons, as well as the nuclear charge, increases by one at each step. It is called an inner shell transition series because the radial probability function for electrons in the 4f shell reaches its maximum well inside those for the filled 5s and 5p shells. This causes the 4f electrons to be rather well shielded from the outside environment, and gives a series of metals and compounds of fairly similar behavior in which trends in physical and chemical properties may be observed, and in which theoretical predictions of these properties may be thoroughly checked.

The optical absorption spectra of liquids and solids, in contrast with the sharp line spectra of gases, are generally characterized by broad diffuse bands without much resolvable structure. Although it is frequently possible to recognize the presence of certain molecular groupings from these

spectra, it is usually very difficult to obtain information on the detailed structure of the material. Early in the history of spectroscopy, however, it was recognized that certain naturally occurring minerals containing lanthanide group elements showed sharp line spectra even at room temperature. It was later found that this occurrence of sharp line spectra was characteristic of atoms or ions possessing a partially filled inner shell of electrons.

The earliest review of these spectra was given by Kayser (1), covering the years before 1905. Following the discovery of the Zeeman effect in 1895 (2) and the subsequent calculation of the effect of a magnetic field on the spectral lines by Lorentz (3), Becquerel (4) and Becquerel et al. (5, 6) studied the Zeeman effect and the Faraday effect of crystals of the naturally occurring rare earth minerals at various temperatures as low as that of liquid helium. In 1925 Hund (7) was able to correlate the paramagnetic susceptibilities of the rare earth salts at room temperature with the spectrographic ground states of the ions. He was the first to show that the ground states arise from $4f^n$ electron configurations, where n is the number of 4f electrons. The agreement with experiment was quite good except in the cases of europium and samarium salts where more precise agreement was later obtained by Van Vleck and Frank (8). Hund's success indicated that the effects upon the magnetic behavior of the free rare earth ion induced by including it in a crystal

lattice were small compared to kT at room temperature and small even in comparison to the multiplet splitting of the ground LS term. These facts were to play an important role in the foundations of later theoretical works.

In the period 1929 to 1940 Spedding (9), Freed (10), Ewald (11), Merz (12), Gobrecht (13), and many others conducted an intensive experimental investigation of the powder and polarized crystal spectra of many rare earth salts at various temperatures and external magnetic field strengths. Among the compounds investigated were the hydrated rare earth chlorides, bromides, iodides, sulfates, bromates, ethylsulfates, perchlorates, molybdates, acetates, the rare earth magnesium nitrates, and the p-dibrombenzolsulfonates. The great improvement of the results, compared to those obtained by the earlier workers was due to the use of synthetic crystals of definite composition in contrast to the naturally occurring mineral crystals, which usually consisted of a mixture of rare earths. Prior to this time there had been little to gain from comparison of the data of two or more workers, even though they had made admirable attempts to identify and subtract lines due to "impurities". The use of synthetic crystals constituted a great advance toward the systemization of the study of rare earth spectra, though by today's standards, largely made possible by ion-exchange technology, the purity of these crystals would be considered

less than desirable.

The spectra of the various rare earth salts were found to follow a general pattern of behavior. That is, the absorption lines occurred in relatively isolated groups, or multiplets, whose widths were on the order of a few hundred wavenumbers, and whose wavelengths were characteristic of the particular rare earth ion being studied, regardless of the negative ions or ligands with which it was associated. The internal structure of the multiplets, on the other hand, their numbers of lines, their polarization effects, and their Zeeman effects, were found to be dependent on the negative ions or ligands and upon the point symmetry of the rare earth ion. The spectra were also found to exhibit a general pattern of behavior when observed at low temperatures. The lines were generally sharper than their room temperature analogs, corresponding to a decrease in the Doppler broadening, and to a decrease in variations in the electric field about the central ion due to the thermal motions of its neighbors. The overall separations of the lines within the various multiplets were generally found to be increased at the lower temperature (14), and this was attributed to an intensification of the electrostatic influence of the ligands caused by contraction of the whole crystal. The number of lines in the multiplets was also found to depend on the temperature. Certain "high temperature lines", appearing mostly on the red side of each multiplet, disappeared at the lower temperatures. This was

found to be due to thermal depopulation of the higher energy levels of the ground multiplet.

Turning to the theoretical explanation of the rare earth spectra, it seems natural now to assume, as suggested by Hund's success in identifying the spectrographic ground states, that the rare earth spectra are mainly characterized by the free ion spectra, slightly modified by the inclusion of the ions in crystals. Suggestions to this effect were made in 1928 and 1929 by Becquerel (15), who expressed the idea of a crystalline electric field, and by Brunetti (16), and Brunetti and Ollano (17), who measured the order of magnitude of this perturbation of the free ion spectrum, and related the splittings observed to the crystalline site symmetry of the ions. Freed and Spedding (18) also developed this assumption, but the classic paper of the time was Bethe's (19). He pointed out, working from group theory considerations, that the number and type of lines arising from any given free ion level is determined only by the symmetry of the crystalline field, and not by its strength. Kramers (20, 21), at the same time, discovered the requirement that the crystal field, if truly of electrostatic origin, must leave every level of systems with an odd number of electrons at least twofold degenerate. The classic works in the theory of complex atomic spectra were the works of Slater (22), and Condon and Shortley (23). More descriptive works were published later by White

(24) and Herzberg (25).

Even though it seemed certain that the spectra could be explained by a small perturbation of the free ion levels by the crystal field, the intensity of the spectra remained a puzzle. Which transitions were responsible for the lines was unknown, and the situation was complicated by an utter lack of detailed information on the free ion spectra. Even today only beginnings have been made toward understanding the transition mechanisms involved. Van Vleck (26) pointed out that the intensity of the lines, when one considers the high concentration of ions present in crystalline samples, must correspond to transitions which are forbidden in ordinary atomic spectra. Van Vleck also calculated the relative probabilities of electric dipole, magnetic dipole, and electric quadrupole radiative transitions within the $4f^n$ configuration. He found no good reason for rejecting any of these as being not responsible for the lines.

Bethe and Spedding (27) and Spedding (28), by including the effects of the intermediate coupling of the spin and orbital momenta of the states, showed that the energies of the sharp line groups could be understood in terms of transitions within the $4f^n$ configuration. Good agreement was obtained between experiment and theory with reasonable magnitudes for the electrostatic and spin-orbit interactions. Broer et al. (29) carefully repeated Van Vleck's estimation of transition

probabilities and concluded that the electric dipole type of transition was the most probable, and indeed, that in most cases the probability was large enough to explain the observed intensities.

Between 1942 and 1949 Racah published a series of papers (30-33) under the title "Theory of Complex Spectra". In these he introduced a number of very powerful concepts which have since found wide use in nuclear as well as in atomic spectroscopy. Among these were the definition and use of irreducible tensor operators and coefficients of fractional parentage, and the application of the theory of continuous groups to the problem of identifying and calculating the energies of terms for configurations of equivalent electrons. His work is of extreme importance in the case of the rare earths because the standard methods of Slater and Condon and Shortley become very cumbersome when applied to systems of more than two equivalent f electrons such as occur in the case of the rare earths. The more recent and more detailed theoretical descriptions by Judd (34) and Wybourne (35) have shifted almost entirely to the techniques and nomenclature given in these first four papers and in the 1959 book by Fano and Racah (36).

Another major advance was the application of paramagnetic resonance techniques to the study of rare earth crystals. Bleaney and Stevens (37) have given a review of this work. The method's advantages are high resolution and accuracy.

Its main advantage is that it is usually only applicable to studies of the lowest energy doublet of the ground multiplet. Several attempts have been made to calculate the crystal field potential from paramagnetic resonance data (38), and from data obtained from heat capacity (39), and magnetic susceptibility (40, 41) measurements. Although reasonable agreement was obtained with experiment in each case, the energy levels of the ground multiplet calculated using this potential were not in agreement with data from optical spectroscopy. This was especially true of the higher energy levels of the ground multiplet. The lack of success in calculating the crystal field potential from heat capacity and magnetic susceptibility measurements is attributed to the relative insensitivity of these statistical properties to the relative positions of all but the lowest two or three levels. In the case of the calculations from paramagnetic resonance measurements not enough experimental data were available for an adequate determination of the crystalline potential.

The period 1940 to the present saw an intense effort to gather high resolution spectral data on rare earth ions in crystals. Important workers in the field were Hellwege, Dieke, and Spedding. In a series of papers (42-47) published in 1948, Hellwege derived crystal quantum numbers and selection rules for electric dipole, magnetic dipole, and electric quadrupole transitions for ions in a number of different crys-

tal symmetries. Viewing the experimental data, he found the selection rules for electric dipole transitions were most often obeyed, though occasionally transitions were observed which obeyed the selection rules for magnetic dipole transitions. Hellwege also studied the hyperfine structure of the absorption lines, and electron-vibration combination frequencies associated with the main lines. More recently, however, he and his associates have shifted their attention to studies of rare earth spectra in magnetically ordered crystals. Dieke demonstrated the importance of combining the results of absorption, fluorescence, and Zeeman measurements for maximum surety in identifying the levels (48), and was one of the few workers who made a serious attempt to determine the field free spectra of the trivalent ions (49, 50). Spedding and his group have made detailed studies of the Zeeman effects of the ethylsulfates. They found a variation of Zeeman splitting and intensity for certain lines when the crystals were rotated about their c axis while the directions of the incident light and magnetic field were kept constant in the hexagonal plane (51). Most of the later high resolution work has been devoted to the ethylsulfates and anhydrous chlorides because of their relatively high symmetry. The point symmetry of a rare earth ion in these crystals is C_{3h} as demonstrated by the structure determinations of Ketelaar (52) and Fitzwater and Rundle (53).

The study of rare earth spectra since 1960 has been

especially marked by the use of large high speed computers. Many workers (54-62) have used these valuable tools to calculate matrix elements, energy levels, eigenfunctions, and to fix theoretical parameters determining the electrostatic, spin-orbit, and crystal field interactions by least squares fitting of the experimental data. The aim of these calculations has largely been to explore the possibilities and limitations of a necessarily simplified theoretical model following Condon and Shortley. Although energy levels calculated with the parameters obtained in this way often agree with the experimentally determined levels within one percent, the experimental energies can be measured to within one part in 10^6. There is therefore much room for improvement in the calculations, particularly in the case of the higher energy levels. It was for this reason that Margolis (63) in his work on praseodymium chloride, considered not only the interactions mentioned above, but also the magnetic orbit-orbit, spin-spin, and spin-other-orbit interactions. For the same reason other workers have explored the possible effects of configuration interaction (64, 65), closed shell correlation (66, 67), and covalent bonding (68). The biggest obstacle to advances in this area of the theory has been the lack of good experimental data on the excited levels.

A recent example of how careful experimental work on the excited levels can stimulate advances in the theory of rare earth spectra has been provided by the group of research-

ers headed by Professors Spedding and Good. Observations of non-linear Zeeman splitting behavior in a number of rare earth ethylsulfates and observations of transitions whose intensities depended on the strength of the magnetic field led to an extensive theoretical treatment of the Zeeman effect for rare earth ions in a crystal field of C_{3h} symmetry (69). In addition to explaining the observed behavior, this work predicted that the Zeeman splittings and intensities of transitions to certain energy levels of systems with an odd number of 4f electrons should be found to be anisotropic with respect to rotation of the crystal about its c axis when the magnetic field is perpendicular to this axis. (The experimental situation in which the magnetic field is perpendicular to the c axis will be referred to hereafter as the HsC case.) It has been commonly believed up to this time that the Zeeman effect would be isotropic in the a plane, although Hamm et al. (70) had observed an anisotropic Zeeman effect for Co^{+2} at cubic and tetragonal sites. For systems with an even number of 4f electrons the same theory predicted only intensity changes on rotation. Experimental results presented in a paper (51) published as a companion to the theoretical work and in the work of Spedding and Bartel (71) confirmed these predictions in the case of erbium and thulium ethylsulfate. Here the rare earth ions have $4f^{11}$ and $4f^{12}$ configurations, respectively. Later experimental work on holmium ethylsulfate (72) likewise supported the theory,

but here, since the magnetic splittings were not small compared to the crystal field splittings, it was necessary to follow the extended theory outlined in reference (51) in order to explain the energy changes observed on rotation for a system with an even number of 4f electrons.

In the past year two new theoretical works on the Zeeman spectra of rare earth ethylsulfates have appeared (73, 74). In the first it was pointed out that when the magnetic field is perpendicular to the c axis the Hamiltonian has a strange symmetry of a type first described by Wigner (75). Studies of this symmetry led to simplifications in the energy level calculations for systems of both even and odd number of 4f electrons, and to the assignment of a new quantum number for each level. In the second work these ideas were applied to the problem of calculating relative intensities and intensity variations on rotation for the Zeeman absorption lines of erbium ethylsulfate. A number of fairly simple examples were treated, and the results were in good agreement with the previously unexplained experimental data.

The Zeeman theory of Murao, Spedding and Good (69) also defined a new property of crystals with C_{3h} point symmetry. This property is the direction of what is known as the x axis. Its direction is determined theoretically by choosing the z axis in the crystallographic c direction, and choosing a direction for the x axis which makes the coefficient of the imaginary part of the V_6^6 crystal field potential vanish.

The direction of the x axis depends on the environment of the rare earth ion, and in general does not coincide with the direction of the crystallographic a axis of the crystal. It can be determined experimentally, and preliminary measurements of $\bar{\phi}$, the angle between the a and x axes, have been presented in references (51) and (71) for erbium and thulium ethylsulfate. The measurements seemed to indicate that there was a small but measurable difference in the values of $\bar{\phi}$ obtained in the pure salts and those obtained when either erbium or thulium ethylsulfate were diluted with yttrium ethylsulfate. If the environment of the rare earth ion in the crystal lattice of the pure salt is different from that in the yttrium ethylsulfate lattice one would expect $\bar{\phi}$ to be different, and if better techniques for aligning the crystals were developed it might be possible to use the $\bar{\phi}$ measurements for rare earth ions in various lattices as a sensitive probe of their immediate environments in mixed crystals.

The aim of the present work is threefold: 1) to observe and report the anisotropic HsC Zeeman effect for dysprosium ethylsulfate, 2) to determine the x axis direction in dysprosium ethylsulfate, and in mixed crystals containing various concentrations of Dy^{+3} in erbium and yttrium ethylsulfate, and 3) to extend the present experimental and theoretical understanding of the excited levels of dysprosium ethylsulfate into the ultraviolet.

Single crystals of dysprosium ethylsulfate (hereafter referred to as DyES) were chosen for this investigation for two reasons. The first is that the theory indicated that the ground state levels of DyES would have a sizeable anisotropy in the HsC Zeeman effect (76). If this were true, the results of earlier Zeeman effect measurements in this orientation would certainly be open to question. In addition, the substantial mixing of the wavefunctions which accompanies the HsC anisotropy would lead to the observance of many transitions which are not visible at zero magnetic field. This would be a big help in the interpretation of absorption lines in the excited multiplets because the more lines we see, the more checks and cross-checks we have. The second reason for choosing DyES was a desire to stimulate further theoretical work on the spectra of ions in crystals. Data on the $4f^9$ levels of Dy^{+3} would be ideal for this because here is a many electron problem in which the wealth of data which can be obtained completely overwhelms the number of theoretical parameters. Such a situation always provides an attractive proving ground for new theories.

THEORY

Field Free Ion States

The spectra of many electron atoms or ions in the absence of external fields has been discussed at length by Condon and Shortley (23) and Slater (22). If the mass of the nucleus is assumed to be infinite, and all relativistic effects except the magnetic interaction of the spin and orbit of each electron are ignored, the Hamiltonian for an N electron system can be written as

$$H=\sum_{i=1}^{N}\left[\frac{\vec{P}_i^2}{2m_i}-\frac{Ze^2}{r_i}+\xi(r_i)\vec{s}_i\cdot\vec{l}_i\right]+\sum_{i>j=1}^{N}\frac{e^2}{r_{ij}}. \qquad (1)$$

The first term is the sum of the kinetic energies of each of the electrons, the second is the sum of the potential energies of the electrons due to their Coulomb attraction to the nucleus, and the third term is the sum of the approximate spin-orbit interactions of each of the electrons. The last term is the sum of the mutual repulsion energies for all pairs of electrons.

Exact solutions of the Schrodinger equation for this Hamiltonian are not possible, but approximate solutions can be obtained by use of the central field approximation. In this approximation each electron is assumed to move independently in the field of the nucleus and a spherically symmetric central field due to the average potential fields of

all of the other electrons. If $U(r_i)$ is the potential energy of an electron in such a field, the central field Hamiltonian is

$$H_{cf} = \sum_{i=1}^{N} \left[\frac{\vec{p}_i^{\,2}}{2m_i} + U(r_i) \right] . \qquad (2)$$

Schrodinger's equation for this Hamiltonian has exact solutions known as the Slater determinantal product wavefunctions. They satisfy the Pauli exclusion principle, and serve as a convenient starting point for a calculation in which the remaining part of the Hamiltonian in Equation 1 is treated as a perturbation. The perturbation Hamiltonian is written as

$$H_{pert} = \sum_{i=1}^{N} \left[-U(r_i) - \frac{Z e^2}{r_i} + \xi(r_i) \vec{s}_i \cdot \vec{l}_i \right] + \sum_{i>j=1}^{N} \frac{e^2}{r_{ij}} . \qquad (3)$$

In the case of rare earth spectra we are only interested in the relative energies of the $4f^n$ states, so we can ignore the first two terms in the brackets. They depend on the n and l quantum numbers only, and therefore cannot affect the relative $4f^n$ energies. Condon and Shortley have shown that the sum over electrons in spherically symmetric closed shells in the last two terms may be omitted also, because this part of the sum can only give a shift of the entire $4f^n$ configuration. We are left with a perturbation Hamiltonian of the form

$$H_{pert} = \sum_{i=1}^{n} \xi(r_i) \vec{s}_i \cdot \vec{l}_i + \sum_{i>j=1}^{n} \frac{e^2}{r_{ij}} , \qquad (4)$$

where now the sum is only over the electrons in the 4f shell.

The relative energies of the states are given by the eigenvalues of the matrix M, whose elements are given by

$$M_{ij} = \int \psi_i^{\dagger} H_{pert} \psi_j \, d\tau \, , \tag{5}$$

or, in the Dirac notation,

$$M_{ij} = \langle i | H_{pert} | j \rangle \, . \tag{6}$$

Here ψ_i and ψ_j are the i^{th} and j^{th} functions in a complete ordered set of orthonormal solutions of the central field problem (the Slater determinantal product wavefunctions or unitary rearrangements of them), and $\psi_i^{\dagger}$ is the Hermitian conjugate of ψ_i. The integration is understood to be over all allowed values of the space and spin coordinates of all of the 4f electrons.

The calculation of matrix elements of the perturbation Hamiltonian can be considerably simplified by an intelligent choice of the basis functions ψ. There is a great deal of freedom in this choice because each of the Slater functions, or unitary rearrangements of them, gives the same energy in the central field problem. A particularly useful choice is one in which the basis functions are chosen to be eigenfunctions of operators which commute with the Hamiltonian or its parts. This gives rise to selection rules on the matrix elements which can simplify the work considerably, and the

eigenvalues of the operators can be used as quantum numbers in labelling the states.

In the case of the perturbation Hamiltonian in Equation 4, for example, the well known angular momentum operators (77) $\vec{S}^2$, $\vec{S}_z$, $\vec{L}^2$, and $\vec{L}_z$ commute with each other and with the electrostatic repulsion term. If we choose simultaneous eigenfunctions of these operators for our basis, we find that the matrix of the electrostatic interaction is diagonal in S, M_S, L, and M_L. This means that matrix elements of the electrostatic interaction between functions $\psi(f^n \gamma SM_S LM_L)$ and $\psi(f^n \gamma' S' M_S' L' M_L')$ are zero unless $S = S'$, $M_S = M_S'$, $L = L'$, and $M_L = M_L'$. Here f^n tells what configuration we are studying, and γ stands for additional numbers used to distinguish functions with the same values of S, M_S, L, and M_L.

The angular momentum stepping operators $\vec{S}_\pm$ and $\vec{L}_\pm$ also commute with this part of the Hamiltonian, and give us the additional information that matrix elements of electrostatic interaction are independent of M_S and M_L. Solutions of the electrostatic part of the perturbation problem are completely characterized therefore by stating values of γ, S, M_S, L, and M_L, and states with the same values of γ, L, and S have the same energy.

The total angular momentum operators $\vec{J}^2$ and $\vec{J}_z$ commute with each other and with both the electrostatic and spin-orbit parts of the Hamiltonian. They also commute with $\vec{S}^2$

and $\vec{L}^2$. If we choose simultaneous eigenfunctions of these four operators for our basis set, we get selection rules for both parts of the Hamiltonian. The matrix of the electrostatic interaction is diagonal in S, L, J, and M, and is independent of J and M, while the matrix of the spin-orbit interaction is diagonal in J and M, and is independent of M. The matrix elements do not depend on M because the stepping operators $\vec{J}_+$ and $\vec{J}_-$ commute with the entire Hamiltonian. These facts greatly reduce the amount of work in calculating the field free ion energy levels and eigenfunctions because they reduce the number of matrix elements that have to be calculated, and because they reduce the size of the matrices that have to be diagonalized.

Racah (30-33) has shown that an additional classification of the $4f^n$ wavefunctions can be attained by studying their properties under certain groups of transformations. This is especially important for configurations of more than two equivalent f-electrons because some way is needed to distinguish between states with the same values of L and S. The additional classification is not quite as useful as that furnished by the angular momentum operators because in general the group operators do not commute with the Hamiltonian. Nevertheless it does simplify the calculation of matrix elements, and yields quantum numbers which are very useful in labelling the states.

The classification of states of f^n configurations by group theory depends on the fact that the states for a given S and M_S form a basis for a single irreducible representation of U_7, the continuous group of unitary transformations in seven dimensions. The representation does not depend on M_S, so identifying it by some label is equivalent to specifying the spin. The process of using the labels of irreducible representations as quantum numbers can be continued because U_7 has a succession of subgroups. The subgroups have irreducible representations too, and the labels of these can be used as additional quantum numbers. The succession of subgroups is written

$$R_3 \subset G_2 \subset R_7 \subset U_7,$$

where $\subset$ is read as "is a subgroup of". R_3 and R_7 are the rotation groups in three and seven dimensions, respectively, and G_2 is a special group unique to f^n configurations.

Just as specifying the irreducible representation of U_7 is equivalent to specifying S, specifying the irreducible representation $\mathcal{D}_L$ of R_3 is equivalent to specifying L. Racah's method lets us further classify the states according to the irreducible representations of the intermediate subgroups R_7 and G_2. In this way states with the same values of L and S can usually be distinguished, and the calculation of matrix elements can be simplified by rearranging the Hamiltonian into parts which separately transform according

to one or the other of the irreducible representations of these groups. The basis states are completely specified by writing $\psi(f^n \tau\, WUSM_S LM_L)$ or $\psi(f^n \tau\, WUSLJM)$. Here $W \equiv (w_1 w_2 w_3)$ and $U \equiv (u_1 u_2)$ are sets of integers which serve to identify the irreducible representations of R_7 and G_2 according to which the states transform, and τ is an additional number used to distinguish between pairs of states with the same values of W, U, S, and L which occur for U = (31) and U = (40). The numbers have much more significance than just labels, but that does not concern us here. The reader is referred to Judd (34) for an extensive discussion of their group theoretical significance.

The states which arise from the $4f^9$ configuration of Dy^{+3} have been classified by Wybourne (78) and are given in Table 1. They are the same as those which arise from the $4f^5$ configuration because, as Condon and Shortley have shown, the quantum mechanical problem for n f-electrons is the same as that for 14-n positive holes. Wybourne has also calculated matrix elements of electrostatic (79) and spin-orbit (80) interaction appropriate for Dy^{+3}, and has calculated the free ion energy levels in intermediate coupling (81). This last calculation was also a least squares determination of the values of the radial parameters of electrostatic and spin-orbit interaction, F_2 and ζ which give the best fit of the calculated energy levels to the experimental crystal levels determined by Rosa (82), Dieke and Singh (83), Gram-

Table 1. Field free ion states of the $4f^9$ configuration of Dy^{+3}

W	U	SL
(110)	(10)	^6F
	(11)	$^6P^6H$
(211)	(10)	^4F
	(11)	$^4P^4H$
	(20)	$^4D^4G^4I$
	(21)	$^4D^4F^4G^4H^4K^4L$
	(30)	$^4P^4F^4G^4H^4I^4K^4M$
(111)	(00)	^4S
	(10)	^4F
	(20)	$^4D^4G^4I$
(221)	(10)	^2F
	(11)	$^2P^2H$
	(20)	$^2D^2G^2I$
	(21)	$^2D^2F^2G^2H^2K^2L$
	(30)	$^2P^2F^2G^2H^2I^2K^2M$
	(31)	$^2P^2D^2F^2F^2G^2H^2H^2I^2I^2K^2K^2L^2M^2N^2O$
(210)	(11)	$^2P^2H$
	(20)	$^2D^2G^2I$
	(21)	$^2D^2F^2G^2H^2K^2L$
(100)	(10)	^2F

berg (84), and Crosswhite and Dieke (85). The values of F_4 and F_6 were fixed by assuming hydrogenlike ratios for F_4/F_2 and F_6/F_2.

Wybourne's calculation showed that the effect of intermediate coupling is very pronounced in Dy^{+3}, and that it is impossible in most cases to assign physically significant values of L and S quantum numbers. He therefore followed the procedure of labelling the energy levels by their position and J value, and listed percent contributions for the major LS states. The agreement with the experimental energies was quite good for the levels below 22000 cm^{-1}, but there was insufficient data on the higher energy levels for a satisfactory interpretation.

Crystal Field Levels

Rare earth ions in a crystal lattice are subjected to the electric field of all the other atoms and ions in the crystal. The spherical symmetry of the free ion problem is destroyed, and the (2J+1)-fold degenerate levels of the free ion split under the influence of the field. The Hamiltonian for an ion in a crystal is

$$H = H_{ion} + V, \qquad (7)$$

where H_{ion} is the free ion Hamiltonian and V is the potential energy arising from interaction with the crystalline environment. Since the 4f electrons of the rare earth ions are well

shielded from the surroundings, the crystal field splittings in most cases will be small compared to the separation of the free ion levels. Therefore it is appropriate to treat the crystal field potential as a perturbation on the free ion levels. The basis states are taken to be the solutions of the free ion problem, and the crystalline potential is expanded in terms of spherical harmonics (34).

The potential energy of the 4f electrons is given by $V = \sum_i V_i$, where

$$V_i = -\sum_j q_j e^2 / |\vec{R}_j - \vec{r}_i| \qquad (8)$$

and the sum is over the 4f electrons. Here $q_j e$ is the effective charge on the j^{th} ion and the sum on j runs over all the ions in the crystal other than the one under consideration. $\vec{R}_j$ is the position vector of the j^{th} ion and $\vec{r}_i$ is the position vector of the i^{th} 4f electron. The factor $1/|\vec{R}_j - \vec{r}_i|$ can be expanded as an infinite series of Legendre polynomials $P_k(\cos w_{ij})$, where w_{ij} is the angle between the position vectors, to give

$$1/|\vec{R}_j - \vec{r}_i| = \sum_{k=0}^{\infty} (\vec{r}_<^{\,k} / \vec{r}_>^{\,k+1}) P_k(\cos w_{ij}) \cdot \qquad (9)$$

Here $\vec{r}_<$ is the lesser of $\vec{R}_j$ and $\vec{r}_i$, and $\vec{r}_>$ is the greater. The spherical harmonic addition theorem (34) gives

$$P_k(\cos w_{ij}) = (4\pi/2k+1)\sum_{q=-k}^{k} Y^*_{kq}(\theta_j,\phi_j)\, Y_{kq}(\theta_i,\phi_i)\,, \tag{10}$$

so if we define

$$C^{(k)}_q(i) = \sqrt{(4\pi/2k+1)}\; Y_{kq}(\theta_i,\phi_i)\,, \tag{11}$$

the potential energy of the i^{th} electron can be written as

$$V_i = \sum_j \sum_{k=0}^{\infty} -(q_j e^2 r_<^k / r_>^{k+1}) \sum_{q=-k}^{k} C^{(k)*}_q(j)\, C^{(k)}_q(i)\,. \tag{12}$$

The potential is real so if we sum it and its complex conjugate and divide by two we get the same result. This gives

$$V_i = \sum_j \sum_{k=0}^{\infty} (A_{jk}/2) \sum_{q=-k}^{k} \left[C^{(k)*}_q(j) C^{(k)}_q(i) + C^{(k)}_q(j) C^{(k)*}_q(i)\right]\,, \tag{13}$$

where A_{jk} has been substituted for $(-q_j e^2 r_<^k / r_>^{k+1})$. The terms which depend on the angular coordinates i and j can be further separated, and the sum on q can be restricted to positive values if we write the potential in the form

$$V_i = \sum_j \sum_{k=0}^{\infty} A_{jk} \sum_{q=0}^{k} \left[\begin{array}{l} \left[\dfrac{C^{(k)}_q(j) + C^{(k)*}_q(j)}{2}\right] \left[C^{(k)}_q(i) + C^{(k)*}_q(i)\right] \\ \\ -i \left[\dfrac{C^{(k)}_q(j) - C^{(k)*}_q(j)}{2i}\right] \left[C^{(k)}_q(i) - C^{(k)*}_q(i)\right] \end{array} \right] \tag{14}$$

Here $\underline{i}$ stands for $\sqrt{-1}$.

Now the sum on j can be performed to give

$$V_i = \sum_{k=0}^{\infty} \sum_{q=0}^{k} \left\{ \alpha_{kq} \left[C_q^{(k)}(i) + C_q^{(k)*}(i) \right] + \underline{i} \beta_{kq} \left[C_q^{(k)}(i) - C_q^{(k)*}(i) \right] \right\}. \quad (15)$$

Here

$$\alpha_{kq} = \sum_j (-q_j e^2 r_<^k / r_>^{k+1}) \left[\frac{C_q^{(k)}(j) + C_q^{(k)*}(j)}{2} \right] \quad (16)$$

and

$$\beta_{kq} = \sum_j (+q_j e^2 r_<^k / r_>^{k+1}) \left[\frac{C_q^{(k)}(j) - C_q^{(k)*}(j)}{2\underline{i}} \right].$$

The crystal field potential must have the same symmetry as the environment of the rare earth ion. The potential must therefore be invariant under the group operations of the rare earth ion point symmetry group. This requirement considerably restricts the sum on k and q in Equation 15. In the case of the rare earth ethylsulfates the point group is C_{3h} (52, 53), and the group operators are the six powers of the operator,

$$O = \underline{i}^n \exp(\underline{i} \pi \vec{J}_z / 3) P, \quad (17)$$

defined by Murao, Spedding, and Good (69). Here P is the parity operator. The only terms in Equation 15 which fulfill the symmetry requirement are those with q equal to an integer multiple of three and k+q even. All other terms must be zero.

The sum can be further restricted in the case of the

energy calculation because we are only interested in matrix elements of V_i between single 4f electron states. The first reduction in this case is based on the parity argument. Both of the states in any $4f^n$ matrix element have parity $(-1)^n$, and the potential operators have parity $(-1)^k$. In order for the matrix element to be nonzero, the product of the parities of the two states times the parity of the operator must be (+1). Therefore the only potential terms which can contribute to nonzero matrix elements are those with k even.

The final reduction is made by applying the Wigner-Eckart theorem (34) for matrix elements of irreducible tensor operators. An irreducible tensor operator of rank k is defined by Racah (31) as an operator $T^{(k)}$ whose (2k+1) components $T_q^{(k)}$ satisfy the same commutation properties with the total angluar momentum operators, $\vec{J}_+$, $\vec{J}_-$, and $\vec{J}_z$, as do the spherical harmonics. Because of the definition in Equation 11, it is clear that the $C_q^{(k)}$'s are components of an irreducible tensor operator. We are interested in sums of matrix elements of the form $(nlm_\ell\ m_s | C_q^{(k)}(i) |\ nlm'_\ell\ m'_s)$. The operator $C_q^{(k)}(i)$ is independent of m_s, so the Wigner-Eckart theorem gives

$$(nlm_\ell\ m_s | C_q^{(k)}(i) |\ nlm'_\ell m'_s)$$

$$= \delta(m_s, m'_s)(-1)^{l-m_\ell} \begin{pmatrix} l & k & l \\ -m_\ell & q & m'_\ell \end{pmatrix} (nl \| C_q^{(k)}(i) \| nl). \tag{18}$$

The factor $(nl||C_q^{(k)}(i)||nl)$ is called the reduced matrix element of $C_q^{(k)}$, and the factor $\begin{pmatrix} l & k & l \\ -m_\ell & q & m'_\ell \end{pmatrix}$ is a 3-j symbol (86). Together with $(-1)^{\ell-m}$ it contains all of the m_ℓ and m'_ℓ dependence of the matrix elements. One of the properties of the 3-j symbol, written in general as $\begin{pmatrix} j_1 & j_2 & j_3 \\ m_1 & m_2 & m_3 \end{pmatrix}$, is that it is zero unless the triangular conditions

$$j_1 + j_2 - j_3 \geq 0;\ j_1 - j_2 + j_3 \geq 0;\ -j_1 + j_2 + j_3 \geq 0 \tag{19}$$

are satisfied. Thus, in the case of matrix elements of 4f electron states, we get zero contribution from all terms in V with $k > 6$. The only terms which need to be considered in the energy calculation when all the restrictions have been taken into account are those given in Table 2.

Table 2. Significant crystal field terms for C_{3h} energy calculation

k	q
2	0
4	0
6	0
6	± 6

The odd parity terms of the crystal field potential which are not eliminated by symmetry requirements have been shown by the parity argument to have no effect on the energy levels when the calculations are carried out within a basis of $4f^n$ states. However these terms are very important in the determination of the intensities of the spectral lines. They represent the strongest odd parity interaction in the Hamiltonian, and are important in mixing states of opposite parity. It is the mixing of configurations of opposite parity which permits electric dipole transitions within the $4f^n$ configuration. The terms in the C_{3h} crystal field expansion which need to be considered in intensity calculations are given in Table 3.

Table 3. Significant crystal field terms for C_{3h} intensity calculations

k	q
3	± 3
5	± 3
7	± 3

The requirement that the crystalline potential have the same symmetry as the environment of the rare earth ion does much more than tell us what potential terms to retain. If

we study the properties of the operator O whose powers generate the C_{3h} point group we can predict the number of crystal field levels to be expected from each of the free ion levels, we can know the transformation properties of the wavefunctions corresponding to the crystal field levels under the O operation, and we can derive selection rules for radiative transitions between the levels.

The O operator is unitary and commutes with the entire Hamiltonian for an ion in a C_{3h} crystal field, so we can find solutions $\psi(\mu i)$ that are eigenfunctions of H and of O simultaneously:

$$H\psi(\mu i) = E(\mu i)\psi(\mu i), \tag{20}$$

and

$$O\psi(\mu i) = \exp(\pm i\pi\mu/3)\psi(\mu i) \tag{21}$$

Here μ is the crystal quantum number defined in (69), and i is a serial number which distinguishes between states with the same values of μ. The solutions may be expanded in terms of solutions of the central field problem, but since the crystal field potential is generally treated as a perturbation on the free ion levels, it is usually more appropriate to expand in terms of the free ion solutions. This gives

$$\psi(\mu i) = \sum_{\gamma,J,M} (\gamma JM|\mu i)\,\psi(\gamma JM), \tag{22}$$

where the sum is over all possible values of the free ion quantum numbers γ, J, M, for the configuration under consideration. The expansion coefficients are represented by $(\gamma JM|\mu i)$, and the connection between the μ and M quantum numbers for Dy^{+3} is given in Table 4.

Table 4. Relation between μ and M quantum numbers for Dy^{+3} in C_{3h} symmetry

μ values	Contributing M values
0	-21/2, -9/2, 3/2, 15/2
3	-15/2, -3/2, 9/2, 21/2
1	-19/2, -7/2, 5/2, 17/2
2	-17/2, -5/2, 7/2, 19/2
-1	-23/2, -11/2, 1/2, 13/2
-2	-13/2, -1/2, 11/2, 23/2

The sixth power of the O operator is equal to the identity operator regardless of the number of electrons, so we can write a single character table for the cases of both even and odd numbers of electrons. The irreducible representations are labelled by the crystal quantum numbers $\mu = 0, \pm1, \pm2$, and 3, for both cases. The character table for the C_{3h} point group is given in Table 5. Using this table one can easily determine how the levels of the free ion will split due to

Table 5. C_{3h} character table for even or odd number of electrons -- $w = \exp(i\pi/3)$

μ	E	O^2	O^4	O	O^3	O^5
0	1	1	1	1	1	1
1	1	w^2	$-w$	w	-1	$-w^2$
2	1	$-w$	w^2	w^2	1	$-w$
3	1	1	1	-1	-1	-1
-1	1	$-w$	w^2	$-w^2$	-1	w
-2	1	w^2	$-w$	$-w$	1	w^2

the crystal field.

Since the free ion levels in the rare earths are well separated in energy we can usually ignore crystal field interactions between them, and we can consider the 2J+1 states of each free ion level as forming the basis of a reducible representation of the symmetry operators of the group. The crystal field splittings are found by diagonalizing the matrix representation of V in this basis, and the number of irreducible representations contained in the reducible representation corresponds to the number of levels into which the original free ion levels will split. The number of times $a^{(\mu)}$ that a given μ representation occurs in any J representation is given by

$$a^{(\mu)} = (1/g) \sum_{G} \chi^{(J)}(G)\, \chi^{(\mu)*}(G) . \qquad (23)$$

Here g is the order of the group, and the sum is over the G elements of the group. The reader is referred to Tinkham (87) for further information on the group theory.

The characters $\chi^{(J)}(O^k)$, for C_{3h} symmetry are given by the expression

$$\chi^{(J)}(O^k) = (i^n \alpha)^k \frac{\sin(J+\frac{1}{2})(k\pi/3)}{\sin(k\pi/3)} \qquad (24)$$

Here α is the parity of the configuration, and n is the number of electrons not in closed shells. The $\chi^{(\mu)}(G)$'s are read from the character table given in Table 5. The C_{3h} character table for the half-integral J representations which occur in the Dy^{+3} $4f^9$ configuration are given in Table 6, and the number of times the various μ representations occur for each J value are given in the right hand half of the table.

Time Reversal

Further progress on how the free ion levels split in the crystal field is made by studying the time reversal operator,

$$T = \prod_{j=1}^{n} (-i\sigma_y)_j K . \qquad (25)$$

Here σ_y is the y-component of the Pauli spin matrices, and

Table 6. C_{3h} character table for half integer J representations in the $4f^9$ configuration of Dy^{+3}

J	E	O^2	O^4	O	O^3	O^5	$a^{(0)}$	$a^{(1)}$	$a^{(2)}$	$a^{(3)}$	$a^{(-1)}$	$a^{(-2)}$
1/2	2	-1	-1	$-i\sqrt{3}$	0	$i\sqrt{3}$	0	0	0	0	1	1
3/2	4	1	1	$-i\sqrt{3}$	0	$i\sqrt{3}$	1	0	0	1	1	1
5/2	6	1	1	0	0	0	1	1	1	1	1	1
7/2	8	0	0	$i\sqrt{3}$	0	$-i\sqrt{3}$	1	2	2	1	1	1
9/2	10	2	2	$i\sqrt{3}$	0	$-i\sqrt{3}$	2	2	2	2	1	1
11/2	12	1	1	0	0	0	2	2	2	2	2	2
13/2	14	0	0	$-i\sqrt{3}$	0	$i\sqrt{3}$	2	2	2	2	3	3
15/2	16	2	2	$-i\sqrt{3}$	0	$i\sqrt{3}$	3	2	2	3	3	3
17/2	18	1	1	0	0	0	3	3	3	3	3	3
19/2	20	0	0	$i\sqrt{3}$	0	$-i\sqrt{3}$	3	4	4	3	3	3
21/2	22	2	2	$i\sqrt{3}$	0	$-i\sqrt{3}$	4	4	4	3	3	3
23/2	24	1	1	0	0	0	4	4	4	4	4	4

K is an operator which takes the complex conjugate of its operand. The serial numbers of the electrons are denoted by j. The time reversal operator commutes with the Hamiltonian for an ion in a crystal field, so if $\psi(\mu)$ is a solution of the Schrodinger equation with energy $E(\mu)$ then so is $T\psi(\mu)$. If $T\psi(\mu)$ is orthogonal to $\psi(\mu)$ it is a distinctly different state, but with the same energy as $\psi(\mu)$. The degeneracy which results is known as the time reversal or Kramers degeneracy, and $\psi(\mu)$ and $T\psi(\mu)$ are said to be Kramers conjugate states.

For a system with an odd number of electrons the time reversal operator commutes with the even powers of O and anticommutes with the odd powers. Thus

$$\begin{aligned} O^k\left[T\psi(\mu)\right] &= (-1)^k TO^k\psi(\mu) \\ &= (-1)^k T\chi^{(\mu)}(O^k)\psi(\mu) \\ &= (-1)^k\chi^{(\mu)*}(O^k)\left[T\psi(\mu)\right], \end{aligned} \tag{26}$$

and we see that the state $T\psi(\mu)$ belongs to a new irreducible representation of the symmetry group with crystal quantum number $\tilde{\mu}$. We can substitute $\chi^{(\mu)}(O^k)\psi(\mu)$ for $O^k\psi(\mu)$ in this equation because the representations are all one dimensional, and the matrix representations of O^k are therefore just the

characters of the representations. The characters of the new representations are given by

$$\chi^{(\tilde{\mu})}(O^k) = (-1)^k \chi^{(\mu)*}(O^k) . \qquad (27)$$

When we look these up in the character table we find that $\tilde{\mu} = -\mu \pm 3$. The states which remain twofold degenerate in the crystal field are $\psi(\mu=0)$ with $\psi(\mu=3)$, $\psi(\mu=1)$ with $\psi(\mu=2)$, and $\psi(\mu=-1)$ with $\psi(\mu=-2)$. In the experimental description the degenerate levels will be written for convenience as (0,3), (1,2), and (-1,-2). The number of twofold degenerate levels into which each Dy^{+3} free ion level will split under the influence of the crystal field is $J + 1/2$.

The Zeeman Splitting of the Levels

The Hamiltonian for the interaction of an atom or ion with an external magnetic field is given by Condon and Shortley (23). It can be written as

$$H' = -\beta \vec{H} \cdot (\vec{L} + 2\vec{S}) , \qquad (28)$$

where β is the Bohr magneton ($e\hbar/2mc$), and the $\vec{L}$ and $\vec{S}$ operators have the $\hbar$ taken out of them. $\vec{H}$ is the magnetic field vector. The Hamiltonian can also be written in the form

$$H' = g(\gamma J)\beta \vec{H} \cdot \vec{J} , \qquad (29)$$

where J also has its $\hbar$ factor removed, and $g(\gamma J)$ is an effective Lande' g factor defined by

$$g(\gamma J) = \sum_{\alpha SL} (\alpha SL|\gamma J)^2 g(SLJ). \qquad (30)$$

Here $g(\alpha SLJ)$ is the Lande' g factor for a Russell-Saunders state with quantum numbers αSLJ (23), and the numbers $(\alpha SL|\gamma J)$ are coefficients in the expansion of the free ion states $|\gamma J)$ in terms of Russell-Saunders states.

The Hamiltonian for an ion in the presence of an external magnetic field does not commute with the time reversal operator, so the Kramers degeneracy is removed. Each level of the free ion splits into 2J+1 components and in the case of Dy^{+3}, which has an odd number of 4f electrons, every C_{3h} crystal field level splits into two components if the field is large enough.

Koster and Statz (88, 89) have studied the magnetic field interaction for various symmetries, but confined most of their calculations to the unfilled d-shell in crystals with cubic symmetry. Their method used the same considerations of group theory and time reversal as does the method of Murao, Spedding and Good (69). The studies of reference (69) and the later work of Murao et al. (73) were confined to the magnetic interaction of rare earth ions in C_{3h} symmetry, so these works are more applicable for discussion of the experimental results obtained in this work.

Magnetic field parallel to the c axis

The Hamiltonian for the magnetic field interaction in the case where the field is parallel to the c axis of the crystal (HpC case) is, from Equations 28 and 29,

$$H_p' = -\beta H(\bar{L}_z + 2\bar{S}_z), \tag{31}$$

or equivalently

$$H_p' = g(\gamma J)\beta H \bar{J}_z . \tag{32}$$

Here the z axis has been taken in the c direction, and H is the magnitude of the magnetic field. The complete Hamiltonian for an ion in a C_{3h} crystal field plus HpC Zeeman interaction is given by

$$H = H_{ion} + V + H_p' . \tag{33}$$

It commutes with the operators of the C_{3h} symmetry group so we can find solutions $\psi(\mu i)$ which are simultaneous eigenfunctions of H and O, just as we did in the crystal field problem.

$$H\psi(\mu i) = E(\mu i)\psi(\mu i), \tag{34}$$

and

$$O\psi(\mu i) = \exp(i\pi\mu/3)\psi(\mu i). \qquad (35)$$

The solutions may be expanded in terms of solutions of the central field problem, but since the crystal field and magnetic splittings are usually small compared to the free ion splittings, it is more appropriate to expand in terms of the free ion solutions. The expansion is similar to that given in Equation 22 for the solution to the crystal field problem; only the values of the expansion coefficients are changed.

If the crystal field and magnetic splittings are of a comparable size, but small compared to the separation of the free ion levels, we can treat $V + H_p'$ as a perturbation on the free ion levels and ignore matrix elements of the perturbation between them. The splittings caused by the combined effects of the crystal and HpC magnetic fields can then be calculated by diagonalizing the matrix representation of $V + H_p'$ in the basis formed by the 2J+1 functions of each free ion level.

If the magnetic splittings are small compared to both the free ion and crystal field splittings, H_p' is treated as a perturbation on the crystal field levels. Here the basis functions are taken to be the $\psi(\mu i)$, and the usual approach is to use ordinary first or second order perturbation theory to solve for the eigenvalues and eigenfunctions. Bartel and Spedding (71) used this method to show that the HpC splitting

for a twofold degenerate crystal field level described by $(\mu,\tilde{\mu})_i$ is given to second order by

$$\Delta_p(\mu,\tilde{\mu})_i = 2|(\mu_i|H'_p|\tilde{\mu}_i)|$$
$$= 2\beta H g(\gamma J)\sum_M \left(C^{i\mu}_{\gamma JM}\right)^2 M \qquad (36)$$

Here $\sum_M \left(C^{\mu i}_{\gamma J M}\right)^2 M$ gives the effective M value of the crystal field level, and we see that to this order of the approximation the HpC Zeeman splittings should be linear in the magnetic field strength.

Magnetic field perpendicular to the c axis

The Hamiltonian for the magnetic field interaction in the case where the field is perpendicular to the c axis of the crystal (HsC case) is given by

$$H'_s = -\beta\left[H_x(\vec{L}_x + 2\vec{S}_x) + H_y(\vec{L}_y + 2\vec{S}_y)\right], \qquad (37)$$

or equivalently

$$H'_s = g(\gamma J)\beta\left[H_x\vec{J}_x + H_y\vec{J}_y\right] \qquad (38)$$

The z axis has been taken in the c direction as before, and H_x and H_y are the components of the magnetic field along the x and y directions of the crystal. The x axis is taken so

that the factor β_{66} which occurs in the crystal field expansion of Equation 15 vanishes. If ϕ_m is the angle between the magnetic field and the x axis the Hamiltonian can be written in the form (73)

$$H_s' = -(\beta H/2)\left[e^{-i\phi_m}(\vec{L}_+ + 2\vec{S}_+) + e^{+i\phi_m}(\vec{L}_- + 2\vec{S}_-)\right] \quad (39)$$

or

$$H_s' = g(\gamma J)(\beta H/2)\left[e^{-i\phi_m}\vec{J}_+ + e^{+i\phi_m}\vec{J}_-\right]. \quad (40)$$

Here H is the magnitude of the magnetic field and $\vec{S}_\pm$, $\vec{L}_\pm$, and $\vec{J}_\pm$ are the usual angular momentum stepping operators without the $\hbar$ factor.

The complete Hamiltonian for an ion in a C_{3h} crystal field plus HsC magnetic field is given by

$$H = H_{ion} + V + H_s'. \quad (41)$$

It does not commute with the operators of the C_{3h} point group or with the time reversal operator because the H_s' term does not commute with these operators. If the magnetic splittings are small compared to the crystal field splittings an appropriate way to treat the problem is by perturbation theory. This is the method employed in (69). The basis functions are taken to be the solutions $\psi(\mu i)$ for the crystal field prob-

lem, and H_s' is treated as a perturbation. The results from (69) which are pertinent to the present work can be summarized as follows:

1) (0,3) levels may show HsC Zeeman splittings which depend on the angle ϕ_m between the x axis and the magnetic field. Since the (0,3) splitting can only occur by virtue of a considerable magnetic interaction with both (1,2) and (-1, -2) levels, the HsC splittings of these levels might also depend on ϕ_m.

2) The HsC Zeeman splittings should be proportional to H^3 for (0,3) levels, and should be periodic by 60° about the c axis according to Equation 42,

$$S \propto H^3 \left| A\exp(i6\phi_m) + B \right| , \qquad (42)$$

where A and B are characteristic of each level.

3) The maximum or minimum splitting of all levels should occur at $\phi_m = 0 + n60^\circ$, where n is any integer.

4) The HsC Zeeman splittings of (1,2) and (-1,-2) levels should be linear in the magnetic field strength if these levels are well separated in energy from other levels.

5) The intensities of the lines, if they vary at all, must be periodic by 60°. However, the maximum or minimum intensities of all of the lines need not occur at the same angle.

While the conclusions from perturbation theory are in agree-

ment with the experiment (51, 71, 72) at low magnetic field strengths, there are many observable cases where the magnetic splittings at finite magnetic fields are comparable to the crystal field splittings. Here the agreement is understandably less satisfactory.

In (73) the theory of the HsC Zeeman effect was extended to the case where the magnetic and crystal splittings are comparable. It was shown, for both even and odd numbers of 4f electrons, that the energies of all the levels as functions of ϕ_m do not cross, have 60° periodicity, and have extreme values when the magnetic field is parallel to any one of the twelve equivalent x axes for a rare earth ion in C_{3h} symmetry. These features of the energy levels are in better agreement with the observations at high magnetic fields (51, 72) than those predicted by the earlier theory. In (73) the combined effects of the crystal and magnetic fields were treated as a perturbation on the free ion functions $\psi(\gamma JM)$, and only the consequences of the symmetry of the problem were used. The results therefore apply as long as the splittings are small compared to the energy separation of the free ion states, and the details of the wavefunctions are not needed.

In (73) it was also pointed out that although the complete Hamiltonian for the HsC Zeeman effect does not commute with the C_{3h} or time reversal operators, it does have a symmetry of the type first discussed by Wigner (75). The symmetry

operator in this case is O^3T, "time reverse and reflect in the plane perpendicular to the c axis." O^3T is an antiunitary (75) operator, it commutes with the full Hamiltonian for the HsC Zeeman effect, and its second power is the identity operator for both even and odd number of electrons. As usual this symmetry property leads to quantum numbers for the states, selection rules on the matrix elements, and simplifications in the work required to solve the problem.

Since there is no degeneracy in the HsC case the eigenfunctions of the full Hamiltonian must also be eigenfunctions of O^3T. This led the authors of (73) to choose the functions

$$\chi(JIMI\xi) = (2)^{-1/2}\left[\Psi(JIMI) + \xi\Psi(J-IMI)\right] \qquad (43)$$

for their basis of free ion functions. These functions have the advantage that they are eigenfunctions of O^3T,

$$O^3T\chi(JIMI\xi) = (-1)^{J+\frac{1}{2}n}\,\xi\chi(JIMI\xi)\,, \qquad (44)$$

so the selection rules arising from the O^3T symmetry may be used in setting up the perturbation matrix.

The matrix to be considered for the HsC Zeeman effect is $h^{II}(\phi_m)$, with matrix elements

$$h^{II}(\phi_m)_{IM'I\xi',IMI\xi} = \int \chi^{\dagger}(JIM'I\xi')\left[V^e + H'_s\right]\chi(JIMI\xi)\,. \qquad (45)$$

The selection rule which results from the commutation of O^3T with the Hamiltonian is

$$\left[\int \chi^{\dagger}(J\,|M'|\,\xi')\left[V^e + H_s'\right]\chi(J\,|M|\,\xi)\right]^* = \xi'\xi\int \chi^{\dagger}(J\,|M'|\,\xi')\left[V^e + H_s'\right]\chi(J\,|M|\,\xi) \qquad (46)$$

so the matrix must have the form

	$\xi = 1$	$\xi = -1$
$\xi = 1$	real	purely imaginary
$\xi = -1$	purely imaginary	real

Here only magnetic field terms proportional to H_y are non-diagonal in ξ, so the problem uncouples into two smaller matrices when $\vec{H}$ is parallel to the x axis.

If the perturbation matrix is set up with the basis functions $\chi(J|M|\,\xi = +1)$ and $i\chi(J|M|\,\xi = -1)$, then it is real and symmetric for all values of ϕ_m. It must be possible to write the solutions in the forms

$$\psi(\phi_m, \xi = +1) = \sum_{|M|}\left[D_{|M|}(\phi_m)\chi(J\,|M|+1) + iE_{|M|}(\phi_m)\chi(J\,|M|-1)\right] \qquad (47)$$

and

$$\psi(\phi_m, \xi = -1) = \sum_{|M|} \left[F_{|M|}(\phi_m) \chi(J\,|M|-1) + iG_{|M|}(\phi_m) \chi(J\,|M|+1) \right] \quad (48)$$

where the coefficients $D_{|M|}(\phi_m)$, $E_{|M|}(\phi_m)$, etc., are real and contain all of the ϕ_m dependence of the solutions. Each solution has one or the other of these forms, and has quantum number ξ such that

$$O^3T(\phi_m, \xi) = (-1)^{J+n/2} \xi \psi(\phi_m, \xi). \quad (49)$$

For free ion states with half integer J values there are $J + 1/2$ levels with $\xi = +1$ and $J + 1/2$ with $\xi = -1$.

The relationships between the solutions at various angles ϕ_m have been thoroughly studied in (73), and are summarized below.

$$\psi(\phi_m - \tfrac{\pi}{3}, \xi) = \pm i^n O \psi(\phi_m, \xi) \quad (50)$$

$$\psi(-\phi_m, \xi) = \psi^*(\phi_m, \xi) \quad (51)$$

The sign which is to be used on the right hand side of Equation 50 depends on the state under consideration. States with the plus sign are called type A, those with the minus sign type B. The ξ numbers of type B states are sensitive to the choice of x axis, while those of type A states are not. If there is effective D_{3h} symmetry in the crystal field terms

important for intensities, there is an experimental distinction between absorption transitions of the type A to A or B to B, and transitions of the type A to B or B to A.

Interaction with Electromagnetic Radiation

The perturbation Hamiltonian for interaction of electrons with electromagnetic radiation is given by Schiff (90) as

$$H_{rad} = -(e/mc)\sum_{j=1}^{n}\vec{A}(\vec{r}_j,t)\cdot\vec{p}_j \quad . \tag{52}$$

Here $\vec{P}_j$ is the momentum operator for the j^{th} electron (or hole) and $\vec{A}(\vec{r}_j,t)$ is the instantaneous vector potential of the radiation at the j^{th} electron with coordinates $\vec{r}_j$. The absorption part of $\vec{A}$ is

$$\vec{A}_{abs}(\vec{r}_j,t) = \vec{A}_o\exp(i\vec{k}\cdot\vec{r}_j + i2\pi\nu\, t), \tag{53}$$

where $\vec{A}_o$ is the polarization vector of the radiation with propagation vector k and frequency ν.

Time dependent perturbation theory gives the probability per unit time for absorption of a photon and transition from an initial state ψ_i to a final state ψ_f as

$$W = (e^2/2\pi m^2 c\,\nu^2\hbar^2)I(\nu)\cdot\left|\int\psi_f^{\dagger}\sum_{j=1}^{n}\exp(i\vec{k}\cdot\vec{r}_j)\vec{e}\cdot\vec{p}_j\,\psi_i\,d\tau\right|^2 \tag{54}$$

Here ν is the transition frequency, $I(\nu)d\nu$ is the intensity

of the light shone inside the frequency range $d\nu$, and $\vec{e}$ is a unit vector in the polarization direction of the light. So far nothing has been assumed about the parity of the functions. All we know is that in the case of the rare earth ethylsulfates the functions ψ_i and ψ_f will be eigenfunctions of O in the H = 0 or HpC case, and of O^3T in the HsC case. They therefore have μ or ξ as good quantum numbers regardless of whether or not their parity is well defined.

The usual procedure in calculating transition probabilities from Equation 54 is to assume that $\vec{k}\cdot\vec{r}$ is small. Then we can expand $\exp(i\vec{k}\cdot\vec{r})$ in an infinite series

$$\exp(i\vec{k}\cdot\vec{r}_j) = 1 + i\vec{k}\cdot\vec{r}_j + \ldots \qquad (55)$$

and keep only the first few terms. This is justified in the case of optical absorption in atoms or ions because the wavelength of the light is large compared to the atomic dimensions, but it is not justified if the wavelength is in the X-ray region. In the latter case the higher order terms are more important and lead to scattering phenomena.

If we replace $\exp(i\vec{k}\cdot\vec{r}_j)$ by only the first term in the expansion we get

$$W = (e^2/2\pi m^2 c\,\nu^2\hbar^2) I(\nu) \left| \int \psi_f^{\dagger} \sum_{j=1}^{n} \vec{e}\cdot\vec{p}_j \, \psi_i d\tau \right|^2 , \qquad (56)$$

but

$$\left| \int \psi_f^{\dagger} \sum_j \vec{e}\cdot\vec{p}_j \psi_i d\tau \right|^2 = m^2 \left| \frac{d}{dt} \int \psi_f^{\dagger} \sum_j \vec{e}\cdot\vec{r}_j \psi_i d\tau \right|^2$$

$$= (m^2/\hbar^2)(E_f - E_i)^2 \left| \int \psi_f^{\dagger} \sum_j \vec{e}\cdot\vec{r}_j \psi_i d\tau \right|^2$$

$$= 4\pi^2 m^2 \nu^2 \left| \int \psi_f^{\dagger} \sum_j \vec{e}\cdot\vec{r}_j \psi_i d\tau \right|^2 . \quad (57)$$

Making this substitution in Equation 56 gives

$$W = (2\pi e^2/c\hbar^2) I(\nu) \left| \int \psi_f^{\dagger} \sum_j \vec{e}\cdot\vec{r}_j \psi_i d\tau \right|^2 , \quad (58)$$

and transitions for which this approximation may be used are called electric dipole transitions. This is because only matrix elements of the electric dipole moment in the direction of the polarization vector are involved.

The next term in the expansion of the vector potential, as Condon and Shortley have shown, contains all of the magnetic dipole contribution and part of the electric quadrupole contribution to the intensities. The probability for magnetic dipole transitions is proportional to the square of the absolute value of the matrix element

$$\int \psi_f^{\dagger} \sum_j \beta(\vec{l}_j + 2\vec{s}_j) \psi_i \, d\tau , \quad (59)$$

where β is the Bohr magneton. The probability for allowed magnetic dipole transitions is generally several orders of magnitude less than that for allowed electric dipole transitions. This is because of the additional factor of $|\vec{k}\cdot\vec{r}|^2$ which enters into the expression for the transition probabilities in the magnetic dipole case. This factor comes from the expansion of the vector potential, and for light in the visible region of the spectrum has a value of approximately 10^{-5}.

Selection rules for electric and magnetic dipole transitions have been worked out in (69) and (73) for ions in C_{3h} symmetry. In the absence of an external magnetic field the conclusion is that the transition probabilities are zero unless the conditions listed in Table 7 are fulfilled for the crystal quantum numbers of the initial and final states.

Table 7. Selection rules for transitions between C_{3h} crystal states of a $4f^n$ configuration

Polarization direction	Electric dipole transitions	Magnetic dipole transitions
EsC, MpC	$\Delta\mu = \pm 2, \pm 4$	$\Delta\mu = 0$
EpC, MsC	$\Delta\mu = \pm 3$	$\Delta\mu = \pm 1, \pm 5$

The symbols EpC and EsC are used here to specify the direction of the electric vector of the incident radiation with respect

to the c axis of the crystal. EpC means that it is parallel to the c axis; EsC that it is perpendicular. The symbols MpC and MsC are used in the same way to specify the direction of the magnetic vector.

In the case where an external magnetic field is applied parallel to the c axis of the crystal (HpC case) the selection rules are the same as for the zero magnetic field case. This is because the Hamiltonian is still invariant to the operators of the C_{3h} group, and the crystal quantum number is still a good quantum number.

When the external magnetic field is perpendicular to the c axis (HsC case) the symmetry of the Hamiltonian is reduced, as we have seen, and the crystal quantum numbers no longer have any meaning. However, we can still get information on the transition probabilities by using the O operator. We know from Equation 50 that

$$\Psi(\phi_m - \tfrac{\pi}{3}, \xi) = \pm i^n O \Psi(\phi_m, \xi). \tag{50}$$

Therefore if the transition probability when the field is at angle ϕ_m with respect to the x axis is

$$W(\phi_m) = k\left|\int \Psi_f O_p \Psi_i d\tau\right|^2, \tag{60}$$

then the probability for the same transition when the field

is at angle $\phi_m - \pi/3$ is

$$W(\phi_m - \tfrac{\pi}{3}) = k\left|\int \left[\pm i^n O \psi_f\right]^\dagger O_p \left[\pm i^n O \psi_i\right] d\tau\right|^2$$

$$= k\left|\int \psi_f^\dagger \left[O^{-1} O_p O\right] \psi_i \, d\tau\right|^2. \qquad (61)$$

Here k is a real positive proportionality factor which depends on the frequency and intensity of the incident light, and on whether the transition mechanism is electric or magnetic dipole. The operator in the matrix element, written here as Op, depends on the transition mechanism, and on the polarization of the incident light. The operators to be used in Equations 60 and 61 for the various cases of polarization and transition mechanisms are given in Table 8.

Table 8. Electric and magnetic dipole moment operators for various polarizations of the incident light

Transition mechanism	Polarization direction	Moment operator
Electric dipole	EpC	$\sum_j z_j$
Electric dipole	EsC	$\sum_j (x_j \cos\phi_m + y_j \sin\phi_m)$
Magnetic dipole	MpC	$\sum_j \beta(\ell_z + 2s_z)_j$
Magnetic dipole	MsC	$\sum_j \beta[(\ell_x + 2s_x)_j \cos\phi_m + (\ell_y + 2s_y)_j \sin\phi_m]$

Here the directions of the c axis, the magnetic field, and the propagation vector of the incident light are assumed to be mutually perpendicular. Then the polarization vector in the EsC or MsC case is parallel to the magnetic field, and is at an angle ϕ_m from the x axis of the crystal. This is the experimental situation in the present work.

There are no angle dependent factors in k in Equations 60 and 61 so we can relate the transition probabilities for various angles by studying the transformation properties of the operators in Table 8 under the O operator. The result is that the transition probabilities for both electric and magnetic dipole transitions must be 60° periodic when the directions of the magnetic field and the incident light are kept constant and only the crystal is rotated.

EXPERIMENTAL INVESTIGATION

The Spectrograph and Optical Arrangement

A Jarrell-Ash 3.4 meter Ebert spectrograph (91-93) was used to photograph the absorption spectra observed in this work. Most of the photographs were obtained using this instrument with an interferometrically ruled 300 line/mm Harrison plane grating blazed for 57000 Å in the first order at 59°. The spectra of the various line groups were observed in the seventh through the nineteenth orders near the blaze angle, and the order of interest was isolated on the plate by using either a Jarrell-Ash order sorter (94) or a Jarrell-Ash 1/4 meter grating monochromator as a predispersing instrument. The linear dispersion ranged from 0.62 Å/mm in the seventh order to 0.23 Å/mm in the 19th order. Schematic drawings of the optical arrangement for these two cases are shown in Figures 1 and 2.

When the order sorter was used several orders were obtained at once, and they were displayed on the plate one above the other. However, to get a separation of the orders with the relatively low vertical dispersion of this instrument, it was necessary to use a rather small vertical aperture at the slit of the order sorter. This limited the height of each spectral order to about two millimeters, and made it very difficult to place a useful reference spectrum adjacent to the order which was to be measured. There is no doubt that

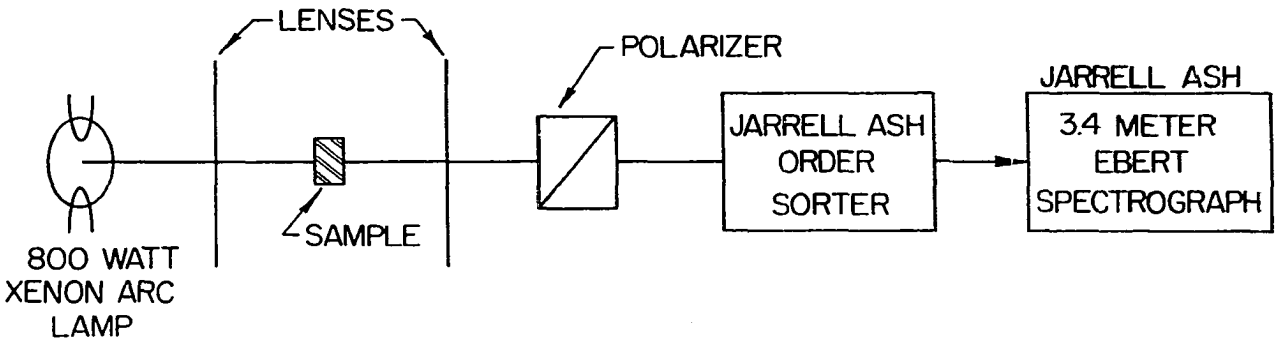

Figure 1. Schematic drawing of the optical arrangement when the order sorter is used

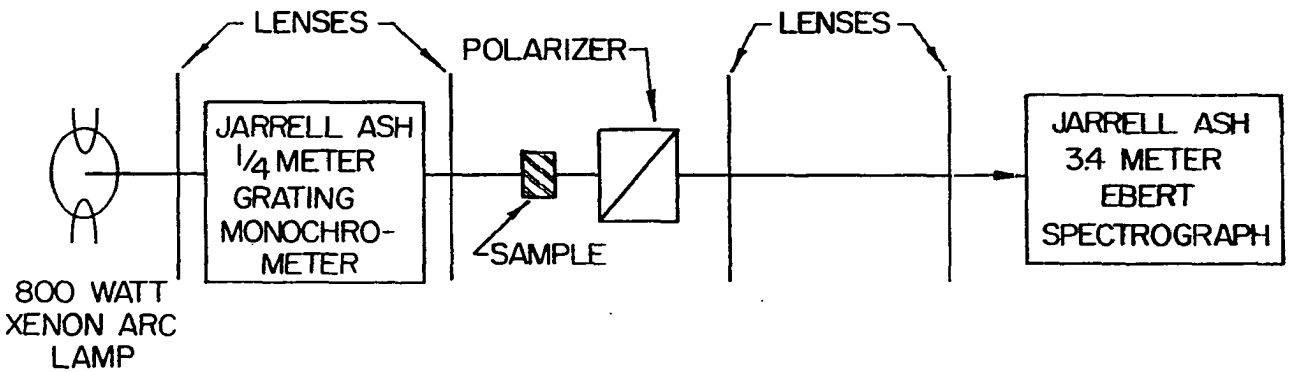

Figure 2. Schematic drawing of the optical arrangement when the grating monochrometer is used

the use of the order sorter reduced the resolution and accuracy which could have been obtained with the main spectrograph.

When the grating monochromator was used as the predispersing instrument only one spectral order was obtained on the plate. However, since this instrument dispersed the light in the same direction as the main spectrograph, there was no limitation on the vertical apertures. The full height of the spectrograph slit could be used, and the Hartmann diaphram could be used to place reference spectra above and below the spectrum to be measured. This is the optimum condition for accurate measurement of the absorption lines.

Some of the photographs were obtained in only the second or third order with a 600 line/mm grating in the main spectrograph. The dispersion in these photographs was only about one tenth that obtained with the 300 line/mm grating in high orders, but this seemed to make the very weak and very broad absorption lines much easier to observe and measure. For these photographs neither the order sorter or the monchromator was used because the limited spectral sensitivity of the photographic plates was enough to isolate the order of interest.

The procedure in obtaining the absorption spectra was to place the sample in the position indicated in Figures 1 and 2. The sample absorbs light of certain wavelengths from the

continuous spectrum emitted by the high pressure xenon lamp, and only a fraction of the light with these wavelengths reaches the photographic plate. The absorptions were observed as unexposed or only partly exposed portions on the plate and the wavelengths which were absorbed were measured with respect to a standard reference spectrum.

The reference spectrum in this work was obtained by removing the sample and replacing the xenon source with a hollow iron cathode discharge tube (95). Many of the wavelengths emitted by tubes of this type have been measured by interferometry techniques, and are the accepted standards for wavelength measurements (96).

In order to determine the polarization of the light which was absorbed by the sample, a Glan (97) polarizing prism was used. The polarizer was lined up so that the electric vector of the light which reached the spectrograph was either parallel or perpendicular to the c axis of the sample. The polarizations will be referred to as EpC and EsC, respectively.

The Magnet

For the Zeeman studies the magnetic field was supplied by an Arthur D. Little electromagnet. The current was supplied by a 100 kilowatt D.C. generator driven by an A.C. motor, and the current was regulated by controlling the current through the field windings of the generator. During each

exposure of the spectrum the current in the magnet was monitored by measuring the voltage drop across a 1200 Ω shunt. The maximum field obtainable in the 1-9/16 inch gap, for 5-3/4 inch pole faces tapered from 11 inches, was 27912 Gauss. The field strengths were measured with a Type 820 Rawson-Lush rotating coil Gaussmeter and Type 501 meter type indicator. The probable error for the magnetic field measurements was less than 0.15% for all field values.

The Dewar

A stainless steel dewar, pictured in Figure 3, contained the samples in contact with up to six liters of liquid helium or liquid hydrogen. If the outside radiation shield was kept filled with liquid nitrogen the helium lasted up to ten hours, and the hydrogen up to one hundred hours. The transparent tip and plane windows were UV grade fused quartz to allow the transmission of ultraviolet light.

Preparation of the Rare Earth Ethylsulfates

The single crystal samples used in this work were grown by Mr. H. O. Weber of Dr. Spedding's chemistry group. The rare earth ethylsulfates were obtained by reacting the rare earth chlorides with sodium ethylsulfate. The rare earth chlorides were prepared from 99.95% pure oxides obtained from the ion exchange group of the Ames Laboratory of the U.S.A.E.C. The sodium ethylsulfate was purchased from Amend Drug and

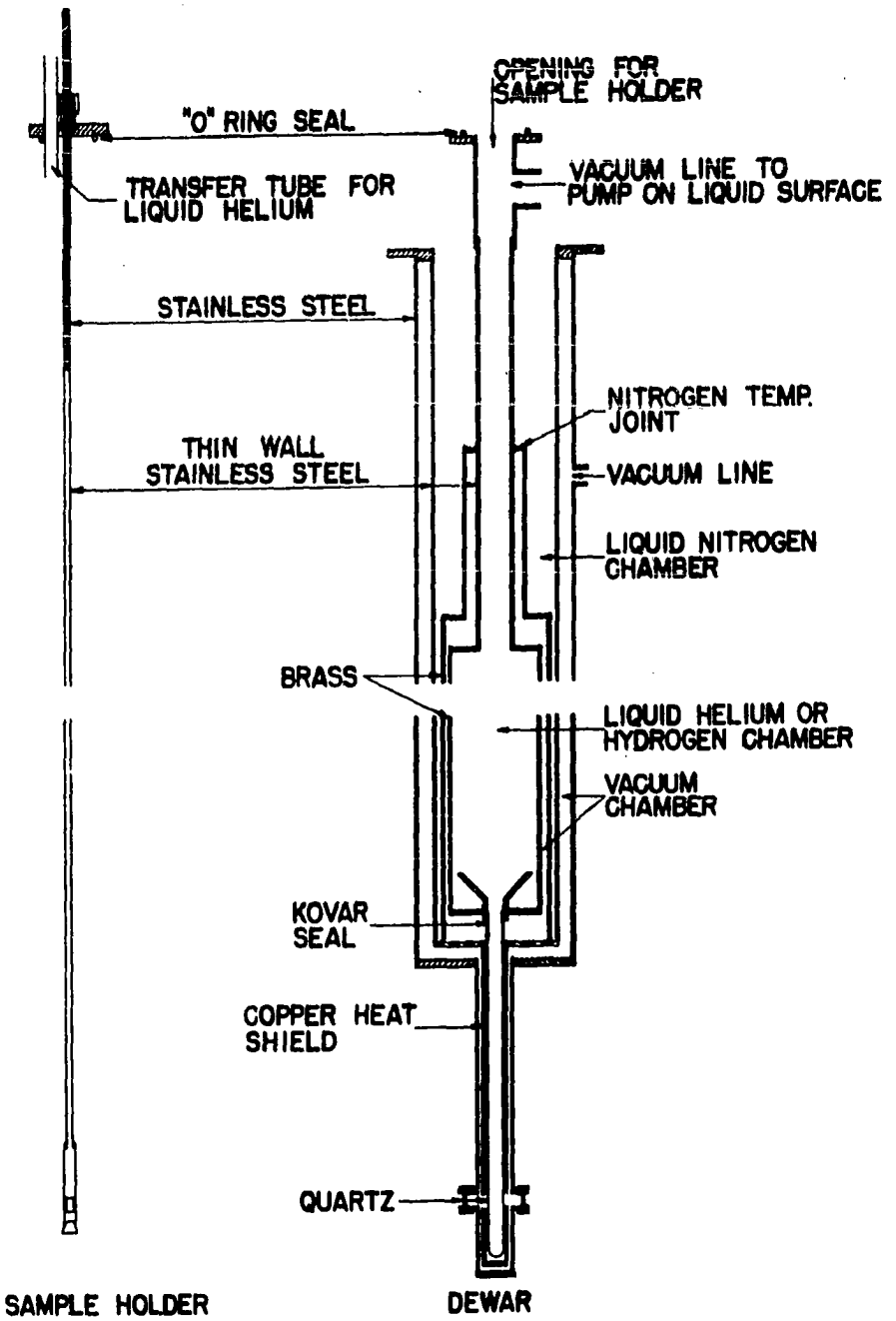

Figure 3. Dewar and sample rod

Chemical Company, New York.

The rare earth oxide was reacted with an equivalent amount of C.P. hydrochloric acid in water with a conductivity of 5×10^{-7} mhos. This mixture was heated just below the boiling point until almost all of the oxide had reacted. Water was added to adjust the concentration of the rare earth chloride to about two molar. A one percent excess of rare earth oxide was added to the solution and it was heated for two more hours. The excess oxide was filtered off, and the pH of the filtrate was adjusted to 3.0 by carefully adding dilute HCl. The solution was heated for one hour to destroy any colloidal rare earth oxide or oxychloride and then was cooled. The pH of the solution was checked, and the above process repeated until the pH remained unchanged after heating. The resulting solution was evaporated to the point where crystals formed. This solution was cooled slightly, and about 500 ml of absolute alcohol were added to it. The resulting rare earth chloride solution was added slowly with stirring to a one percent excess of sodium ethylsulfate in alcohol, and the sodium chloride precipitate was digested overnight. The alcoholic supernatant containing the rare earth ethylsulfate was decanted and the alcohol was distilled off under reduced pressure at 30° C. The salt remaining was dissolved in a minimum amount of conductance water and this solution was filtered. The salt was then purified by frac-

tional crystallization to remove any sodium chloride or sodium ethylsulfate that may have been present. Finally some of the purified rare earth ethylsulfate was dissolved in absolute alcohol in a sidearm flask and the alcohol was distilled off under reduced pressure until the solution was nearly saturated. At this point it was set aside in a glove box whose temperature was kept at 25° C. Hexagonal crystals of the rare earth ethylsulfate nonahydrates grew (71) as the alcohol slowly escaped through the small sidearm orifice.

Grinding, Mounting, and Alignment Procedures

The crystals normally grew to a size of about 3 mm by 5 mm by 2 mm thick, and all of the crystals used in this work were checked on a polarizing microscope to determine the direction of the c axis and to verify that they were indeed single crystals. When white light is passed through the crystal perpendicular to the c axis and through the crossed nicol prisms of the microscope, a null in the intensity is observed every 90° as the crystal is rotated. The direction of the null corresponds to a direction either parallel or perpendicular to the c axis. The c axis was found to lie parallel to the long dimension of all of the crystals used in this work.

In order to obtain samples thin enough to resolve certain features of the spectrum it was often necessary to grind the single crystals. Fine rayon polishing cloth and ethyl alco-

hol were used for the initial grinding, and cotton swabs moistened with alcohol were used for the final reduction and polishing. Typical crystal thicknesses used in the experiments were 0.1, 0.2, 0.5, 1.0, and 4.4 mm.

Two crystals were mounted for each experiment, one with its c axis parallel to the magnetic field, and one with its c axis perpendicular to the field. The sample holder pictured in Figure 4 was used to make the alignment as accurate as possible. It provides three axes of rotation for each crystal by means of the small adjusting screws, and it can be screwed into a standard optical goniometer head. Care was exercised in grinding the crystals so that one broad natural face of each crystal was not disturbed. Optical reflections from these faces were later observed on the goniometer and were used to aid in the crystal alignment procedure. The crystals were mounted over the holes in the outer plates of the sample holder with Duco cement and masking tape, and were aligned under the polarizing microscope so that their c axes were perpendicular to each other.

The sample holder was next mounted on the optical goniometer and both crystals were adjusted by means of the small screws above and below each crystal so that their broad natural faces were parallel to the long axis of the sample holder. The situation at this point in the alignment procedure is shown in Figure 5. Here only the broad natural faces

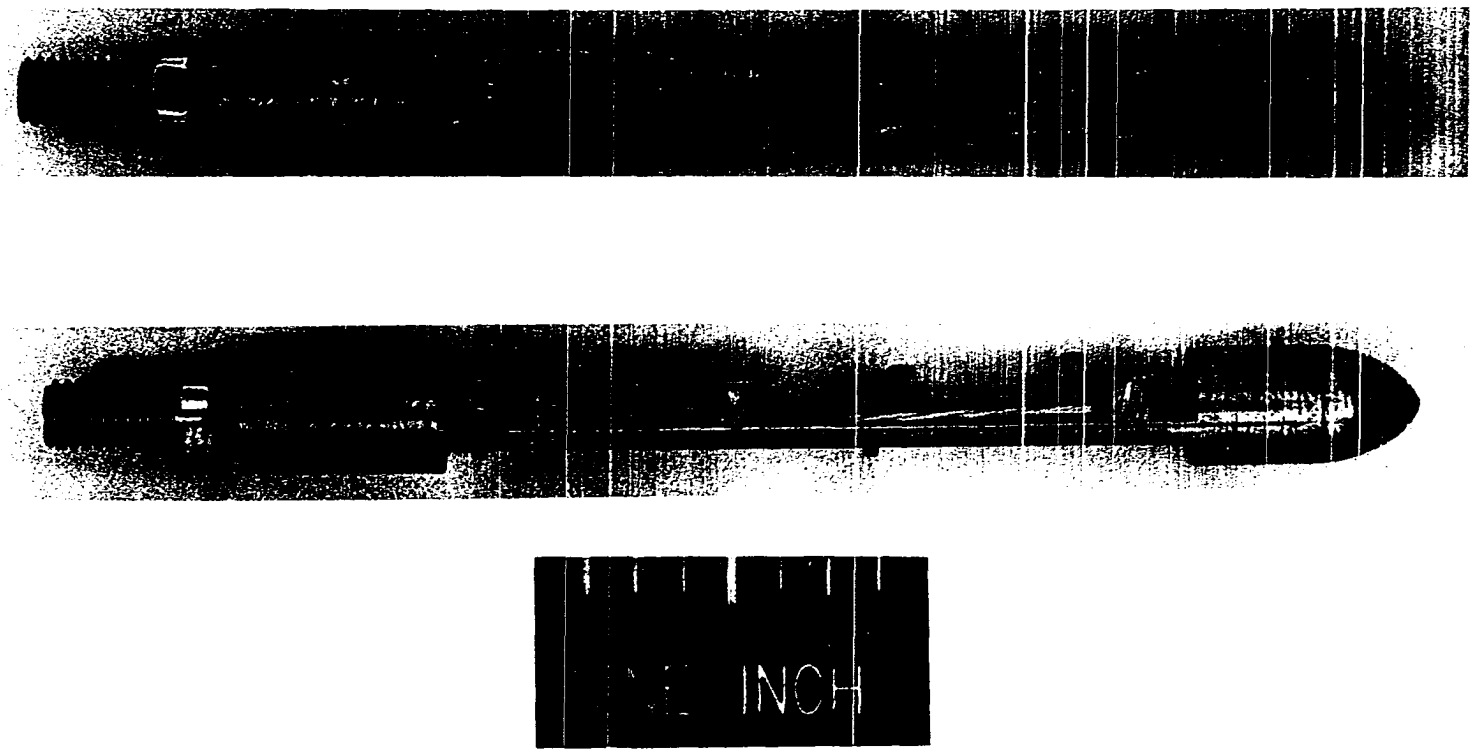

Figure 4. Front and side views of the single crystal sample holder

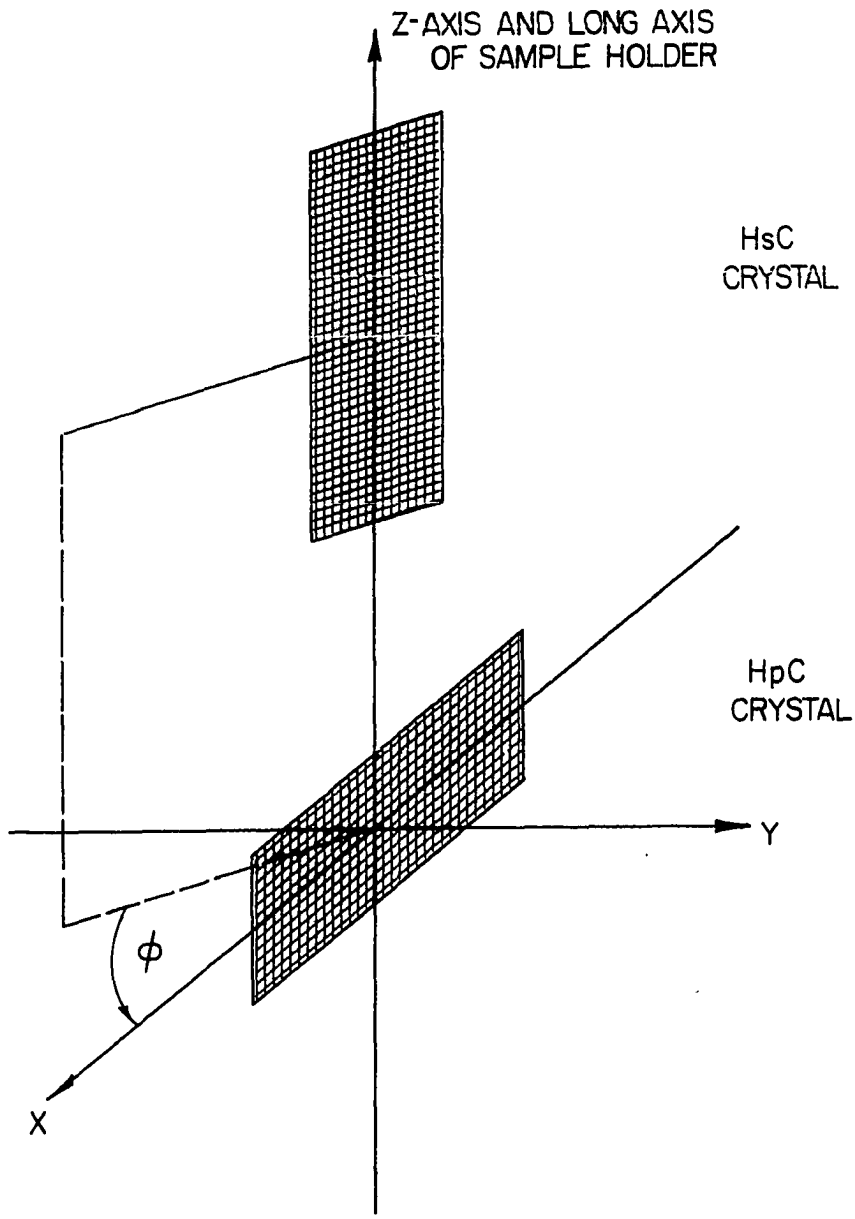

Figure 5. Alignment schematic showing only the broad natural faces of the single crystal samples

are shown for simplicity, and both faces are parallel to the long axis of the sample holder.

The next step in the alignment procedure was a determination of the angle $\emptyset$ subtended in the x-y plane by the broad natural faces of the two crystals. See Figure 5. This was important for determination of the angle between the a and x axes of the crystals because for this one needs to know the angle between the magnetic field and the a axis of the HsC crystal. In this work the a axis was assumed to be parallel to the broad natural face of the crystal. Therefore when $\emptyset$ and the angle between the magnetic field and the c axis of the HpC crystal were known, the angle between the magnetic field and the a axis was also known. The angle $\emptyset$ was measured on the optical goniometer, and the sample holder was returned to the polarizing microscope for a final check of the c axis directions. The latest version of the sample holder had provision for aligning the crystals so that $\emptyset = 0$ while the sample holder was in position on the optical goniometer. Experience showed that the measurements and adjustments performed on the optical goniometer were accurate to within plus or minus one tenth of one degree.

The sample holder was threaded into the bottom of a stainless steel tube running the length of the dewar and a pointer was attached at the top. The crystals were rotated by simply turning the sample tube, and the angles of rotation

were read from a dial which was firmly attached to the body of the dewar. For later measurements in this work the upper end of the sample rod was held in the angle measuring device shown in Figure 6. The inner plate and dome of this device held the sample rod and the outer base plate was firmly attached to the dewar. The inner plate and sample holder were rotated by means of the worm gear drive, and the angles of rotation were measured with respect to the vernier scale on the base plate. The upper portion of the sample rod was milled flat and had a reference line scribed lengthwise on the flat part. To shift either the HsC or HpC crystal into the light path without disturbing the orientation of the crystals with respect to the magnetic field direction, one merely had to raise or lower the sample rod and make sure that the reference line remained in line with a similar reference line scribed on the top of the dome. When the dewar was removed from the light path for the recording of the reference spectrum, rotation was prevented by moving the dewar on a slot wheeled carriage which rode on an angle iron track.

Crystal alignment in the external magnetic field

The accurate alignment of crystals in the magnetic field is the single most critical and most vexing problem encountered in low temperature studies of the Zeeman effect of single crystals. It is a particularly annoying problem be-

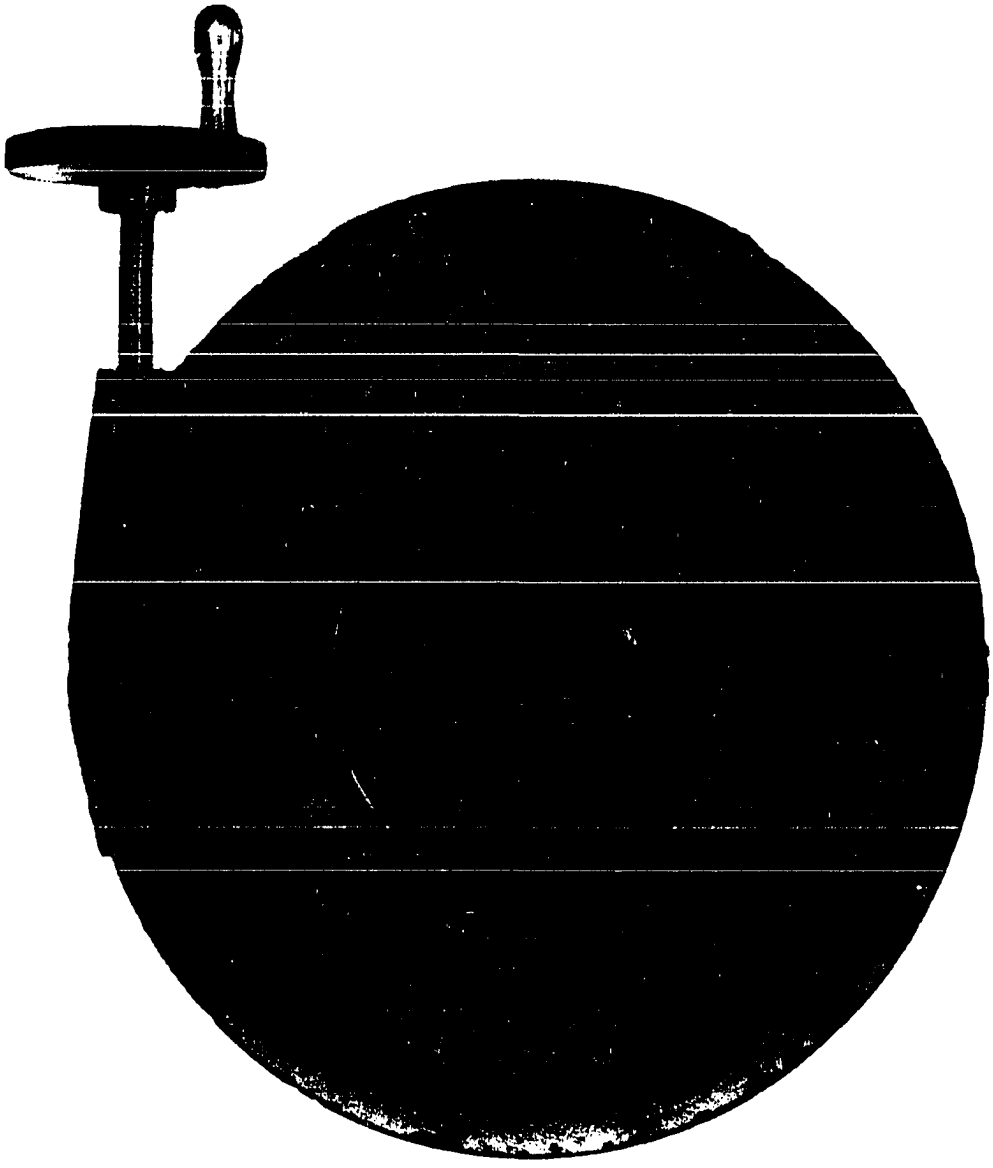

Figure 6. Top view of angle measuring device

cause misalignment is usually not discovered until after numerous plates have been prepared and measured. For example, Dieke, who was well known as a careful worker in this field, reported the possibility of a 12 degree misalignment in his paper with Singh (98) dealing with the spectrum of $ErCl_3$. Hellwege et al. (99) tried to solve the problem by recording the spectra of two crystals mounted at right angles to each other. They then calculated the Zeeman splittings for each level from the splittings resulting from the nominally parallel and from the nominally perpendicular crystals. The difficulty with this method is that a perpendicular component of the Zeeman splitting can still result from misalignment of the nominally parallel crystal in the horizontal plane, and the calculations take no account of this possibility.

The methods used the present work for aligning the crystals and for checking their alignment in the magnetic field were similar to those previously described for erbium ethylsulfate (51). When these methods were used good alignment was obtained and the alignment checks allowed quick verification of proper alignment. With the use of these methods it was possible to forego the lengthy measurement and analysis procedures until after it had been demonstrated that the crystals were properly aligned.

HpC alignment Photographs of the high field Zeeman spectrum were taken as the c axis of the crystal was rotated in the horizontal plane by 2° increments through 10° on either side of the suspected aligned position. Photographs such as those shown in Figure 7 resulted. The c axis was parallel to the magnetic field when the EsC lines at 24966 cm^{-1} and 24980 cm^{-1} vanished. The angle of best alignment was noted and the other degree of freedom was then checked by observing the spectrum of the HsC crystal mounted at 90° to the HpC crystal. See below. If both crystals were aligned at the same angle, one could proceed with the measurement and analysis of the HpC spectrum with considerable confidence that the crystal was properly aligned to within less than 0.5°.

For some of the photographs in this work even more precise HpC alignment was obtained by using a larger range of angles in the alignment photographs. When this was done the splittings of some of the more sensitive levels changed enough so that the angle of maximum or minimum splitting could be calculated to within a few tenths of a degree from the measured splittings at various angles. The most sensitive levels are those with large HpC splittings and small HsC splittings, or vice versa.

HsC alignment check Photographs of the high field Zeeman spectrum were made as the HsC crystal was rotated

Figure 7. Typical HpC alignment photograph

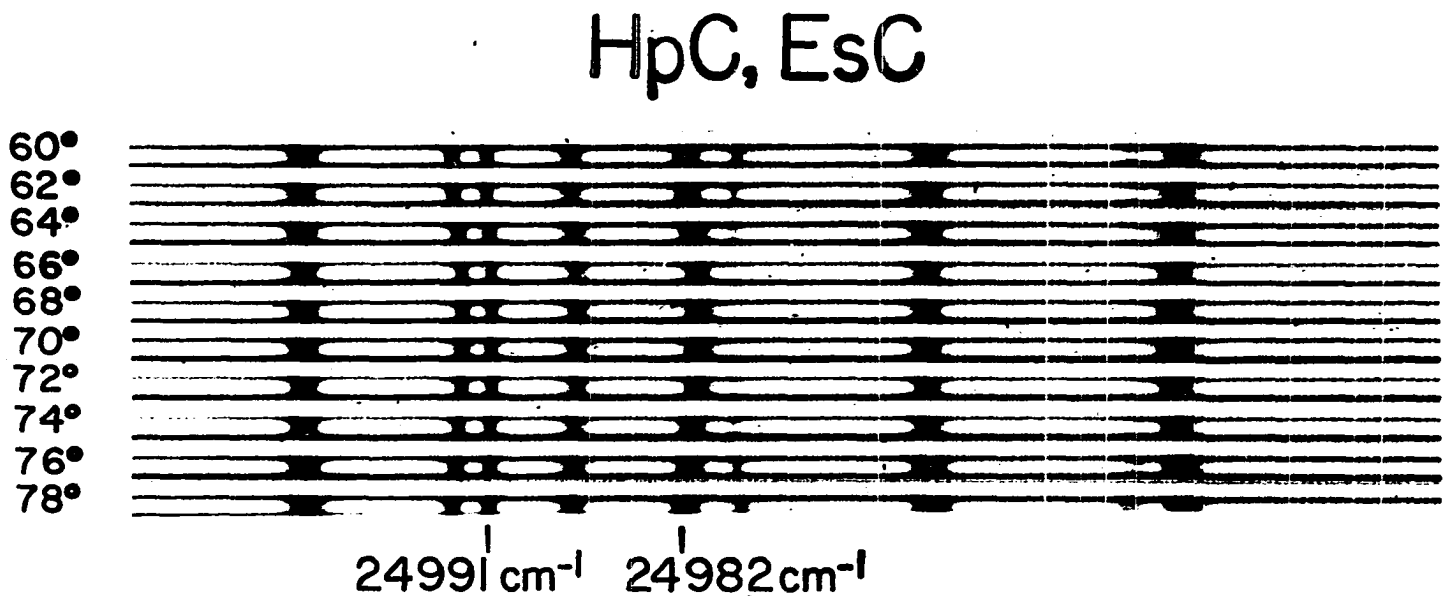

Figure 7. Typical HpC alignment photograph

through 70° about its c axis in 10° increments. The crystalline c axis was perpendicular to the magnetic field when the separation of the EsC lines at 25007.1 cm^{-1} and 25008.0 cm^{-1} did not change by more than 0.1 cm^{-1} for this range of angles. The splitting of these lines corresponds to the HsC splitting of the (0,3) level of the ground state, and changes of up to 0.1 cm^{-1} could be attributed to anisotropy in the HsC splitting of this level if the separations repeated every 60°. However due to the large HpC splitting of this level, changes of 0.2 cm^{-1} over this range of angles corresponded to a crystal misalignment of 1.9°. This was determined experimentally by photographing the spectrum of a crystal deliberately misaligned by 5°. For the experiments in which mixed crystals of dysprosium and erbium ethylsulfate were used, the HsC alignment check previously reported for erbium ethylsulfate was used because this was a more sensitive check. In this case the c axis was perpendicular to the field when the EpC lines of erbium ethylsulfate at 18466.7 cm^{-1} and 18455.5 cm^{-1} exhibited no splitting. These lines correspond to transitions from the (-1,-2) levels of the ground state to a (0,3) level in the excited state. According to the theory of the HsC Zeeman effect (69) it should not split if the field is precisely perpendicular to the c axis.

The alignment of all the crystals used in this work

were checked by the procedures described above and none had to be realigned. This was probably due to the extreme care in aligning the crystals on the polarizing microscope and optical goniometer prior to their insertion in the dewar.

Preparation and Measurement of Plates

The photographs of the spectra for this investigation were obtained on 4" by 10" glass spectroscopic plates, Eastman Kodak types 103aO and 103aF. They were developed for four minutes in Kodak D-19 developer, stopped in dilute acetic acid, and fixed in Kodak general purpose hardening fixer. The plates were dried by passing warm air over them.

Since the standard iron reference spectrum interfered with the observation of the absorption spectrum when the order sorter was used, the plates obtained with the order sorter were photographed and measured as described below. Alternate exposures of the spectrum of the hollow iron cathode and of the absorption spectrum were photographed at intervals down the plate. The plates were always carefully racked in the same direction from start to finish in order to eliminate any possibility of racking backlash within the spectrograph.

The plates were measured on a Jarrell-Ash model 23-500 recording microphotometer. They were carefully aligned so that the recording slit of the microphotometer tracked pre-

cisely in the order of interest. The precision microphotometer screw and the strip chart of the recorder were driven by synchronous motors at constant speeds of 1 mm/min and 127 mm/min, respectively. Thus 1 mm at the plate was expanded to 127 mm on the strip chart. A switching device activated by a pin on the crank of the precision microphotometer screw placed fiduciary marks on the chart at intervals corresponding exactly to each revolution of the screw. By measuring the distance between these marks it was possible to check the relative drive speeds of the screw and the strip chart.

The positions of the absorption lines and of the standard iron lines in the appropriate order were measured from the strip chart, and the vertical positions of the exposures were measured from a vernier scale on the microphotometer stage. The data for each plate were treated in a linear least squares calculation to find equations describing the horizontal positions of the iron lines versus the vertical plate position. The equations were then used to project the standard iron lines into the positions they would have occupied had the iron spectrum been superimposed upon the absorption spectrum. The plates were always racked vertically from the same direction in order to eliminate microphotometer backlash, and the racking of the precision screw for the horizontal position was carried out with the same caution.

The equations were found to fit the experimental positions to within ± 0.0055 mm on the average or, in the regions of special interest here, to within ± 0.002 Å. The small errors seemed to justify the use of the projected iron line positions as good position references for the measurement of the absorption lines.

Calibration of plates

The energies of the absorption lines in any order are not linearly related to their positions on the plate so it was necessary to obtain a calibration. The first step in the calibration was the identification of the standard iron lines in the order of interest. When there were too few standard lines in the same order as the absorption spectrum it was necessary to include lines from adjacent orders. The wavelengths of these lines were converted to wavelengths in the order of interest by the relation

$$\lambda' = n\lambda/n', \tag{62}$$

where n and n' are the order numbers of the order in which the line occurs and the order of interest, respectively, and λ and λ' are the wavelength in the order in which the line occurs and the wavelength in the order of interest. The wavelengths were then converted into wavenumbers in vacuum by means of the Bureau of Standards tables (100).

Two of the standard iron lines were chosen as end iron

lines for calculation of the dispersion. They were in the same order as the absorption spectrum and bracketed the region of absorption. The linear wavenumber dispersion was calculated from

$$D = (\sigma_2 - \sigma_1)/(p_2 - p_1), \tag{63}$$

where σ_1 and σ_2 are the wavenumbers in vacuum of the two end iron lines, and p_1 and p_2 are their respective millimeter positions at the plate. The approximate vacuum wavenumbers of the other iron lines were calculated by means of

$$\overline{\sigma}_i = \sigma_1 + (p_i - p_1)D. \tag{64}$$

Here i is a serial number to distinguish between the different iron lines. The differences between the wavenumbers calculated in this way and the true wavenumbers of the lines, σ_i, which had been found from the tables, were then used to determine a calibration curve of $\overline{\Delta}_i = (\sigma_i - \overline{\sigma}_i)$ versus $(\overline{\sigma}_i - \sigma_i)$. Figure 8 shows a typical calibration curve. The second order equation of the type

$$\overline{\Delta}_i = A(\overline{\sigma}_i - \sigma_1)^2 + B(\overline{\sigma}_i - \sigma_1) + C, \tag{65}$$

which best fit the experimental points in the least squares sense was found by solving the normal equations,

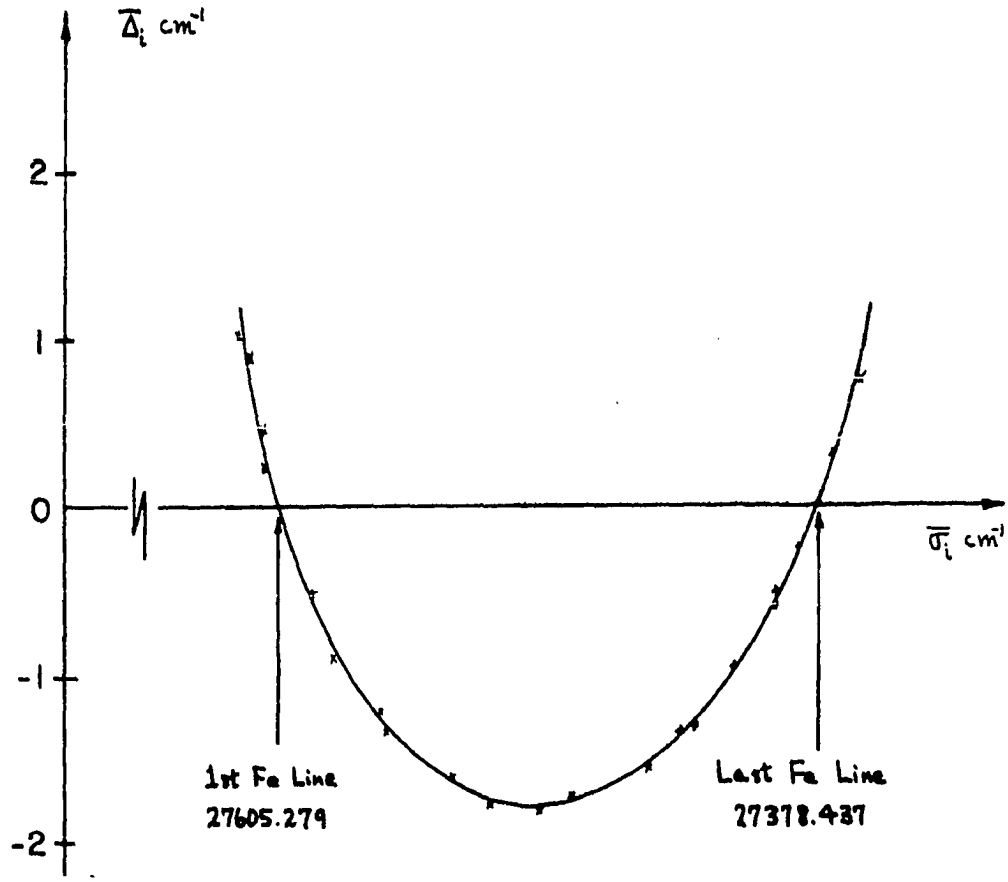

Figure 8. A typical calibration curve. The true wavenumber of every line is given by $\overline{\sigma}_i + \overline{\Delta}_i$

$$\begin{bmatrix} x_1^2 & x_2^2 & \cdots & x_n^2 \\ x_1 & x_2 & \cdots & x_n \\ 1 & 1 & \cdots & 1 \end{bmatrix} \begin{bmatrix} x_1^2 & x_1 & 1 \\ x_2^2 & x_2 & 1 \\ \cdot & \cdot & \cdot \\ \cdot & \cdot & \cdot \\ \cdot & \cdot & \cdot \\ x_n^2 & x_n & 1 \end{bmatrix} \begin{bmatrix} A \\ B \\ C \end{bmatrix}$$

$$= \begin{bmatrix} x_1^2 & x_2^2 & \cdots & x_n^2 \\ x_1 & x_2 & \cdots & x_n \\ 1 & 1 & \cdots & 1 \end{bmatrix} \begin{bmatrix} \overline{\Delta}_1 \\ \overline{\Delta}_2 \\ \cdot \\ \cdot \\ \cdot \\ \overline{\Delta}_n \end{bmatrix} \qquad (66)$$

for A, B, and C. For simplicity ($\overline{\sigma}_i - \sigma_1$) has been replaced in the above equations by x_i, and n is the total number of iron lines. The wavenumber of an unknown line was given by the sum of Equations 64 and 65.

In this work the second order approximation was found, by use in the measurement of many exposures of the standard hollow iron cathode spectrum, to yield results accurate to within $\pm$ 0.005 cm^{-1} in the thirteenth order, $\pm$ 0.006 cm^{-1} in the fourteenth, $\pm$ 0.004 cm^{-1} in the fifteenth, and $\pm$ 0.012 cm^{-1} in the sixteenth order. These were considered to be good results because the hollow iron cathode lines have been

estimated to be accurate to within ± 0.001 Å in general. In the thirteenth order ± 0.001 Å corresponds to ± 0.004 cm^{-1}, and in the sixteenth order the same wavelength error corresponds to ± 0.008 cm^{-1}. The errors in measuring and calculating by the second order calibration method were comparable to the errors in the energies of the standard iron lines. The method used here is believed to be superior to many methods described in the literature for grating plates because of its accuracy when the proper polynomial is used and its speed when the calculations are performed by an electronic computer. In addition it eliminates the need to first calculate wavelengths and then to convert these to wavenumbers in vacuum for every unknown line.

Calculation of vacuum wavenumbers for absorption lines

The determination of the energies of the absorption lines in vacuum wavenumbers proceeded as follows. The millimeter positions of the absorption lines were measured from the strip charts, and the positions of the first and last iron lines in the order of interest were calculated by means of the previously described projection method. The dispersion was calculated using Equation 63 and the projected positions of the iron lines, and approximate vacuum wavenumbers for the absorption lines were calculated using Equation 64. The measured energies of the absorption lines were given by the sum of the results of Equations 64 and 65.

Estimation of error arising from the measuring procedure

If one assumes that the only sources of error in the energies of the absorption lines arise from 1) not having the standard spectrum superimposed on the absorption spectrum when the order sorter was used, 2) error in the calculated correction curve, and 3) error in the estimation of line centers, then the probable error ranges from $\pm$ 0.013 cm^{-1} in the thirteenth order to $\pm$ 0.028 cm^{-1} in the sixteenth order. This estimate was obtained by adding the probable errors arising from 1) and 2), and by assuming that the errors in estimation of line centers were already included in the estimates given for 1) and 2). This assumption is not quite true, however, since it was usually easier to estimate the centers of the iron lines than it was to estimate the centers of absorption lines. Better estimates of the errors for the absorption lines will be obtained in a later section of this work.

EXPERIMENTAL RESULTS

Initial Survey and General Observations

The initial photographs of the spectrum were obtained with 0.5 mm and 1.0 mm dysprosium ethylsulfate crystals immersed in liquid hydrogen. These photographs were taken to find those line groups with sharp lines and closely spaced energy levels which would yield the best measurements of any basal plane anisotropy in the HsC Zeeman effect. Line groups I through S, as previously labelled by Crosswhite and Dieke (85), were observed in the second order with the 600 line/mm grating, and groups D through W were observed in orders seven through nineteen with the 300 line/mm grating and order sorter. Some examples of the HsC Zeeman spectra as observed in the second order are shown in Figures 9 through 11; examples of the higher order spectra will be given later. The absorption of groups D, E, J, L, N, and Q was quite strong, even in a 1.0 mm crystal, and one could not be sure that the lines were completely resolved. The absorption of groups E' and K was so weak and the lines were so diffuse that they were not observed in the high order spectrum. Groups G, I, M, O, P, R, and S had very sharp and intense absorption lines, and because of the short exposure times required for groups G and I, these two groups were thought to be the most suitable for studies of basal plane anisotropy in the HsC Zeeman effect.

Figure 9. HsC spectra of DyES group I -- 1.0 mm crystal at $20^{o}K$

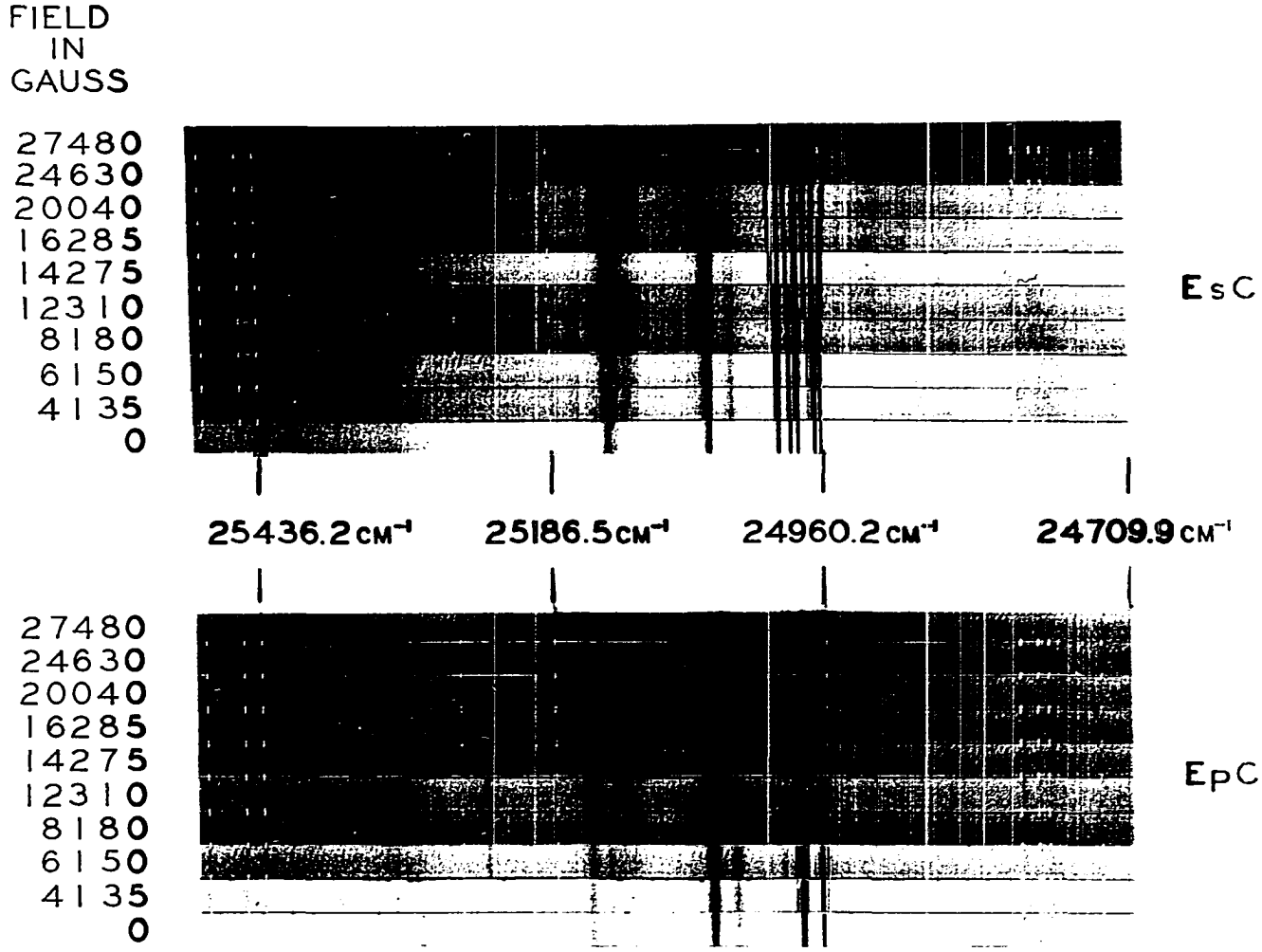
FIELD
IN
GAUSS
27480
24630
20040
16285
14275
12310
8180
6150
4135
0
EsC
25436.2 cm⁻¹
25186.5 cm⁻¹
24960.2 cm⁻¹
24709.9 cm⁻¹
27480
24630
20040
16285
14275
12310
8180
6150
4135
0
EpC

Figure 10. HsC spectra of DyES groups K and J -- 1.0 mm crystal at $20^{\circ}K$

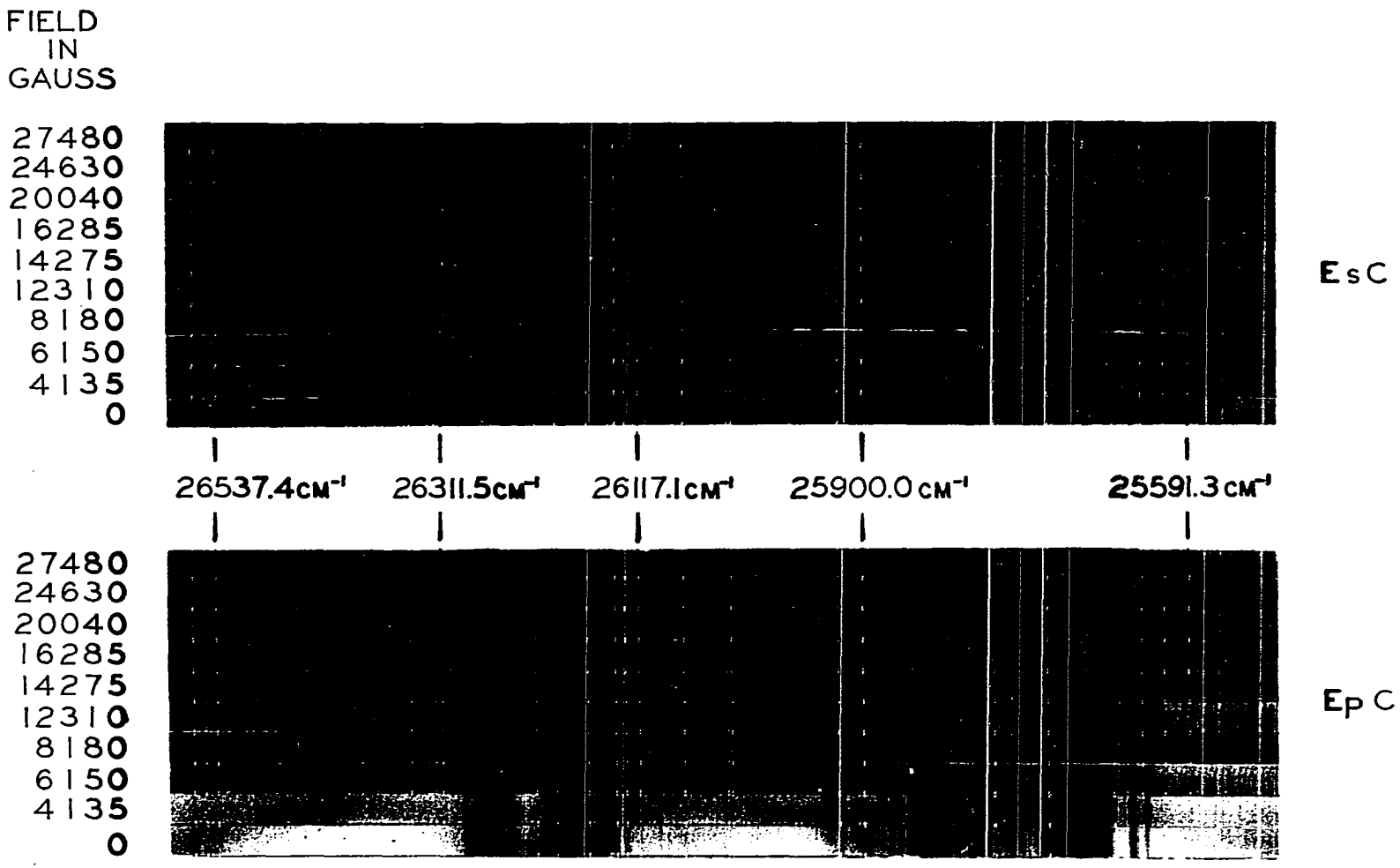
FIELD IN GAUSS
27480
24630
20040
16285
14275
12310
8180
6150
4135
0
E s C
26537.4cm⁻¹
26311.5cm⁻¹
26117.1cm⁻¹
25900.0 cm⁻¹
25591.3 cm⁻¹
27480
24630
20040
16285
14275
12310
8180
6150
4135
0
E p C

Figure 11. HsC spectra of DyES groups M and L -- 1.0 mm crystal at 20°K

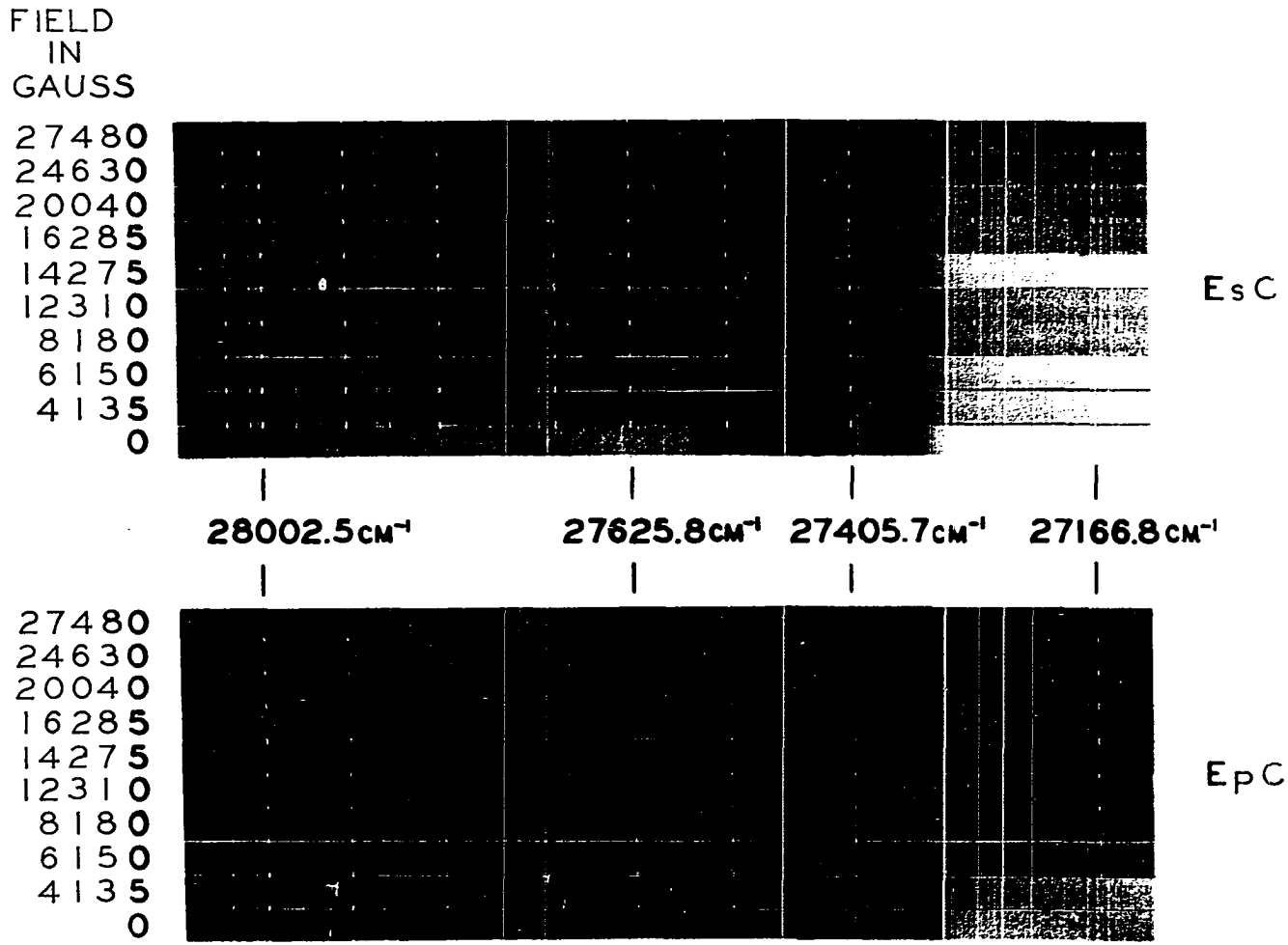
FIELD
IN
GAUSS
27480
24630
20040
16285
14275
12310
8180
6150
4135
0
EsC
28002.5cm⁻¹
27625.8cm⁻¹
27405.7cm⁻¹
27166.8cm⁻¹
27480
24630
20040
16285
14275
12310
8180
6150
4135
0
EpC

In the absence of an external magnetic field, and when a magnetic field was applied parallel to the c axis, most of the absorption lines observed in this work obeyed the selection rules for electric dipole transitions. For the lines of group G however, an appreciable contribution from magnetic dipole transitions was observed. This observation is in agreement with the earlier findings of Gramberg (84). For the case where the magnetic field was perpendicular to the c axis additional lines appeared with increasing magnetic field strength which seemed to obey the selection rules for magnetic dipole transitions. They were in fact electric dipole transitions, but were reflecting the fact that, since the matrix elements of the HsC Zeeman effect connect states with $\Delta\mu = \pm 1$, μ is not a good quantum number for this case. The observation of transitions which are forbidden in the absence of the perpendicular field gives added incentive for studying the HsC Zeeman effect because their observation must certainly lead to less chance of error in measuring the centers of gravity and in assigning term symbols for the various line groups.

Table 9 compares the approximate energies of the line groups of Dy^{+3} in DyES with the free ion energy levels of Dy^{+3} as calculated in the intermediate coupling scheme by Wybourne (81), and with some previously reported line group energies for Dy^{+3} in other salts. The values given for the infrared groups Y through W and A through E' of DyEs were

Table 9. Calculated free ion energy levels and observed line group energies for Dy^{+3} in various salts

Term symbol	Empirical label	Calculated free ion levels[a]	DyES	$DyCl_3$[b]	$DyCl_3 \cdot 6H_2O$[c]	$Dy_2(SO_4)_3 \cdot 8H_2O$[d]	$Dy(NO_3)_3 \cdot 6H_2O$[e]
$^6H_{15/2}$	Z	0	0	0	0		
$^6H_{13/2}$	Y	3457	3600	3517	3588		
$^6H_{11/2}$	X	5778	6000	5835	5857		
$^6H_{9/2}$	W	7613	7740	7650	7665		
$^6F_{11/2}$		7920					
$^6H_{7/2}$	A	9033	-	8987	8973		
$^6F_{9/2}$		9164	9025		9043		

[a]From Wybourne (81).

[b]From Crosswhite and Dieke (85).

[c]From Dieke and Singh (83).

[d]From Rosa (82).

[e]From Gramberg (84).

Table 9. (Continued)

Term symbol	Empirical label	Calculated free ion levels[a]	DyES	$DyCl_3$[b]	$DyCl_3 \cdot 6H_2O$[c]	$Dy_2(SO_4)_3 \cdot 8H_2O$[d]	$Dy(NO_3)_3 \cdot 6H_2O$[e]
$^6H_{5/2}$	B	10089	10171	10138	10157		
$^6F_{7/2}$	C	11130	11004	10925	11018	10939	
$^6F_{5/2}$	D	12550	12383	12323	12447	12358	
$^6F_{3/2}$	E	13299	13178	13116	13202	13182	
$^6F_{1/2}$	E'	13843	13729	-	-	-	
$^4F_{9/2}$	F	20216	21100	20963	21112	21049	21170
$^4I_{15/2}$	G	21427	22140	21954	22150	22117	22180
$^4G_{11/2}$	H	22442	23450	23303	23450	23420	23500
$^4M_{21/2}$	I	22734	25070	24940	25060		25120
$^4K_{17/2}$	J	23428	25730	25581	25770		25790
$^4M_{19/2}$	K	23903	26220	26098	26290		26340
$^4I_{13/2}$	L	24296	27420	27280			
$^4F_{7/2}$	M	24720	27920	27827			
$^4M_{15/2}$	N	26170	28520	28326			

Table 9. (Continued)

Term symbol	Empirical label	Calculated free ion levels[a]	DyES	$DyCl_3$[b]	$DyCl_3 \cdot 6H_2O$[c]	$Dy_2(SO_4)_3 \cdot 8H_2O$[d]	$Dy(NO_3)_3 \cdot 6H_2O$[e]
$^4I_{11/2}$	O	26224	29570	29480			
$^4P_{3/2}$	P	26529	29980	29867			
$^4M_{17/2}$	Q	27662	30690	30583			
$^4F_{5/2}$	R	27752	31125	30996			
$^4I_{9/2}$	S	27772	31560	31462			
$^4G_{9/2}$	T	28592	33110	32985			
$^4L_{19/2}$	U	28949	33400	33262			
$^6P_{5/2}$	V	29161	33530	33444			
$^4K_{15/2}$	W	29167	33920	33781			

obtained from the work of Sutherland (101) and Hellwege et al. (102), respectively. It can be seen from the table that the energies of the line groups are fairly similar in the various salts. However, the energies of the nitrate groups for which data are available are all about 200 cm^{-1} greater than those of the corresponding anhydrous chloride groups, and the energies of the hydrated chloride, sulfate, and ethylsulfate groups are about 100 cm^{-1} greater than those of the anhydrous chloride. In the rare earths the line groups are due to transitions between the energy levels of the $4f^n$ configuration and the 4f electrons are well shielded from their external environment by filled shells of 5p and 6s electrons. Therefore the observed line group energies for a rare earth ion in any salt are very near what would be observed for the free rare earth ion. The small changes in the energies which are observed in various salts are attributed to small changes in the covalency of the chemical bonds of the rare earth ion to its nearest neighbors (103). It has been suggested (104) that as the covalency of the bonding increases, the "tail" of the 4f electron radial distribution function is enlarged, and that this leads to a decrease in the electrostatic interaction between the 4f electrons which decreases the separation of the $4f^n$ energy levels. The expansion of the 4f electron charge cloud, known as the nephelauxetic effect, is thought to be a direct result of the

screening of the 4f electrons by overlapping charge clouds from the surrounding ligands.

The results given in Table 9 are in agreement with previous work on compounds of Pr^{+3} (105) which established that the energy of the line groups decreases and the covalency of the rare earth--ligand bonds increases in the order RF_3, $R^{+3}\cdot xH_2O$, RCl_3, RBr_3, R_2O_3, where R stands for one of the rare earths. However the data for $Dy(NO_3)\cdot 6H_2O$ suggest that the nearest neighbors of the Dy^{+3} ion in this case are not all waters of hydration, as is true for DyES, but that the nitrate ions must be making an appreciable contribution to coordination complex. The data thus tend to support the results of a recent determination of the crystal structure of $Pr(NO_3)_3\cdot 6H_2O$ by Rumanova et al. (106), in which it was proposed that the Pr^{+3} ion has a coordination of ten, with four waters of hydration and six nitrate oxygens in the coordination polyhedron.

It can also be seen from Table 9 that while the agreement of the observed and calculated energies and J values is good in the infrared the agreement deteriorates rapidly for the groups beyond 24000 cm^{-1}. For these groups no significance can be attached to the fact that a particular term symbol and calculated free ion energy level corresponding to that state appears opposite one of the observed line groups. It was therefore clear at the outset of this work that much more work, both theoretical and experimental, remained to be

done before a clear understanding of the higher energy levels could be obtained.

Basal Plane Anisotropy in the HsC Zeeman Effect

When the HsC Zeeman effects of groups D through P of DyES were observed as a function of the angle between the x axis of the crystal and a static external magnetic field of approximately 28 kG, variations with a 60° periodicity were observed for the energy and/or intensity of absorption lines in many of the line groups. Some examples of the observations are given in Figures 12 through 14. Of the line groups observed, only groups D, K, and N showed no dependence of the observed pattern on the angle between the x axis and the external magnetic field.

When the HsC Zeeman effects of groups G and I were examined in detail as a function of the angle between the a axis of the crystal and a static external magnetic field of approximately 28 kG, it was determined that the energy of each absorption line obeys a relation of the type

$$E_i(\phi_e) = E_{oi} + A_i \cos 6(\phi_e - \bar{\phi}) \qquad (67)$$

within experimental error. $E_i(\phi_e)$ is the measured energy of the i^{th} absorption line and is a function of the magnetic field strength and of ϕ_e, the angle between the a axis and the external magnetic field. E_{oi} is that part of the energy of the i^{th} absorption line which is dependent on the magnetic

Figure 12. HsC spectrum of DyES group G as a function of the angle between the magnetic field and the x axis of the crystal. This is a 1.89 mm crystal at 20°K and the magnetic field is 27488 G

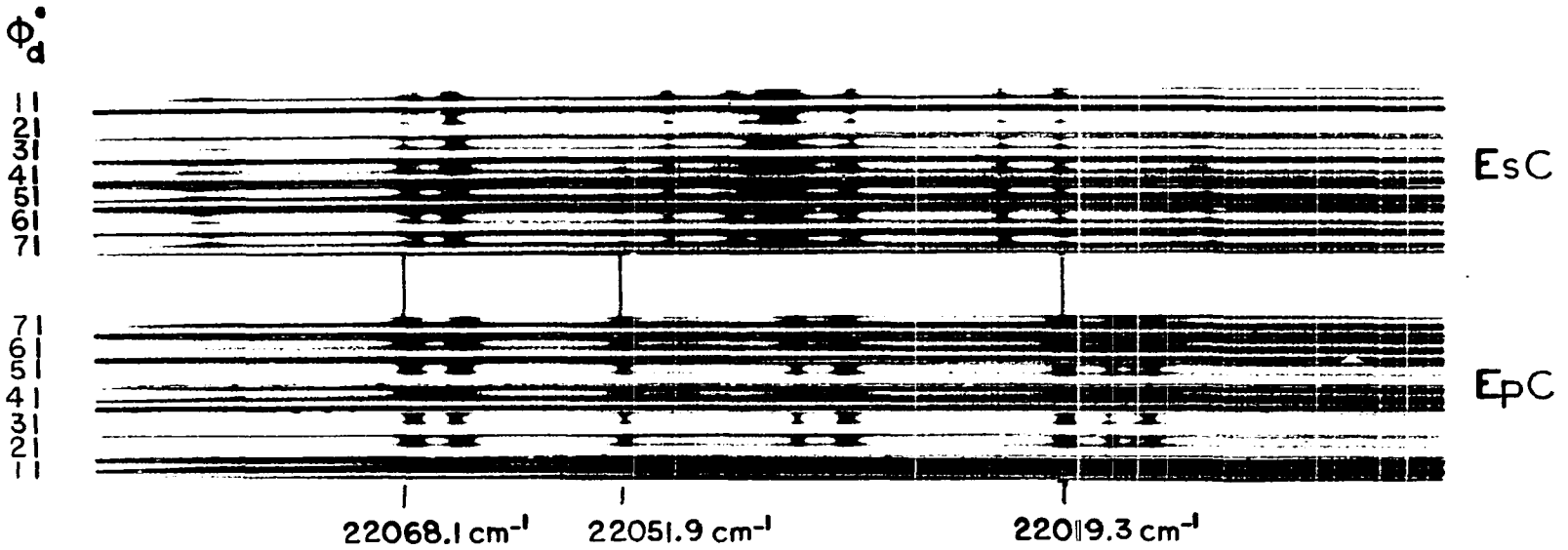

Figure 12. HsC spectrum of DyES group G as a function of the angle between the magnetic field and the x axis of the crystal. This is a 1.89 mm crystal at 20°K and the magnetic field is 27488 G

Figure 13. HsC spectrum of DyES group H as a function of the angle between the magnetic field and the x axis of the crystal. This is a 1.0 mm crystal at 20°K and the magnetic field is 27912 G

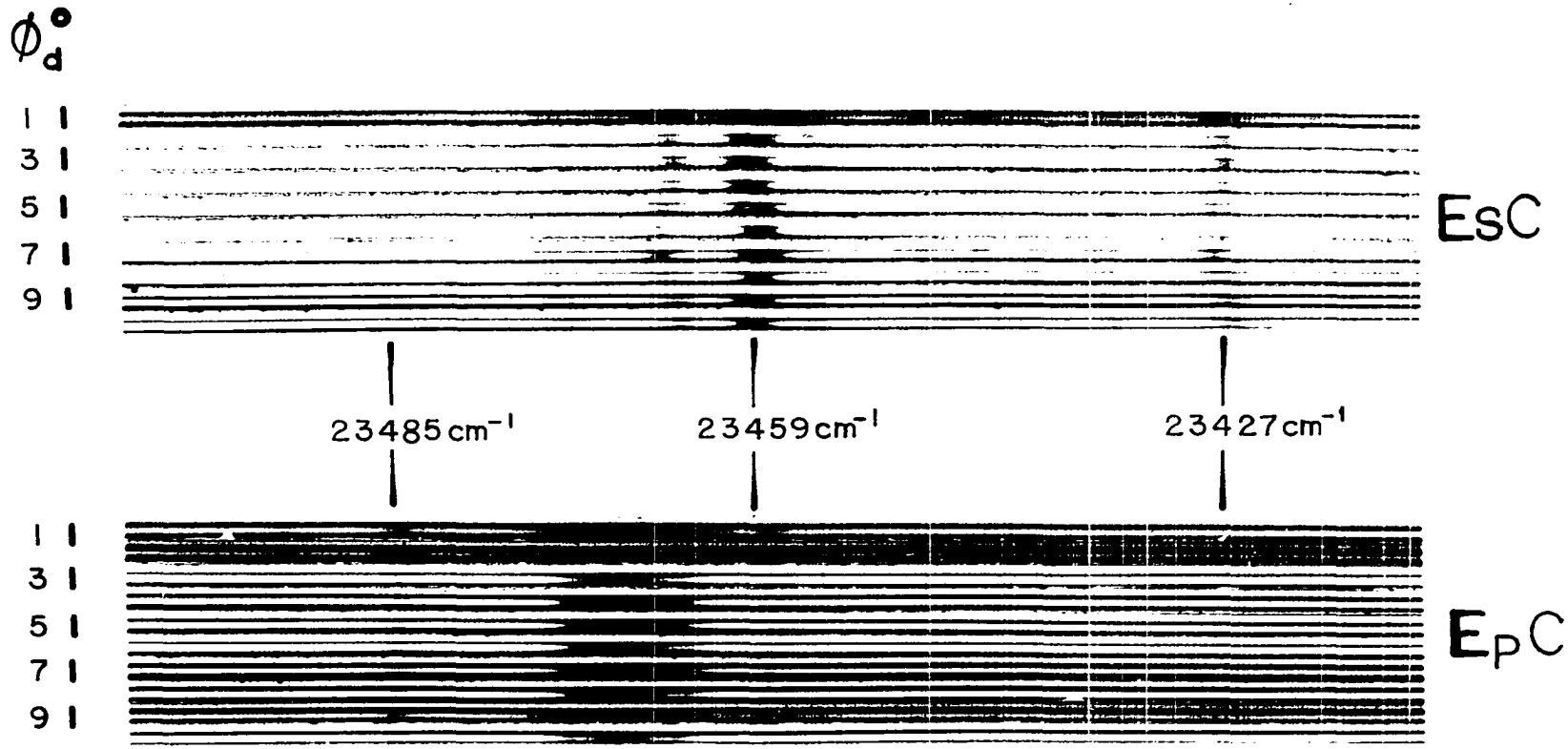
ϕ_d°
1
3
5
7
9
EsC
23485 cm⁻¹
23459 cm⁻¹
23427 cm⁻¹
1
3
5
7
9
EpC

Figure 14. HsC spectrum of DyES group I as a function of the angle between the magnetic field and the x axis of the crystal. This is a 1.0 mm crystal at 20°K and the magnetic field is 27475 G

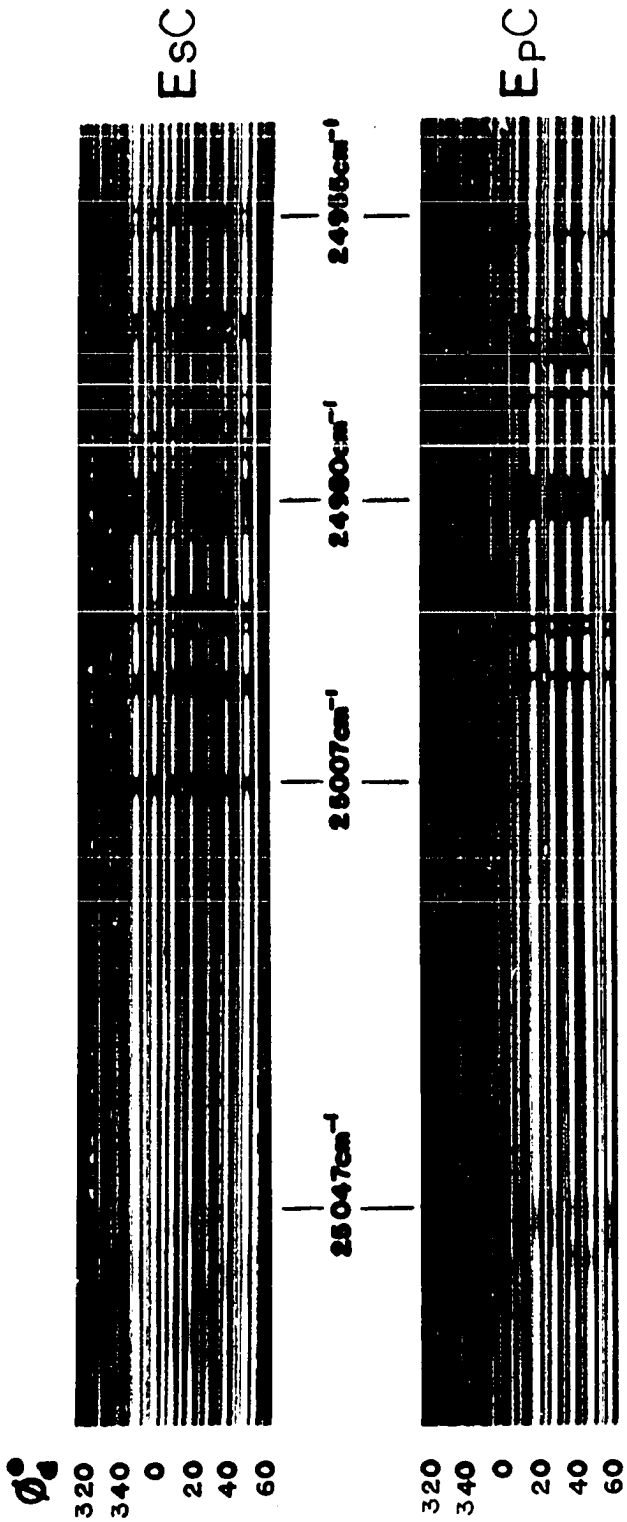
EsC
EpC
25047cm⁻¹
25007cm⁻¹
24980cm⁻¹
24918cm⁻¹
320
340
0
20
40
60

field strength, but which is independent of ϕ_e. A_i, the rotation coefficient for the i^{th} line, gives the amplitude of the variation in energy about E_{oi} which occurs when the crystal is rotated about its c axis in the HsC magnetic field. $\bar{\phi}$ has been defined previously as the angle between the a and x axes of the crystal.

In the preliminary analysis of the data an equation of the type 67 was found for each line by solving the least squares normal equations

$$\begin{bmatrix} \cos6\phi_{e1} & \cos6\phi_{e2} & \cdots & \cos6\phi_{en} \\ \sin6\phi_{e1} & \sin6\phi_{e2} & \cdots & \sin6\phi_{en} \\ 1 & 1 & \cdots & 1 \end{bmatrix} \begin{bmatrix} \cos6\phi_{e1} & \sin6\phi_{e1} & 1 \\ \cos6\phi_{e2} & \sin6\phi_{e2} & 1 \\ \cdot & \cdot & \cdot \\ \cdot & \cdot & \cdot \\ \cos6\phi_{en} & \sin6\phi_{en} & 1 \end{bmatrix} \begin{bmatrix} A \\ B \\ E_o \end{bmatrix}$$

$$= \begin{bmatrix} \cos6\phi_{e1} & \cos6\phi_{e2} & \cdots & \cos6\phi_{en} \\ \sin6\phi_{e1} & \sin6\phi_{e2} & \cdots & \sin6\phi_{en} \\ 1 & 1 & \cdots & 1 \end{bmatrix} \begin{bmatrix} E_i(\phi_{e1}) \\ E_i(\phi_{e2}) \\ \cdot \\ \cdot \\ E_i(\phi_{en}) \end{bmatrix} \qquad (68)$$

for A, B, and E_o. Here n is the number of distinct angle settings, A is equal to $A_i\cos6\bar{\phi}$, and B is equal to $A_i\sin6\bar{\phi}$. A_i is therefore given by

$$A_i = A/\cos6\bar{\phi}, \qquad (69)$$

where

$$6\bar{\phi} = \arctan(B/A). \tag{70}$$

Examples of the results obtained for E_{oi} and A_i are given in Tables 10 and 11.

The Roman numerals used to identify the initial state for each absorption line are the numbers previously assigned by Gramberg to identify the three lowest lying crystal field levels of the ground term, and the μ quantum numbers used to identify the final states are the crystal quantum numbers of Murao, Spedding, and Good. See Table 4. The plus and minus signs are used to identify the higher and lower energy Zeeman level of each of the crystal field states, and the primes serve to distinguish between crystal field states with identical crystal quantum numbers.

The column headed by σ_i in the tables is defined by

$$\sigma_i = \left[\frac{\sum_{i=1}^{n} (E_{icalc} - E_{iobs})^2}{n - 1} \right]^{1/2} . \tag{71}$$

It indicates the goodness of fit of the type 67 equations to the observed energies of the lines in wavenumbers. Here the E_{icalc} are obtained from the i^{th} Equation 67 for the n values of ϕ_e, and the E_{iobs} are the corresponding observed energies of the i^{th} absorption line.

The phase angle $\bar{\phi}$, which according to the theory of (69) should be a measure of the angle between the a and x

Table 10. Angular dependence of DyES group G absorption lines for 1.89 mm crystal at 20°K

Transition	E_o in cm^{-1}	A in cm^{-1}	Polarization	σ_i
	$22162.58 \pm .12$	$.37 \pm .17$	P	$\pm .33$
	$22157.61 \pm .04$	$.14 \pm .05$	P	$\pm .13$
	$22141.11 \pm .02$	$.07 \pm .02$	P	$\pm .06$
	$22132.82 \pm .13$	$.30 \pm .18$	P	$\pm .36$
	$22122.11 \pm .08$	$.22 \pm .11$	S	$\pm .28$
	$22121.87 \pm .03$	$.04 \pm .04$	P	$\pm .10$
	$22107.93 \pm .02$	$.05 \pm .03$	P	$\pm .06$
	$22107.87 \pm .01$	$.02 \pm .01$	S	$\pm .03$
I_- to $-1,-2_+$	$22068.08 \pm .03$	$.03 \pm .04$	S	$\pm .09$
I_+ to $-1,-2_+$	$22067.27 \pm .03$	$-.05 \pm .04$	S	$\pm .09$
I_- to $-1,-2_-$	$22064.52 \pm .01$	$.04 \pm .01$	S	$\pm .03$
I_+ to $-1,-2_-$	$22063.68 \pm .03$	$.07 \pm .04$	S	$\pm .08$
II_- to $-1,-2_+$	$22051.88 \pm .01$	$.04 \pm .02$	P	$\pm .04$
II_- to $-1,-2_-$	$22048.27 \pm .01$	$.02 \pm .02$	S	$\pm .04$

Table 10. (Continued)

Transition	E_o in cm^{-1}	A in cm^{-1}	Polarization	σ_i
II_+ to -1,-2_+	22043.98±.05	-.51±.08	S	±.16
III_- to -1,-2_+	22042.56±.02	.60±.03	S	±.06
I_- to -1,$-2'_+$	22039.89±.01	.01±.03	S	±.02
I_+ to -1,$-2'_+$	22038.98±.00+	-.02±.01	P	±.02
I_- to -1,$-2'_-$	22035.57±.00+	.04±.00+	P	±.01
I_+ to -1,$-2'_-$	22034.70±.01	.05±.02	S	±.05
II_- to -1,$-2'_+$	22023.62±.01	.02±.01	S	±.02
II_- to -1,$-2'_-$	22019.32±.01	.03±.01	S	±.02
II_+ to -1,$-2'_+$	22015.84±.02	-.38±.03	P	±.08
III_- to -1,$-2'_+$	22014.31±.03	.48±.04	P	±.10
III_+ to -1,$-2'_+$	22012.94±.01	-.21±.01	P	±.02
II_+ to -1,$-2'_-$	22011.59±.04	-.47±.06	P	±.12
III_- to -1,$-2'_-$	22010.05±.03	.62±.03	S	±.06
III_+ to -1,$-2'_-$	22008.62±.05	-.27±.07	S	±.16

Table 11. Angular dependence of DyES group I absorption lines for 2.1 mm crystal at 20°K

Transition	E_o in cm^{-1}	A in cm^{-1}	Polarization	σ_i
I_- to $-1,-2_+$	$25008.02 \pm .01$	$-.03 \pm .01$	S	$\pm .03$
I_+ to $-1,-2_+$	$25007.17 \pm .00+$	$.04 \pm .00+$	S	$\pm .01$
I_- to $-1,-2_-$	$24997.87 \pm .01+$	$-.09 \pm .01$	S	$\pm .02$
I_+ to $-1,-2_-$	$24997.03 \pm .00+$	$-.04 \pm .00+$	P	$\pm .01$
I_- to $1,2_+$	$24992.96 \pm .01$	$.27 \pm .01$	P	$\pm .03$
I_+ to $1,2_+$	$24992.10 \pm .01$	$.35 \pm .01$	S	$\pm .04$
II_- to $-1,-2_+$	$24991.69 \pm .01$	$-.03 \pm .02$	P	$\pm .04$
I_- to $1,2_-$	$24991.04 \pm .01$	$-.33 \pm .01$	S	$\pm .03$
I_+ to $1,2_-$	$24990.17 \pm .01$	$-.24 \pm .01$	S	$\pm .03$
II_+ to $-1,-2_+$	$24983.76 \pm .02$	$.42 \pm .02$	S	$\pm .07$
III_- to $-1,-2_+$	$24982.27 \pm .03$	$-.55 \pm .05$	S	$\pm .06$
II_+ to $-1,-2_+$ I_- to $0,3_+$	$24981.00 \pm .00+$	$.15 \pm .00+$	P	$\pm .01$

Table 11. (Continued)

Transition	E_o in cm^{-1}	A in cm^{-1}	Polarization	σ_i
I_+ to $0,3_-$	$24980.93 \pm .01$	$.20 \pm .02$	S	$\pm .05$
I_+ to $0,3_+$	$24980.14 \pm .02$	$.08 \pm .02$	S	$\pm .07$
I_- to $0,3_-$	$24980.01 \pm .01$	$-.12 \pm .01$	S	$\pm .04$
I_+ to $0,3_-$	$24979.17 \pm .00+$	$-.11 \pm .01$	P	$\pm .02$
II_- to $1,2_+$	$24976.62 \pm .01$	$.26 \pm .01$	S	$\pm .04$
II_- to $1,2_-$	$24974.69 \pm .01$	$-.33 \pm .01$	S	$\pm .03$
III_- to $-1,-2_-$	$24972.16 \pm .02$	$-.64 \pm .04$	S	$\pm .10$
III_+ to $-1,-2_-$	$24970.73 \pm .01$	$+.14 \pm .01$	P	$\pm .04$
III_+ to $-1,-2_-$	$24970.75 \pm .02$	$+.18 \pm .02$	S	$\pm .06$
III_- to $1,2_+$	$24967.21 \pm .01$	$-.31 \pm .01$	P	$\pm .03$
II_+ to $1,2_-$	$24966.86 \pm .01$	$.14 \pm .02$	P	$\pm .06$
III_+ to $1,2_+$	$24965.82 \pm .02$	$.53 \pm .03$	S	$\pm .07$
II_- to $0,3_+$	$24964.64 \pm .02$	$.10 \pm .04$	S	$\pm .08$

Table 11. (Continued)

Transition	E_o in cm^{-1}	A in cm^{-1}	Polarization	σ_i
II_- to $0,3_+$	24964.66±.01	.14±.01	P	±.04
II_- to $0,3_-$	24963.84±.02	-.15±.03	P	±.07
II_- to $0,3_-$	24963.68±.00+	-.18±.01	S	±.02
I_+ to $0,3_-$	24979.19±.01	-.14±.01	S	±.03

axes of the crystals, was found to be the same within experimental error for all observed lines. It has therefore not been tabulated. The fact that $\bar{\phi}$ was the same for all lines in each crystal means that, within experimental error, every line attained either its maximum or minimum energy when an x axis was parallel to the magnetic field. This finding is in agreement with the theoretical findings of (73). Further discussion of the determination of $\bar{\phi}$ for the various crystals studied in this work will be presented in a later section.

The standard deviations associated with the quantities given in the tables were derived from the variance-covariance matrix for each set of Equations 68 by the ordinary methods for studies of the propagation of error (107). In the present case the variance-covariance matrix is the inverse of the product of the first two matrices on the left hand side of Equation 68. According to the theory of propagation of error, if

$$f = f(A, B, E_o), \tag{72}$$

then the standard deviation for determination of f from values of A, B, and E_o is given by

$$S_f = \left[\begin{array}{l} \left(\frac{\partial f}{\partial A}\right)^2 \sigma_A^2 + \left(\frac{\partial f}{\partial B}\right)^2 \sigma_B^2 + \left(\frac{\partial f}{\partial E_o}\right)^2 \sigma_{E_o}^2 \\ + \left(\frac{\partial f}{\partial A}\right)\left(\frac{\partial f}{\partial B}\right) \sigma_{AB} + \left(\frac{\partial f}{\partial A}\right)\left(\frac{\partial f}{\partial E_o}\right) \sigma_{AE_o} + \left(\frac{\partial f}{\partial B}\right)\left(\frac{\partial f}{\partial E_o}\right) \sigma_{BE_o} \end{array} \right]^{1/2} \tag{73}$$

Here σ_i is the standard deviation of the measurements from which A, B, and E_o were determined, and the quantities σ_A^2, σ_B^2, etc., are defined by

$$\begin{aligned} \sigma_A^2 &= \sigma_i^2 C(1,1) \\ \sigma_B^2 &= \sigma_i^2 C(2,2) \\ \sigma_{E_o}^2 &= \sigma_i^2 C(3,3) \end{aligned} \tag{74}$$

and

$$\sigma_{AB} = \sigma_i^2 C(1,2)$$

The C(I,J) are the elements of the variance-covariance matrix. Application of Equations 73 and 74 to Equations 67, 69, and 70 gives the expressions used to calculate the standard deviations of the derived quantities, E_o, A_i, and $\bar{\phi}$:

$$S_{E_{oi}} = \sigma_i \sqrt{C(3,3)} \tag{75}$$

$$S_A = (\sigma_i / |A_i|) \sqrt{A_i^2 C(1,1) + B^2 C(2,2) + 2AB\,C(1,2)} \tag{76}$$

$$S_{\bar{\phi}} = (\sigma_i / 6A_i^2) \sqrt{B^2 C(1,1) + A^2 C(2,2) - 2AB\,C(1,2)} \tag{77}$$

It should be noted that the error in determination of the rotation coefficient A_i is inversely proportional to $|A_i|$, and that the error in determination of $\bar{\phi}$ is inversely proportional to A_i^2. Thus, as we might expect, the best determina-

tions of rotation coefficients, and of the angle between the a and x axes, are obtained from absorption lines with large rotation coefficients.

Energy level scheme for the anisotropic HsC Zeeman effect

The next step in the analysis of the basal plane anisotropy in the HsC Zeeman effect was the determination of an energy level scheme such that the energy differences between the various energy levels would have the same angular dependence as the observed absorption lines. In general the determination of the energy line scheme is complicated for DyES because the energy levels of both the initial and final states in each transition may depend upon the direction of the magnetic field with respect to the x axis. When this is the case the energy of each of the absorption lines as a function of ϕ_e is given by

$$E_{\substack{\text{absorption}\\\text{line}}}(\phi_e) = E_{\substack{\text{final}\\\text{level}}}(\phi_e) - E_{\substack{\text{initial}\\\text{level}}}(\phi_e). \qquad (78)$$

The quantities on the left hand side are obtained directly from the experiment, and what are needed for the energy level diagram are the quantities on the right, the energies of the initial and final levels as functions of ϕ_e.

We know from (69) and (73) that the variations in the energies of the levels all have the same phase and 60° peridicity, so the energies of the levels should be given by the

same type of equation as that used for the energies of the absorption lines. Thus we can substitute the right hand sides of equations like Equation 67 for $E_{\substack{\text{final}\\\text{level}}}(\phi_e)$ and $E_{\substack{\text{initial}\\\text{level}}}(\phi_e)$ in Equation 73 to obtain

$$E_{\substack{\text{absorption}\\\text{line}}}(\phi_e) = (E_{o\ \substack{\text{final}\\\text{level}}} - E_{o\ \substack{\text{initial}\\\text{level}}}) + (A_{\substack{\text{final}\\\text{level}}} - A_{\substack{\text{initial}\\\text{level}}})\cos 6(\phi_e - \bar{\phi}) \ . \quad (79)$$

Equating coefficients of $\cos 6(\phi_e - \bar{\phi})$ in Equations 67 and 79 gives

$$E_{o\ \substack{\text{absorption}\\\text{line}}} = E_{o\ \substack{\text{final}\\\text{level}}} - E_{o\ \substack{\text{initial}\\\text{level}}} \ , \quad (80)$$

and

$$A_{\substack{\text{absorption}\\\text{line}}} = A_{\substack{\text{final}\\\text{level}}} - A_{\substack{\text{initial}\\\text{level}}} \ . \quad (81)$$

For each pair of initial and final energy levels the E_o's and A's on the left hand sides are known from the experiment, and to construct the energy level diagram we have to solve for the E_o's and A's on the right. However, since only energy differences are observed in the experiment, not absolute energies, these equations have no unique solution unless additional conditions are imposed.

Any additional conditions which provide a reference point for the measurement of energy and energy variations will allow

a unique solution for the E_o's and A's of the energy levels. For example, if one can observe absorption lines resulting from transitions from ground term Zeeman levels to a group of excited state levels whose center of gravity is not affected by the magnitude or direction of the applied HsC magnetic field, a good choice of extra conditions would be to take the center of gravity of the group of levels at zero magnetic field as the reference for energy measurements, and to restrict the solution for the A's such that the sum of the A's of all of the excited state levels in the group is equal to zero. This is a very useful condition because it allows determination of the shifts of the levels with respect to their zero magnetic field positions, and because it gives the rotation coefficients of the levels with respect to the center of gravity of the configuration. This makes it easy to compare them with the results of theoretical calculations.

The difficulty with using this choice of side conditions is that large amounts of experimental data are required to determine that the center of gravity of any group of excited state energy levels is independent of the direction and magnitude of the external magnetic field. The difficulty can be circumvented, however, if, proceeding under the assumption that the side conditions outlined in the previous paragraph are fulfilled for two or more relatively isolated groups of excited state levels, one obtains identical results for the

E_o's and A's of the ground levels. This is true because deviations from the assumed conditions would be reflected in the results obtained for the ground levels, and because it is unlikely that two or more relatively isolated groups of excited levels would have exactly the same dependence upon the direction or magnitude of the external magnetic field.

In the present work the simultaneous Equations 80 and 81 were solved for the absorption lines between 22005 and 22070 cm^{-1} in group G, and for the lines between 24950 and 25010 cm^{-1} in group I, under the assumption that the center of gravity of the group of final levels in each case was independent of the direction and magnitude of the external magnetic field. The lines treated for group G result from transitions from the Zeeman levels of the three lowest lying crystal field states of the ground term to the Zeeman levels of the (-1,-2) and (-1,-2)' crystal field states of the excited term. These levels of the excited term are separated by approximately 27 cm^{-1} at zero magnetic field, and the next nearest level is some 44 cm^{-1} away, so the assumption is certainly expected to be fulfilled. The lines treated in Group I result from transitions from the same levels in the group term to the Zeeman levels of (0,3), (1,2), and (-1,-2) levels in the excited term. These levels occur within the space of only 14 cm^{-1} at zero magnetic field and the next nearest level is 59 cm^{-1} away, so again the assumption is

expected to be fulfilled.

The results obtained for the E_o's and A's which describe the energy variations of the ground term levels are given in Tables 12 and 13. Apart from the second order shifts which are expected from the difference in the strength of the external magnetic field, the results obtained from groups G and I are within experimental error. The conclusion is that the centers of gravity of both groups of excited levels are independent of the direction and magnitude of the external magnetic field as was assumed, and that in both cases the correct E_o's and A's were obtained for the ground levels. The results obtained for the levels of groups G and I are given in Tables 14 and 15.

Table 12. HsC anisotropy of the low lying levels of the ground term of DyES as determined from group G H = 27488 G

Level	E_o	A
I_-	$-3.14\pm.02$	$+.03\pm.02$
I_+	$-2.28\pm.02$	$+.01\pm.02$
II_-	$13.11\pm.02$	$+.03\pm.02$
II_+	$20.91\pm.02$	$-.45\pm.03$
III_-	$22.40\pm.02$	$+.57\pm.03$
III_+	$23.81\pm.03$	$-.24\pm.04$

Table 13. HsC anisotropy of the low lying levels of the ground term of DyES as determined from group I
H = 27912 G

Level	E_o	A
I_-	$-3.26\pm.01$	$+.03\pm.01$
I_+	$-2.41\pm.01$	$-.01\pm.01$
II_-	$13.07\pm.01$	$+.04\pm.01$
II_+	$20.95\pm.01$	$-.41\pm.02$
III_-	$22.47\pm.01$	$+.59\pm.02$
III_+	$23.88\pm.01$	$-.22\pm.02$

Table 14. Observed HsC anisotropy of low lying (-1,-2) levels of DyES group G
H = 27488 G

Level	E_o	A
$(-1,-2)_+$	$22064.96\pm.02$	$.02\pm.02$
$(-1,-2)_-$	$22061.39\pm.02$	$-.02\pm.03$
$(-1,-2)'_+$	$22036.73\pm.01$	$.01\pm.02$
$(-1,-2)'_-$	$22032.44\pm.01$	$-.01\pm.02$

Table 15. Observed HsC anisotropy of some low lying levels of DyES group I
H = 27912 G

Level	E_o	A
$(-1,-2)_+$	$25004.75\pm.01$	$.02\pm.01$
$(-1,-2)_-$	$24994.62\pm.01$	$-.05\pm.02$
$(1,2)_+$	$24989.69\pm.01$	$.31\pm.01$
$(1,2)_-$	$24987.78\pm.01$	$-.28\pm.02$
$(0,3)_+$	$24977.72\pm.01$	$.13\pm.02$
$(0,3)_-$	$24976.76\pm.01$	$-.12\pm.01$

The angular dependence of the Zeeman splitting of any pair of levels can be obtained from the quantities given in the tables by using Equation 82, and the center of gravity of any two levels can be obtained by using Equation 83.

$$S_{i-j}(\phi_m) = (E_{oi} - E_{oj}) + (A_i - A_j)\cos 6\phi_m \qquad (82)$$

$$C_{i-j}(\phi_m) = 1/2(E_{oj} + E_{oj}) + 1/2(A_i + A_j)\cos 6\phi_m \qquad (83)$$

Here $\phi_m = \phi_e - \overline{\phi}$ is the angle between the x axis and the external magnetic field, and i and j are labels to distinguish between the higher and lower energy levels of the pair. For example, the splitting and center of gravity of the II_+

and II_- levels of the ground term are given by

$$S_{II_+} - {}_{II_-}(\phi_m) = (E_{oII_+} - E_{oII_-}) + (A_{II_+} - A_{II_-})\cos 6\phi_m \tag{84}$$

$$C_{II_+} - {}_{II_-}(\phi_m) = 1/2(E_{oII_+} - E_{oII_-}) + 1/2(A_{II_+} + A_{II_-})\cos 6\phi_m. \tag{85}$$

A comparison of the observed E_o's and A's of the absorption lines and those calculated from the E_o's and A's obtained for the energy levels is given in Tables 16 and 17. The agreement is quite good considering that in group G there were 20 absorption lines involving transitions between only 6 initial and 4 final energy levels, and that in group I there were 26 absorption lines involving transitions between only 6 initial and 6 final energy levels. The standard deviation between the observed and calculated E_o's and A's of the absorption lines in group G was $\pm$ 0.037 cm^{-1} and $\pm$ 0.054 cm^{-1}, respectively, and for the lines of group I $\pm$ 0.019 cm^{-1} and $\pm$ 0.031 cm^{-1}, respectively.

Another useful choice of side conditions for the solution of the simultaneous equations is to require E_o and A for the lowest Zeeman level of the ground term to be zero for all values of the external magnetic field. This choice makes it especially easy to determine the E_o's and A's of the excited term Zeeman levels by merely watching transitions

Table 16. Comparison of observed E_o's and A's for group G absorption lines with values calculated from the energy level scheme

Observed		Calculated	
E_o	A	E_o	A
22068.08	-.03	22068.09	-.01
22067.27	+.05	22067.23	-.00
22064.52	-.04	22064.52	-.05
22063.68	-.07	22063.66	-.03
22051.88	-.04	22051.85	-.01
22048.27	-.02	22048.28	-.05
22043.98	+.51	22044.05	+.46
22042.56	-.60	22042.55	-.56
22039.89	-.01	22039.87	-.02
22038.98	+.02	22039.01	-.00
22035.57	-.04	22035.58	-.04
22034.70	-.05	22034.72	-.02
22023.62	-.02	22023.62	-.02
22019.32	-.03	22019.34	-.03
22015.84	+.38	22015.82	+.46
22014.31	-.48	22014.33	-.56
22012.94	+.21	22012.92	+.25
22011.59	+.47	22011.54	+.44
22010.05	-.62	22010.04	-.58
22008.62	+.27	22008.63	+.23

Table 17. Comparison of observed E_o's and A's for group I absorption lines with values calculated from the energy level scheme

Observed		Calculated	
E_o	A	E_o	A
25008.02	-.03	25008.01	-.02
25007.17	.04	25007.16	.03
24997.87	-.09	24997.88	-.09
24997.03	-.04	24997.03	-.04
24992.96	.27	24992.95	.27
24992.10	.35	24992.10	.32
24991.69	-.03	24991.67	-.02
24991.04	-.33	24991.04	-.31
24990.17	-.24	24990.19	-.27
24983.76	.42	24983.79	.43
24982.27	-.55	24982.27	-.57
24980.14	.08	24980.14	.14
24980.01	-.12	24980.02	-.16
24979.17	-.11	24979.17	-.12
24976.62	.26	24976.62	.27
24974.69	-.33	24974.70	-.31
24972.16	-.64	24972.14	-.64
24970.73	.14	24970.74	.16
24970.75	.18	24970.74	.16
24967.21	-.31	24967.22	-.28
24966.86	.14	24966.82	.13
24965.82	.53	24965.81	.52
24964.64	.10	24964.65	.09
24964.66	.14	24964.65	.09
24963.68	-.18	24963.68	-.16
24979.19	-.14	24979.17	-.12

from the lowest ground term level to any of the excited term levels. This is because, as can be seen from Equations 80 and 81 with E_o and A for the initial level taken to be zero, the E_o's and A's of the excited term levels are simply equal to the measured E_o's and A's of the absorption lines. This choice of side conditions also has the advantage that nothing at all needs to be known or assumed concerning the behavior of the center of gravity of the excited term. One may proceed immediately with the analysis of the data, and if it is later demonstrated that some group of excited levels is independent of the direction and magnitude of the magnetic field, it is then a simple matter to transform from this set of side conditions to the set described earlier. The disadvantage of this choice of side conditions is that the shifts and rotation coefficients which are obtained are not in the most useful form for comparison with theoretical results.

The method of solving simultaneous equations for the E_o's and A's of the energy levels, no matter what the choice of side conditions, has the disadvantage that, while it is assumed that the variations in the energies of the levels all have the same phase and 60^o periodicity, because of experimental error the equations used to describe the energy variations of the adsorption lines do not all have the same phase. Thus when the E_o's and A's of the absorption lines are taken from tables like Tables 10 and 11, and used in the

solution of the simultaneous equation, phase errors are introduced. It is felt that errors are small however, because the absorption lines whose phases deviate most from the average are those with very small energy variations. The experimental error in determination of the phase angle for these lines therefore makes only a very small error in both the E_o's and A's of the lines, and those of the energy levels.

This conclusion was checked by determining the variations of the ground term energy levels and their phases by another method. In this method the energies of absorption lines due to X to Y transitions were subtracted from the energies of lines due to I_- to Y transitions, and these energy differences and their respective angles for the orientation of the magnetic field were used to determine the type 67 equation which gave the best least squares fit of the data. Here I_- is the lowest Zeeman level of the ground term, X is I_+, II_-, II_+, III_-, or III_+, any one of the higher energy ground levels, and Y is any Zeeman level of the excited term. Equation 78 tells us that the energies of these two types of absorption lines are given by

$$E_{\substack{I \text{ to } Y \\ \text{lines}}}(\phi_e) = E_{Y \text{ level}}(\phi_e) - E_{I_- \text{ level}}(\phi_e), \qquad (86)$$

and

$$E_{\substack{X \text{ to } Y \\ \text{lines}}}(\phi_e) = E_{Y \text{ level}}(\phi_e) - E_{X \text{ level}}(\phi_e), \qquad (87)$$

so the difference in their energies is

$$E_{\substack{I_- \text{ to } Y \\ \text{lines}}}(\phi_e) - E_{\substack{X \text{ to } Y \\ \text{lines}}}(\phi_e)$$

$$= E_{X \text{ level}}(\phi_e) - E_{I_- \text{ level}}(\phi_e). \qquad (88)$$

There is no dependence on the final level so when these energy differences were fit for $X = I_+$, for example, with $Y = (-1,-2)_+$, $(-1,-2)_-$, $(-1,-2)'_+$, and $(-1,-2)'_-$, an equation was obtained which describes the angular variation of the I_+ level and its phase with respect to the energy of the I_- level. The angular variations of the other ground term levels and their phases were obtained in a similar manner. The results are illustrated in Figure 15, and the E_o's and A's for the energy variations of the ground term levels are given in Table 18.

As can be seen by comparison of the results presented in this table and those in Table 19, which were obtained by solution of the simultaneous equations with side conditions $E_{I_-} = 0$ and $A_{I_-} = 0$, the difference method yields more precise results for the E_o's and A's of the ground levels. This is due to the fact that in general several examples of each energy difference are observed for each orientation of the

Figure 15. HsC anisotropy of low lying DyES ground term levels at H = 27488 G. The experimental points were derived by the difference method from the absorption lines of group G between 22005 cm^{-1} and 22070 cm^{-1}, and the smooth curves are the best least squares fits with sixfold periodicity

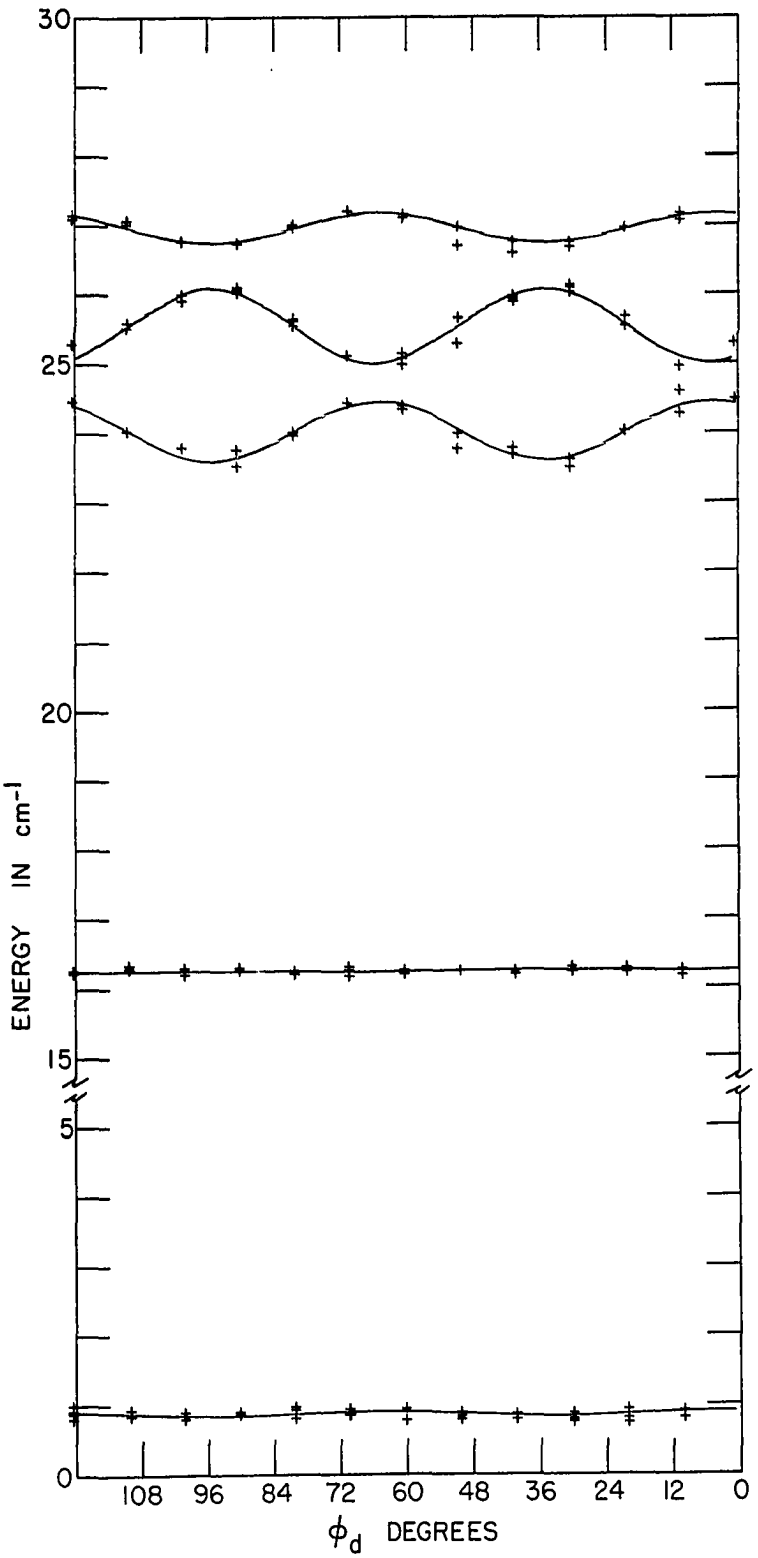
30
25
20
15
5
0
ENERGY IN cm⁻¹
108
96
84
72
60
48
36
24
12
0
ϕ_d DEGREES

Table 18. HsC anisotropy of the low lying levels of the ground term of DyES as obtained from the subtraction method in group G
H = 27488 G

Level	E_o	A		$\bar{\phi}$
I_-	0	0	-	-
I_+	0.87±.01	-0.04±.01	±.05	3.15±3.04°
II_-	16.25±.01	+0.02±.01	±.04	12.00±6.36°
II_+	24.04±.02	-0.44±.03	±.10	5.33± .66°
III_-	25.55±.02	+0.54±.02	±.08	5.59± .41°
III_+	26.96±.01	-0.22±.02	±.05	5.12± .70°

Table 19. HsC anisotropy of the low lying levels of the ground term of DyES as obtained from group G with side conditions $E_o(I_-)$ and $A(I_-) = 0$
H = 27488 G

Level	E_o	A
I_-	0 ±.00	0 ±.00
I_+	.86±.03	-.02±.03
II_-	16.24±.03	-0 ±.03
II_+	24.04±.03	-.48±.03
III-	25.54±.03	+.54±.03
III_+	26.94±.03	-.27±.04

external magnetic field, and to the fact that the error for the measurement of energy differences between absorption lines is about one half that for the measurement of their absolute energies.

Table 18 also shows that there is good agreement for the angle at which each of the levels with large energy variations attains its maximum or minimum energy. The deviations which occur for the levels with very small energy changes are due to the fact that, since the amplitudes of their variations are comparable to the measuring error, it is extremely difficult, if not impossible, to obtain a satisfactory determination of the angle at which their maximum or minimum energy occurs. There is certainly nothing here to contradict the theoretical conclusion reached in (73) that every level must have its maximum or minimum energy at the same angle.

Determination of $\bar{\phi}$

The angle $\bar{\phi}$ between the a translational symmetry axis of the crystal and the x axis direction was determined for several single crystals of dysprosium ethylsulfate, and for mixed crystals of Dy^{+3} in erbium ethylsulfate (ErES) and yttrium ethylsulfate (YES). The results are given in Table 20.

The x axis direction was determined by finding the values of the adjustable parameters S_o, A, and ϕ_x in Equation 89

Table 20. Measured values of $\bar{\phi}$, the angle between the a and x axes, for Dy^{+3} and Er^{+3} in DyES, ErES, and YES single crystals at 20°K

Sample	$\bar{\phi}$ for Dy^{+3}	$\bar{\phi}$ for Er^{+3}
1.0 mm DyES	$9.86° \pm .56°$	-
0.5 mm DyES	$4.93° \pm .34°$	-
1.0 mm DyES	$7.12° \pm .51°$	-
1.9 mm DyES	$5.51° \pm .36°$	-
2.4 mm $(DyES)_{90}(ErES)_{10}$	$6.35° \pm .19°$	$6.63° \pm .26°$
1.4 mm $(DyES)_{50}(ErES)_{50}$	$6.01° \pm .42°$	$6.25° \pm .40°$
2.4 mm $(DyES)_{10}(ErES)_{90}$	$6.23° \pm .17°$	$6.06° \pm .24°$
2.1 mm $(DyES)_{10}(YES)_{90}$	$8.17° \pm .44°$	-
1.0 mm ErES	-	$4.80° \pm .19°$

which gave the best least squares fit of the energy difference between two absorption lines with large rotation coefficients of opposite sign.

$$S(\phi_d) = S_o + A\cos 6(\phi_d - \phi_x) \tag{89}$$

Here ϕ_d is the angle reading at the top of the dewar and ϕ_x is the angle setting for which an x axis is parallel to the external magnetic field. Splittings were fit rather than

absorption line energies because, as noted earlier, the error for measurement of splittings is one half as large as the error for measurement of absolute energies, and because by choosing absorption lines with rotation coefficients of opposite sign, the variation of the splitting as a function of magnetic field direction has a larger amplitude than any of the absorption line energies. The use of splittings thus makes it possible to obtain more precise determinations of ϕ_x.

The absorption lines used for the determination of ϕ_x for Dy^{+3} in the various host lattices were the EsC lines resulting from the III_+ to $(1,2)_+$ and III_- to $(-1,-2)_-$ transitions in group I. (See Table 11.) Those used for the ϕ_x determination for Er^{+3} in DyES and ErES were the EpC lines at 27497 and 27500 cm^{-1} which result from the $(-1,-2)_+$ to $(0,3)_+$ and $(-1,-2)_+$ to $(-1,-2)'_-$ transitions, respectively. (See reference 51.) The variations of both of these splittings as a function of the magnetic field direction had amplitudes of approximately 1.1 cm^{-1} at 27.5 kG.

The angle setting ϕ_a for which an a axis was parallel to the magnetic field was determined by reference to the HpC crystal in each experiment. Knowing the angle setting ϕ_c for which the c axis of the HpC crystal is parallel to the magnetic field, and knowing the angle ϕ between the main faces of the HsC and HpC crystals, ϕ_a is given by

$$\phi_a = \phi_c + \phi. \tag{90}$$

For all of the HsC rotation experiments in this work ϕ_c was determined from spectra such as those shown in Figure 7. This was done by calculating values of S_o, A, and ϕ_c in Equation 91 which gave the best least squares fit of the distance (energy difference) between the absorption lines at 24982 and 24991 cm^{-1} as a function of ϕ_d, the angle reading at the top of the dewar.

$$S(\phi_d) = S_o + A\cos 2(\phi_d - \phi_c) \tag{91}$$

The results obtained in typical ϕ_x and ϕ_c determinations are illustrated in Figures 16 and 17.

The standard deviations for the ϕ_x and ϕ_c determinations were calculated using equations similar to Equation 77 for each of the nine crystals studied. In every case the standard deviations were less than $\pm$ 0.5 degrees; the average for all the determinations was $\pm$ 0.25 degrees. The standard deviations for the $\bar{\phi}$ measurements given in Table 20 were derived from the standard deviations for ϕ_x, ϕ_c, and ϕ. Since

$$\phi_a = \phi_c + \phi, \tag{91}$$

and

$$\bar{\phi} = |\phi_x - \phi_a| , \tag{92}$$

the standard deviation for each $\bar{\phi}$ determination is given by

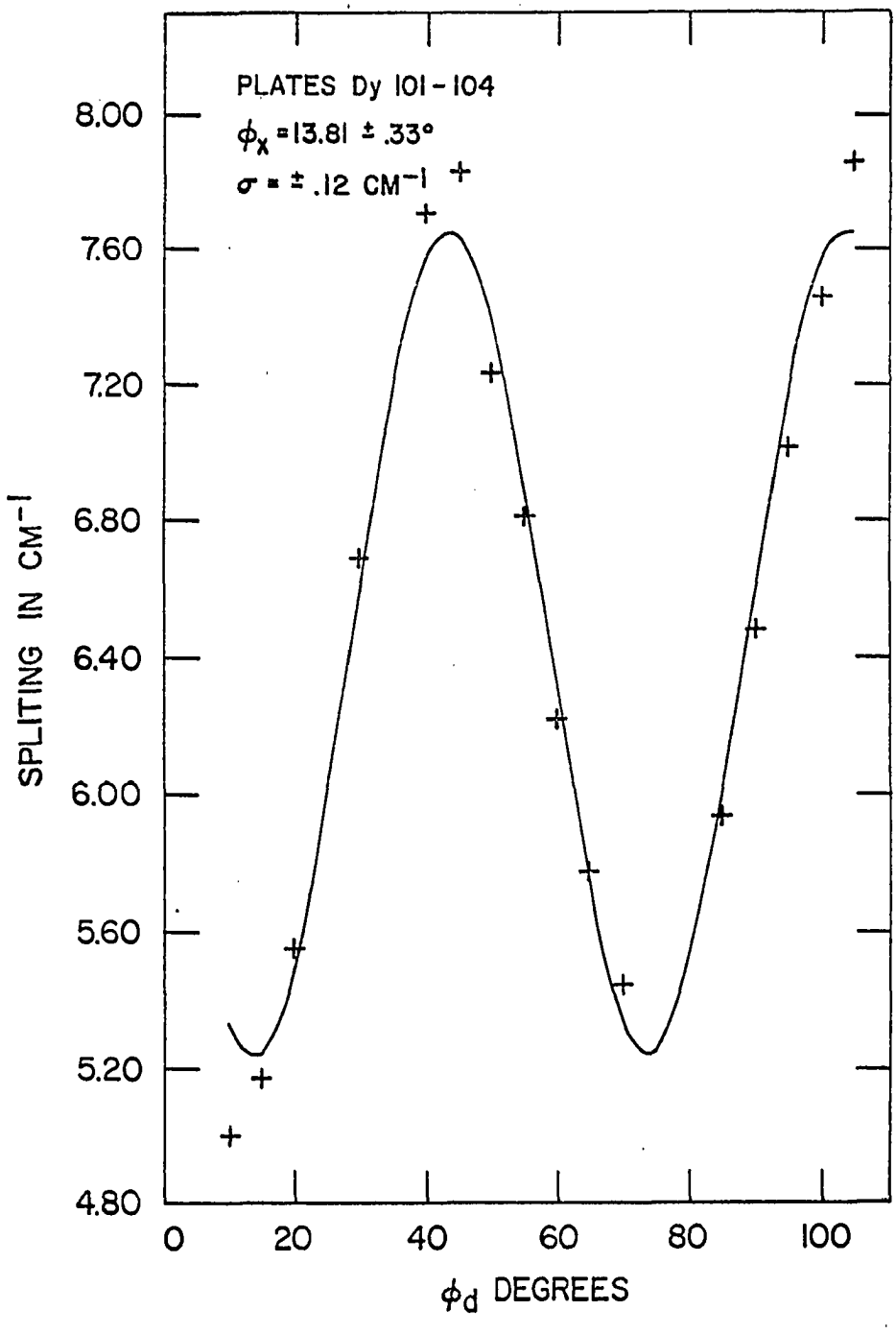

Figure 16. Typical result for ϕ_x determination

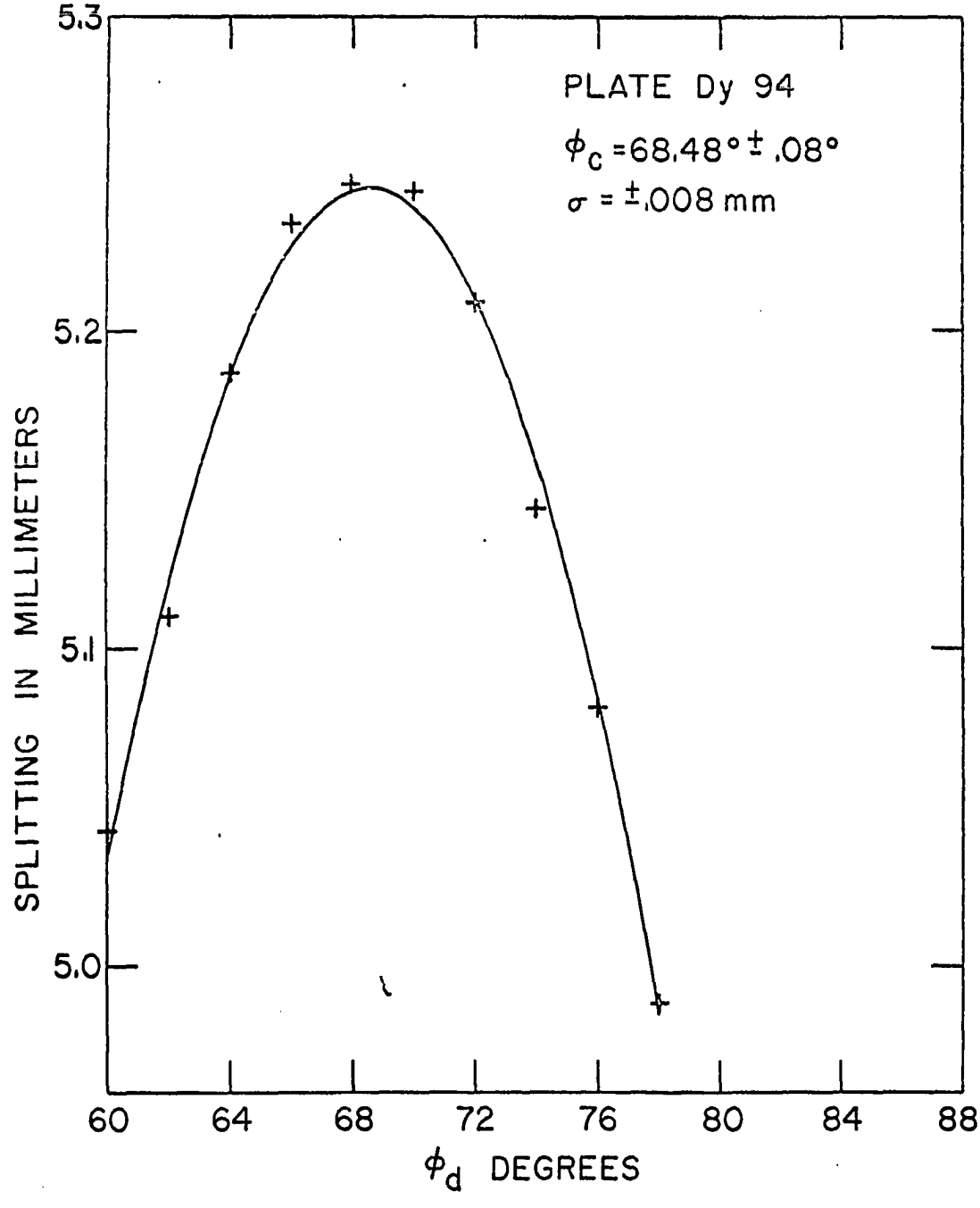

Figure 17. Typical result for ϕ_c determination

$$s_{\bar{\phi}} = \sqrt{s^2_{\phi_c} + s^2_{\phi} + s^2_{\phi_x}} \,. \qquad (93)$$

It is encouraging to note from the results given in Table 20 that fair precision can be obtained for the measurements of $\bar{\phi}$. However, it is also obvious from Table 20 that either $\bar{\phi}$ is not the same for all DyES crystals, or that the present $\bar{\phi}$ determinations are not very accurate. Since $\bar{\phi}$ is defined as the angle between an a translational symmetry axis and a choice of x axis which makes the lattice sum for β_{66} in Equation 16 vanish, one would have expected to obtain similar results for $\bar{\phi}$ measurements in the different single crystal samples of DyES. If the crystal lattices of the various samples were different, or if the lattices were distorted by significantly different amounts when the crystals were cooled to liquid hydrogen temperature, one might expect varying results for $\bar{\phi}$. However these possibilities are extremely unlikely. It is much more likely that the discrepancy results from errors in the determination of ϕ_x, ϕ_c, or ϕ.

Random errors in the measurement of ϕ_x, ϕ_c, and ϕ have been discussed earlier and are well understood. They are too small to account for the discrepancy. Systematic errors have not been discussed however, and it is possible that these are more important than the random errors. There are only two possibilities for systematic errors in the $\bar{\phi}$ deter-

minations. Either ϕ changed because of mounting failure when the crystals were cooled to 20°K, or the sample rod was allowed to rotate slightly when it was lowered to shift from the HpC to the HsC crystal. Examination of the crystals after the experiments, and measurement of ϕ after the crystals had warmed up to room temperature completely discount the possibility of mounting failure. Therefore it seems that the major source of error was failure to prevent rotation when the HsC crystals were lowered into the light path. This error, which leads to a corresponding error in $\bar{\phi}$, is estimated to be on the order of $\pm$ 2°. It could be effectively eliminated in future measurements by using a light source and a mirror attached to the sample rod to check the rotation of the sample rod before and after changing samples.

In view of the large discrepancy in the values of $\bar{\phi}$ obtained for the four DyES crystals, and in view of its probable cause, very little significance can be attached to the fact that the values of $\bar{\phi}$ obtained for different crystals agree or disagree. All that can be said is that $\bar{\phi} = 6.5°$ $\pm$ 1.4° for both Dy^{+3} and Er^{+3} in all the ethylsulfate crystals studied. It is significant, however, that the $\bar{\phi}$ values obtained for Dy^{+3} and Er^{+3} in any given $(DyES)_x(ErES)_{100-x}$ crystal are in agreement. Since the systematic error in $\bar{\phi}$ is the same for Dy^{+3} and Er^{+3} in any one of these mixed crystals, it can be concluded that, within the random error limits given in Table 20, the angle between the a and x axes

is the same for both rare earth ions in the mixed lattice. The $\bar{\phi}$ measurements do not indicate that there is any difference in the environments of Er^{+3} and Dy^{+3} in any given $(DyES)_x(ErES)_{100-x}$ crystal. Before any fruitful comparison of the $\bar{\phi}$ results for different crystals can be made, it is clear that further work must be done in which more care is taken to eliminate the systematic errors in the determination of the a and x axis directions.

Magnetic Field Dependence of the Energy Levels

The Zeeman splittings and shifts of the energy levels of Dy^{+3} in the ethylsulfate lattice were also studied as a function of the external magnetic field strength for groups G through L (22000 cm^{-1} to 27500 cm^{-1}). At least ten values of magnetic field between zero and 27.5 kG were used for each crystal and both the HpC and HsC orientations were studied. In the HsC case the magnetic field dependence was only studied for the case where ϕ_m, the angle between the magnetic field and the x axis was equal to $\bar{\phi}$. This corresponds to the situation in which the magnetic field is perpendicular to the c axis and parallel to an a axis of the crystal.

The crystals were immersed directly in liquid helium or liquid hydrogen. Photographs taken at liquid helium temperature were particularly helpful because only the lowest ground term level is appreciably populated at 4.2°K. This considerably simplified the spectrum and in most cases the

crystal quantum numbers of the final states in the transitions could be easily determined with the help of the selection rules given in Table 7. Also, as previously noted by Gramberg, the lowest crystal field level in the ground term has such a large Zeeman splitting in the HpC case that at 4.2°K the high energy branch becomes depopulated and absorption lines originating from this branch fade out with increasing external magnetic field. This fact is a big help in the analysis of the spectrum.

The center of gravity of each Zeeman pattern was determined with respect to the center of gravity of the lowest ground term crystal field level and the Zeeman splittings of the initial and final states were determined, when possible, for each value of the external magnetic field. The shifts of the centers of gravity of all the patterns and the splittings of the levels as functions of the external magnetic field are summarized in Tables 21 through 39 in terms of coefficients for the polynomial equations which gave the best least squares fit of the experimental data. The equations for the centers of gravity have the form

$$C = \sum_{k=0}^{4} C_k H^k, \tag{94}$$

and those for the splittings have the form

$$S = \sum_{k=1}^{4} C_k H^k. \tag{95}$$

Table 21. HpC pattern centers and Zeeman splittings for DyES group G 1.83 mm single crystal at 20°K

Transition	M	Pattern centers C_0	10^3C_1 ($10^{12}C_3$)	10^8C_2 ($10^{16}C_4$)	N	σ
I 1,2	212	22238.046 ±.104	.1000 ±.0194	-.4308 ±.0705	4	±.10
I -1,-2	212	22158.545 ±.337	-.0444 ±.0486	.2908 ±.1636	8	±.35
III 0,3	11	22154.316 ±.126	-.2558 ±.0085		8	±.16
II -1,-2	4A11	22142.787 ±.110	.0291 ±.0076		5	±.12
I 1,2	4A11	22122.615 ±.007	.0061 ±.0015	-.0595 ±.0075	5	±.01
I 0,3	4A11	22106.292 ±.020	.0153 ±.0045	-.0985 ±.0230	5	±.02
II 0,3	11	22089.916 ±.105	.2274 ±.0236	.1423 ±.0895	4	±.11
III 0,3	212	22085.074 ±.082	.0837 ±.0453	-1.4920 ±.5456	4	±.08

M	ID	Splittings 10^3C_1 ($10^{12}C_3$)	10^8C_2 ($10^{17}C_4$)	Range kG	N	σ
1	GS	.5109 ±.0054		0-27.5	4	±.216
1		.3591 ±.0118		0-27.5	8	±.586
				4.2-24.6		
4	EX	.0127 ±.0036		0-20.1	5	±.116
8	GS	.2649 ±.0084		0-20.1	5	±.269
4	EX	.1282 ±.0081	-.2424 ±.0472	0-20.1	5	±.044
8	GS	.5151 ±.0005		0-20.1	5	±.017
4	EX	.3072 ±.0127	-.2327 ±.0746	0-20.1	5	±.069
8	GS	.5047 ±.0006		0-20.1	5	±.019
				0-20.5		
1	GS+EX	.8749 ±.0304		0- 8.2	4	±.337

Table 21. (Continued)

Transition	M	Pattern centers C_o	10^3C_1 ($10^{12}C_3$)	10^8C_2 ($10^{16}C_4$)	N	σ
I -1,-2	4A11	22062.955 ±.012	-.0045 ±.0017	.1436 ±.0058	8	±.01
II -1,-2	4A11	22046.845 ±.045	-.0038 ±.0098	.1332 ±.0475	5	±.05
III -1,-2	212	22041.867 ±.002	-.0420 ±.0030	.9383 ±.0724	7	±.00
			(-.5608) (±.0553)	(.1311) (±.0132)		
I -1,-2	423	22034.803 ±.043	.0102 ±.0060	-.1587 ±.0204	7	±.043
II -1,-2	4A11	22018.658 ±.012	.0038 ±.0020	-.1211 ±.0070	10	±.015
III -1,-2	323	22013.655 ±.048	.0307 ±.0107	-.2866 ±.0550	5	±.048

M	ID	Splittings 10^3C_1 ($10^{12}C_3$)	10^8C_2 ($10^{17}C_4$)	Range kG	N	σ
4	EX	.4448 ±.0142	-.4321 ±.2456	0-27.5	8	±.019
		(.1704) (±.1355)	(-.3364) (±.2386)			
8	GS	.5149 ±.0005		0-27.5	8	±.026
4	GS	.2892 ±.0046	-.0910 ±.0270	0-20.1	5	±.030
8	EX	.4143 ±.0014	-.0611 ±.0084	0-20.1	5	±.009
1	GS-EX	.2369 ±.0058	.0843 ±.0356	0-20.1	7	±.046
1	GS	.5080 ±.0045	.0209 ±.0191	0-27.4	6	±.042
5	EX	.5724 ±.0033	-.1370 ±.0142	0-27.4	6	±.031
4	GS	.2761 ±.0026	-.0215 ±.0117	0-27.4	10	±.035
8	EX	.5784 ±.0036	-.1595 ±.0164	0-27.4	10	±.049
1	EX	.5332 ±.0164	.1182 ±.0962	12.6-20.1	4	±.089
5	GS	.6186 ±.0206	.1763 ±.1210	12.6-20.1	4	±.056

Table 22. HsC pattern centers and Zeeman splittings for DyES group_G 0.965 mm single crystal at 20°K
$\phi_m = \phi$

Transition	M	Pattern centers C_o	$10^3 C_1$ ($10^{12} C_3$)	$10^8 C_2$ ($10^{16} C_4$)	N	σ
I 1,2	11	22238.537 ±.663	-.1855 ±.1042	.8594 ±.3515	21	±1.039
I 1,2	11	22236.592 ±.182			20	± .813
II 1,2	212	22220.037 ±.374	.1234 ±.0252		10	± .605
I 0,3	212	22202.583 ±.234	.0638 ±.0138		23	± .523
III 0,3	212	22182.138 ±.195			6	± .479
I 0,3	313	22174.566 ±.057	.0180 ±.0136	.1918 ±.0485	11	± .087
	21	22168.313 ±.114	.0605 ±.0178	.1430 ±.0611	23	± .189
	11	22162.943 ±.300	.0304 ±.0669	.3181 ±.3157	10	± .330
I -1,-2	323	22158.605 ±.177	.1107 ±.0255	-.5619 ±.0838	6	± .177
	11	22157.727 ±.128			15	± .497
	11	22152.695 ±.100	.1745 ±.0228		5	± .142

M	ID	Splittings 10^3C_1 ($10^{12}C_3$)	10^8C_2 ($10^{17}C_4$)	Range kG	N	σ
				0-27.4		
				0-27.4		
1		.0802 ±.0244		2.7-27.4	10	±1.143
1		.0815 ±.0121		0-27.4	23	± .988
1		-.0708 ±.0918	1.3813 ± .6963	2.7-15.4	6	± .581
5		.0220 ±.0263	.3301 ± .1059	0-27.4	11	± .232
1		.0023 ±.0290		9.3-15.4	6	± .916
				0-19.1		
1		-.1339 ±.0213	1.0044 ± .0897	26.0-27.2	6	± .235
3		.2962 ±.0440	.2870 ± .1850	12.6-27.2	6	± .485
				0-27.4		
				0- 8.2		

Table 22. (Continued)

Transition	M	Pattern centers C_o	10^3C_1 ($10^{12}C_3$)	10^8C_2 ($10^{16}C_4$)	N	σ
II -1,-2	414	22142.628 ±.285	-.0368 ±.0181		5	± .287
I 1,2	413	22122.772 ±.073	-.0013 ±.0119	.5961 ±.0518	10	± .073
I 0,3	212	22106.275 ±.054	.0083 ±.0084	.1760 ±.0284	24	± .089
III 1,2	212	22101.8			1	-
II 0,3	212	22089.946 ±.114	-.0398 ±.0100		7	± .133
III 0,3	313	22085.002 ±.058	.0256 ±.0099	-.3548 ±.0326	15	± .092
I -1,-2	4A11	22062.954 ±.044	-.0414 ±.0258	1.2616 ± .4565	14	± .044
			(-.5175) (±.2727)	(.0949) (±.0509)		
II -1,-2	4A11	22046.973 ±.059	-.0537 ±.0088	.0864 ±.0304	21	± .086

M	ID	Splittings 10^3C_1 ($10^{12}C_3$)	10^8C_2 ($10^{17}C_4$)	Range kG	N	σ
1	GS&EX	.3614 ±.0160		0-20.1	10	± .737
3	GS	.0006 ±.0027		0-27.4	19	± .264
7	EX	.4441 ±.0152	-.1633 ±.0715	0-27.4	17	± .317
1	GS	-.0008 ±.0024		0-27.4	24	± .192
1	GS	.4833 ±.0421	-.9202 ±.3065	0-17.1	7	± .276
3	EX	-.0070 ±.0044		0-27.4	14	± .223
5	GS	-.0573 ±.0097	.4841 ±.0421	0-27.4	15	± .170
3	GS	-.0258 ±.0055	.1900 ±.0250	0-27.4	21	± .148
7	EX	.1150 ±.0048	.0543 ±.0220	0-27.4	18	± .129
4	EX	.1382 ±.0021	-.0324 ±.0101	0-27.2	21	± .040
8	GS	.4300 ±.0063	-.5338 ±.0297	0-27.2	21	± .119

Table 22. (Continued)

Transition	M	Pattern centers C_0	10^3C_1 ($10^{12}C_3$)	10^8C_2 ($10^{16}C_4$)	N	σ
III -1,-2	423	22041.732 ±.070	.0327 ±.0173	-.3180 ±.0933	8	± .070
I -1,-2	4A11	22034.770 ±.026	.0098 ±.0035	.3002 ±.0108	20	± .030
II -1,-2	4A11	22018.819 ±.062	-.0565 ±.0088	.0468 ±.0285	21	± .081
III -1,-2	423	22013.700 ±.060	.0286 ±.0084	-.4239 ±.0259	8	± .061

M	ID	Splittings 10^3C_1 ($10^{12}C_3$)	10^8C_2 ($10^{17}C_4$)	Range kG	N	σ
3	GS	.1078 ±.0165	-.3489 ±.0973	0-19.1	8	± .086
7	EX	.1311 ±.0018		0-19.1	6	± .072
4	GS	-.0190 ±.0066	.2303 ±.0695	0-27.4	20	± .040
		(-.0182) (±.0174)				
8	EX	.1583 ±.0004		0-27.4	20	± .035
4	EX	.1634 ±.0014	-.0260 ±.0063	0-27.4	21	± .027
8	GS	.4369 ±.0068	-.5737 ±.0310	0-27.4	21	± .134
3	GS	-.0258 ±.0024	.1973 ±.0980	0-27.4	8	± .043
7	EX	.0573 ±.0072	.3692 ±.0294	11.4-27.4	8	± .131

Table 23. HpC pattern centers and Zeeman splittings for DyES group G 1.83 mm single crystal at 4.2°K

Transition	M	Pattern centers C_0	10^3C_1 ($10^{12}C_3$)	10^8C_2 ($10^{16}C_4$)	N	σ
I 1,2	11	22237.507 ±.295	.3434 ±.0484	-.2322 ±.1663	10	±.361
I -1,-2	11	22158.512 ±.203	.2851 ±.0128		10	±.344
I 1,2	323	22122.584 ±.120	-.1046 ±.0407	.4898 ±.3041	5	±.124
Satellite	11	22125.044 ±.104	.1188 ±.0053		4	±.116
I 0,3	423	22106.171 ±.161	-.0291 ±.0337	.2019 ±.1606	7	±.168
I -1,-2	414	22062.968 ±.009	.0022 ±.0024	.1054 ±.0138	7	±.009

M	ID	Splittings 10^3C_1 ($10^{12}C_3$)	10^8C_2 ($10^{17}C_4$)	Range kG	N	σ
				0-27.5		
				0-27.5		
1	EX	.1019 ±.0066		0-24.6	4	±.185
3	GS	.5263 ±.0130		0-12.6	5	±.219
				0-27.5		
1	EX	.2964 ±.0106	-.1012 ±.0476	0-27.5	9	±.139
5	GS	.7163 ±.0403	-1.0858 ±.2456	0-20.1	7	±.320
3	EX	.4489 ±.0043	-.1688 ±.0443	0-27.5	7	±.012
		(-.0171) (±.0108)				
4	EX	.4493 ±.0019	-.1962 ±.0127	0-16.3	4	±.005
7	GS	.5276 ±.0003		0-20.1	5	±.011

Table 23. (Continued)

Transition	M	Pattern centers C_o	10^3C_1 ($10^{12}C_3$)	10^8C_2 ($10^{16}C_4$)	N	σ
I -1,-2	313	22034.690 ±.006			2	±.008

M	ID	Splittings $10^3 c_1$ ($10^{12} c_3$)	$10^8 c_2$ ($10^{17} c_4$)	Range kG	N	σ
8	GS	.5276 ±.0004		0-16.3	4	±.009
1	EX	.5782 ±.0072	-.0131 ±.1399	0-27.5	10	±.019
		(-.0352) (±.0852)	(-.0494) (±.1610)			

Table 24. HsC pattern centers and Zeeman splittings for DyES group G 1.89 mm single crystal at 4.2°K
$\phi_m = \overline{\phi}$

Transition	M	Patter centers C_o	$10^3 C_1$ ($10^{12} C_3$)	$10^8 C_2$ ($10^{16} C_4$)	N	σ
	11	22239.255 ±.190	.0633 ±.0120		10	±.322
	11	22236.536 ±.178	-.0906 ±.0256	.4001 ±.0863	8	±.186
	11	22224.772 ±.209	.0893 ±.0149		9	±.335
I 0,3	11	22173.931 ±.223	.1005 ±.0126		8	±.251
I -1,-2	212	22158.756 ±.065	.0066 ±.0091	.3800 ±.0312	7	±.066
I 1,2	4A11	22122.508 ±.022	.0310 ±.0035	.4819 ±.0136	7	±.023
I 0,3	212	22106.277 ±.056	.0114 ±.0092	.1884 ±.0315	10	±.068
I -1,-2	4A11	22062.974 ±.008	-.0713 ±.0200	1.6822 ±.3128	6	±.008
			(-.6974) (±.1563)	(.1169) (±.0252)		

M	ID	Splittings 10^3C_1 ($10^{12}C_3$)	10^8C_2 ($10^{17}C_4$)	Range kG	N	σ
				0-27.5		
				0-27.5		
				0-24.6		
				6.1-27.5		
1	EX	.3043 ±.0333	.1933 ±.1464	0-27.5	7	±.368
4	GS	-.0241 ±.0089	.1399 ±.0446	0-24.6	7	±.090
8	EX	.4663 ±.0070	-.3169 ±.0353	0-24.6	7	±.071
4	GS	-.0179 ±.0102	.1834 ±.0437	0-27.4	6	±.100
8	EX	.1268 ±.0061	.0331 ±.0261	0-27.4	6	±.060

Table 24. (Continued)

Transition	M	Pattern centers C_0	10^3C_1 ($10^{12}C_3$)	10^8C_2 ($10^{16}C_4$)	N	σ
I -1,-2	4A11	22034.696 ±.013	.0012 ±.0042 (-.0227 ±.0091)	.3875 ±.0381	9	±.014

M	ID	Splittings 10^3C_1 ($10^{12}C_3$)	10^8C_2 ($10^{17}C_4$)	Range kG	N	σ
4	GS	-.0245 ±.0089	.2784 ±.0961	0-27.4	9	±.040
		(-.0280 ±.0244)				
8	EX	.1553 ±.0002		0-27.4	9	±.010

Table 25. HpC pattern centers and Zeeman splittings for DyES group H 4.4 mm single crystal at 20°K

Transition	M	Pattern centers C_o	10^3C_1	10^8C_2	N	σ
I -1,-2	212	23485.321 ±.062	-.0286 ±.0111		3	±.063
II -1,-2[a]	212	23468.915 ±.032	.0179 ±.0017		7	±.039
I 0,3[a]	11	23467.933 ±.218	-.2500 ±.0258	.1582 ±.0696	7	±.069
I 1,2	212	23461.776 ±.050	-.0041 ±.0078	.1088 ±.0264	9	±.056
II 0,3	212	23451.385 ±.021	-.0060 ±.0059	.0519 ±.0323	4	±.021
I 0,3	11	23439.432 ±.031	.4840 ±.0020		10	±.054
III 1,2	212	23440.665 ±.039	-.0196 ±.0113	.1634 ±.0688	7	±.041
I 1,2	212	23429.153 ±.020	-.0047 ±.0034	-.0722 ±.0117	9	±.025
II 0,3	212	23423.225 ±.033	-.0056 ±.0036		4	±.039
III 1,2	423	23408.018 ±.031	-.0059 ±.0052	-.0523 ±.0180	10	±.039
IV 0,3	11	23381.031 ±.087	.1834 ±.0118	.0711 ±.0348	8	±.044

[a]Measured in 0.5 mm crystal.

M	ID	Splittings $10^3 c_1$	$10^8 c_2$	Range kG	N	σ
1	GS-EX	.5476	-.8041	0-7.7	3	-
		-	-			
1	GS-EX	.2160 ±.0038	.0211 ±.0165	0-27.9	7	±.043
				8.2-27.9		
1	GS+EX	.5092 ±.0040	.0419 ±.0183	0-27.4	9	±.054
1	GS-EX	.0426 ±.0069	.6389 ±.0409	0-19.1	4	±.027
				0-27.4		
1	GS+EX	.6480 ±.0058	.1602 ±.0451	0-13.4	7	±.035
1	GS+EX	.6336 ±.0008		0-27.4	9	±.038
1	GS+EX	.7969 ±.0238	-.3906 ±.1922	0-13.4	4	±.071
1	EX	.0857 ±.0672	.0847 ±.0304	0-27.4	10	±.091
5	GS	.6446 ±.0020		0-27.4	7	±.095
				5.8-27.4		

Table 25. (Continued)

Transition	M	Pattern centers C_o	$10^3 C_1$	$10^8 C_2$	N	σ
II -1,-2	212	23374.862 ±.041	-.0028 ±.0064	.0349 ±.0217	7	±.043
IV -1,-2	212	23332.469 ±.088			3	±.153

M	ID	Splittings $10^3 c_1$	$10^8 c_2$	Range kG	N	σ
1	GS+EX	.3677 ±.0026	.0191 ±.0115	0-27.4	7	±.029
1	GS-EX	.2653 -	-.0854 -	0-13.4	3	-

Table 26. HsC pattern centers and Zeeman splittings for DyES group H 4.4 mm single crystal at 20°K
$\phi_m = \phi$

Transition	M	Pattern centers C_o	$10^3 C_1$ ($10^{12} C_3$)	$10^8 C_2$ ($10^{16} C_4$)	N	σ
I -1,-2	312	23485.330 ±.129	-.0446 ±.0296 (-.0801) (±.0406)	.9234 ±.1999	8	±.027
I 0,3	2-	23468.	not resolved			
I 1,2	4A11	23461.914 ±.105	-.0148 ±.0147	.1213 ±.0437	6	±.052
II 0,3	313	23451.316 ±.164	.0168 ±.0116		8	±.235
III 1,2	212	23440.645 ±.030	.0529 ±.0062	-.5684 ±.0234	4	±.030
I 0,3	11	23439.401 ±.057	-.0066 ±.0185 (-.0601) (±.0396)	.7090 ±.1644	10	

M	ID	Splittings 10^3C_1 ($10^{12}C_3$)	Splittings 10^8C_2 ($10^{17}C_4$)	Range kG	N	σ
1	EX	.3455 ±.0045	-.2102 ±.0205	5.8-27.4	8	±.060
3	GS	-.0350 ±.0066	.2507 ±.0341	7.7-24.1	6	±.067
5	GS+EX	.3173 ±.0016		7.7-24.1	6	±.064
				7.7-27.4		
4	GS	-.0164 ±.0122	.1407 ±.0550	5.8-27.4	6	±.146
8	EX	.3079 ±.0139	-.2951 ±.0626	5.8-27.4	6	±.166
1	GS	.2859 -	.0943 -	19.1-24.1	3	-
3	EX	.2311 ±.0215	-.6034 ±.0870	19.1-27.4	4	±.114
5	GS+EX	.4027 ±.0089		0-24.1	8	±.353
1		.2108 ±.0044	-.2239 ±.0178	19.1-27.4	4	±.023
				0-27.4		

Table 26. (Continued)

Transition	M	Pattern centers C_o	10^3C_1 ($10^{12}C_3$)	10^8C_2 ($10^{16}C_4$)	N	σ
I 1,2	212	23429.121 ±.063	.0085 ±.0098	.2231 ±.0331	9	±.071
II 0,3	212	23423.227 ±.023	-.0097 ±.0042	.0308 ±.0168	9	±.027
III 1,2	323	23407.955 ±.107	.0364 ±.0165	-.5390 ±.0561	9	±.120
I -1,-2	11	23390.983 ±.059	-.0395 ±.0185	.6792 ±.1675	9	±.060
			(-.0594 ±.0406)			
IV 0,3	11	23380.854 ±.053	.0140 ±.0100	.1500 ±.0397	9	±.064
II -1,-2	212	23374.939 ±.039	-.0360 ±.0025		10	±.067
IV -1,-2	11	23332.126 ±.121	.0632 ±.0201	-.1133 ±.0696	10	±.150

M	ID	Splittings 10^3C_1 ($10^{12}C_3$)	Splittings 10^8C_2 ($10^{17}C_4$)	Range kG	N	σ
1	EX	.3035 ±.0105	-.2027 ±.0473	0-27.4	9	±.139
1	GS	.4012 ±.0583	-.3942 ±1.3279	0-24.1	9	±.119
		(.0610) (±.9272)	(- .6905) (±1.9900)			
1	GS	-.0869 ±.0196	.7565 ±.0885	0-27.4	9	±.259
3	EX	.4251 ±.0165	-.6602 ±.0745	0-27.4	9	±.218
5	GS+EX	.3381 ±.0181	.0963 ±.0816	0-27.4	9	±.239
				0-27.4		
				0-27.4		
1	GS	.4139 ±.0166	-.4269 ±.0753	0-27.4	10	±.227
				0-27.4		

Table 27. HpC pattern centers and Zeeman splittings for DyES group I 1.0 mm single crystal at 20°K

Transition	M	Pattern centers C_o	10^3C_1	10^8C_2	N	σ
I 0,3	212	25156.879 ±.302	.0368 ±.0142		3	±.303
II 0,3	212	25140.925 ±1.000			1	±1.000
I -1,-2	11	25137.974 ±.221	.2366 ±.0310	.3583 ±.1062	7	±.223
II -1,-2	11	25123.088 ±.394	-.1048 ±.0247		8	±.658
I 0,3 I -1,-2	212	25055.655 ±.057	.0357 ±.0087	-.1487 ±.0293	9	±.063
II -1,-2	11	25036.363 ±.193	.1839 ±.0319	.5278 ±.1096	10	±.237
III 0,3	212	25034.384 ±.212	.0455 ±.0155		5	±.243
I -1,-2	212	24996.655 ±.061	-.0237 ±.0035		8	±.082
I 1,2	212	24986.572 ±.069			5	±.154
I 0,3	212	24982.717 ±.053	-.0128 ±.0029		7	±.064
II -1,-2	3123	24980.346 ±.008			4	±.016

M	ID	Splittings $10^3 c_1$	$10^8 c_2$	Range kG	N	σ
1		.9283 -	-.4654 -	24.6-27.4	3	-
				0		
				0-27.4		
				0-27.4		
1	GS+EX	.5186 ±.0238	.2960 ±.1067	0-27.4	9	±.311
				0-27.4		
1	GS+EX	.5752 ±.0571	.4922 ±.3315	0-20.0	5	±.341
1	GS-EX	.2407 ±.0038	.0366 ±.0167	0-27.4	8	±.046
1	EX-GS	.2989 ±.0191	.0935 ±.0780	0-27.4	5	±.140
1	EX-GS	.1471 ±.0015		0-27.4	7	±.073
1	GS&EX	.3336 ±.0471	-.8444 ±.6602	0-8.2	4	±.107
2	GS&EX	.2706 ±.0004		0-24.6	6	±.014
3	GS&EX	.2538 ±.0162	.1684 ±.1333	0-14.3	6	±.088

Table 27. (Continued)

Transition	M	Pattern centers C_o	$10^3 C_1$	$10^8 C_2$	N	σ
II 0,3	212	24966.582 ±.026	.0088 ±.0068	-.0676 ±.0397	6	±.026
III 1,2	212	24965.481 ±.022	-.0077 ±.0033	.0166 ±.0113	7	±.023
III 0,3	11	24961.628 ±.032	-.0044 ±.0031		7	±.044

M	ID	Splittings $10^3 C_1$	$10^8 C_2$	Range kG	N	σ
1	EX-GS	.3981 ±.0098	-.1471 ±.0703	0-16.3	6	±.056
1	EX-GS	.1861 ±.0010		0-27.4	7	±.046
				0-16.3		

Table 28. HsC pattern centers and Zeeman splittings for DyES group_I 0.965 mm single crystal at 20°K
$\phi_m = \phi$

Transition	M	Pattern centers C_o	$10^3 C_1$ ($10^{12} C_3$)	$10^8 C_2$ ($10^{16} C_4$)	N	σ
I -1,-2	4A11	24996.529 ±.068	.0095 ±.0146 (.0188 ±.0187)	.6952 ±.0940	19	±.016
I 1,2	4A11	24986.347 ±.056	.1339 ±.0092	.2181 ±.0294	17	±.068
II -1,-2	414	24980.605 ±.074	-.0705 ±.0097	.5451 ±.0302	17	±.083
I 0,3	414	24982.881 ±.047	.0713 ±.0083	-.1027 ±.0273	17	±.074

M	ID	Splittings $10^3 c_1$ ($10^{12} c_3$)	Splittings $10^8 c_2$ ($10^{17} c_4$)	Range kG	N	σ
4	GS	-.0018 ±.0043	.0453 ±.0466	6.2-27.2	19	±.027
		(.0252 ±.0121)				
8	EX	.5089 ±.0040	-.5043 ±.0191	6.2-27.2	19	±.077
4	GS	-.0158 ±.0069	.1134 ±.0819	1.8-27.4	17	±.047
		(.0235 ±.0219)				
8	EX	-.0360 ±.0179	.2627 ±.2118	1.8-27.4	17	±.122
		(.0658 ±.0566)				
3	GS	.3783 ±.0238	-.1470 ±.4422	0-27.4	13	±.053
		(.0340 ±.2522)	(-.0420 ±.0452)			
5	EX	.4635 ±.0098	-.1507 ±.0808	0-14.3	8	±.053
10	GS+EX	-.0476 ±.0057	.4317 ±.0244	0-27.4	17	±.100

Table 28. (Continued)

Transition	M	Pattern centers C_0	10^3C_1 ($10^{12}C_3$)	10^8C_2 ($10^{16}C_4$)	N	σ
III -1,-2	313	24975.225 ±.009	.0480 ±.0004		4	±.006
II 1,2	4A11	24970.903 ±.126	.0162 ±.0128	.0876 ±.0306	11	±.016
III 1,2	4A11	24965.433 ±.073	.1198 ±.0137	-.4024 ±.0454	11	±.104
II 0,3	414	24967.147 ±.094	-.1813 ±.0134	-.2232 ±.0423	11	±.100
III 0,3	3123	24961.775 ±.040	-.0261 ±.0188	-1.326 ± .2490	16	±.019
			(.2746) (±.1246)	(- .0439) (± .0216)		

M	ID	Splittings 10^3C_1 ($10^{12}C_3$)	Splittings 10^8C_2 ($10^{17}C_4$)	Range kG	N	σ
1	EX	.5111 ±.0025	-.5069 ±.0099	13.4-27.4	4	±.023
3	GS	.0739 ±.0082	-.1733 ±.0363	13.4-27.4	14	±.125
3	EX	-.0092 ±.0034	.3236 ±.0151	12.6-27.4	15	±.076
7	GS	.4548 ±.0070	-.6507 ±.3080	7.6-27.4	17	±.162
3	GS	-.0204 ±.0032	.1825 ±.0133	0-27.4	16	±.070
7	EX	-.0522 ±.0061	.4860 ±.0253	0-27.4	16	±.132
3	EX	-.0255 ±.0054	.2467 ±.0214	0-27.4	13	±.075
7	GS	.3961 ±.0154	-.0642 ±.1555	9.3-27.4	18	±.075
		(-.1365) (±.0374)				
4	GS&EX	.0238 ±.0044	.0409 ±.0195	1.8-27.4	16	±.108

Table 29. HpC pattern centers and Zeeman splittings for DyES group I 1.83 mm single crystal at 4.2°K

Transition	M	Pattern centers C_0	$10^3 C_1$	$10^8 C_2$	N	σ
	11	25166.034 ±.121	-.2955 ±.0159	1.5618 ±.0464	8	±.058
I 0,3	11	25157.247 ±.102	.3107 ±.0098		7	±.142
I 0,3	212	25143.331 ±.097	.0575 ±.0277	-.1980 ±.1687	5	±.098
I -1,-2	212	25137.571 ±.086	-.0130 ±.0262	.2204 ±.1738	5	±.087
I 0,3	212	25055.674 ±.072	.0295 ±.0074		5	±.084
I -1,-2	11	25053.790 ±.090	.3282 ±.0145		8	±.058
I -1,-2	323	24996.516 ±.014	-.0042 ±.0037	-.0514 ±.0213	6	±.014
I 1,2	313	24986.583 ±.008	-.0013 ±.0005		10	±.014
I 0,3	212	24982.805 ±.015	-.0023 ±.0021	-.0171 ±.0072	7	±.015
II 0,3	11	24966.740 ±.036	-.2004 ±.0023		9	±.060

M	ID	Splittings $10^3 c_1$	Splittings $10^8 c_2$	Range kG	N	σ
				6.1-27.5		
				0-16.3		
1	GS-EX	1.0965 ±.1777	-5.8676 ±1.2698	0-16.3	5	±1.005
1		.5061 ±.0261	.4993 ±.2088	0-14.3	5	±.121
1	GS+EX	.5485 ±.0111		0-14.3	5	±.241
				0-24.6		
3	GS-EX	.2584 ±.0028	-.0521 ±.0199	0-16.3	6	±.016
5	EX-GS	.3398 ±.0018	-.0415 ±.0083	0-27.5	10	±.025
1	EX-GS	.1481 ±.0020	-.0274 ±.0087	0-27.5	7	±.022
				0-27.5		

Table 30. HsC pattern centers and Zeeman splittings for DyES group_I 1.89 mm single crystal at 4.2°K
$\phi_m = \phi$

Transition	M	Pattern centers C_o	$10^3 C_1$ ($10^{12} C_3$)	$10^8 C_2$ ($10^{16} C_4$)	N	σ
I 0,3	3123	25056.061 ±.718	-.0730 ±.0761	.4966 ±.1890	6	±.095
I -1,-2	323	25052.635 ±.051	.0495 ±.0074	-.0347 ±.0250	8	±.054
Satellites	212	24998.766 ±.004			2	±.006
I -1,-2	4A11	24996.513 ±.005	-.0062 ±.0074	.9425 ±.1508	6	±.005
			(-.1197) (±.0957)	(.0247) (±.0184)		
	11	24996.556 ±.136	-.2283 ±.0153	.9770 ±.0407	5	±.013
Satellite	11	24988.092 ±.455	.2024 ±.0213		3	±.456
I 1,2	4A11	24986.457 ±.106	.0959 ±.0207	.3365 ±.0695	7	±.122

M	ID	Splittings 10^3C_1 ($10^{12}C_3$)	10^8C_2 ($10^{16}C_4$)	Range kG	N	σ
1	EX	.3825 ±.0184	-.1657 ±.0822	0-27.5	9	±.240
3		.3386 ±.0172	.0929 ±.0754	12.6-27.5	6	±.189
3	EX	.4241 ±.0123	-.1909 ±.0546	0-27.5	8	±.150
1		.3467 .0		0- 8.2	2	±.0
4	GS	-.0129 ±.0030	.1481 ±.0134	8.2-27.5	6	±.035
8	EX	.5155 ±.0064	-.5395 -.0290	8.2-27.5	6	±.076
				12.6-24.6		
				0		
4	GS	-.0165 ±.0035	.1726 ±.0144	0-27.5	7	±.037
8	EX	-.0154 ±.0213	.0517 ±.2771	0-27.5	7	±.092
		(.1192) (±.0763)				

Table 30. (Continued)

Transition	M	Pattern centers C_0	10^3C_1 ($10^{12}C_3$)	10^8C_2 ($10^{16}C_4$)	N	σ
I 0,3	212	24983.117 ±.069	-.1156 ±.0100	.0419 ±.0312	9	±.048
II 0,3	11	24966.865 ±.102	.0914 ±.0168	-.7490 ±.0579	10	±.126

M	ID	Splittings 10^3C_1 ($10^{12}C_3$)	Splittings 10^8C_2 ($10^{16}C_4$)	Range kG	N	σ
				4.2-27.5		
				0-27.5		

Table 31. HpC pattern centers and Zeeman splittings for DyES group I 2.1 mm $(DyES)_{10}(YES)_{90}$ crystal at 20°K

Transition	M	Pattern centers C_o	10^3C_1 ($10^{12}C_3$)	10^8C_2 ($10^{16}C_4$)	N	σ
I 0,3	11	25055.463 ±.101	.2962 ±.0054		7	±.122
I -1,-2	212	24996.409 ±.013	-.0012 ±.0020	-.0730 ±.0070	10	±.016
I 1,2	212	24986.497 ±.006			9	±.019
I 0,3	212	24982.696 ±.007	.0057 ±.0022	-.0634 ±.0002	10	±.007
			(.0074 ±.0046)			
II -1,-2	3123	24980.273 ±.012	-.0034 ±.0020	-.0467 ±.0067	9	±.014
II 0,3	212	24966.567 ±.015	-.0049 ±.0028	.0172 ±.0109	9	±.018
III 1,2	212	24965.372 ±.004	.0006 ±.0002		10	±.006
III 0,3	11	24961.586 ±.018	-.0072 ±.0041	.0207 ±.0196	8	±.020

M	ID	Splittings $10^3 c_1$ ($10^{12} c_3$)	Splittings $10^8 c_2$ ($10^{17} c_4$)	Range kG	N	σ
				0-27.9		
1	GS-EX	.2437 ±.0008	.0180 ±.0040	0-27.9	10	±.011
1	EX-GS	.3232 ±.0014	-.0093 ±.0062	0-27.9	9	±.018
1	EX-GS	.1382 ±.0003		0-27.9	10	±.013
1		.2270 ±.0019	-.0167 ±.0082	0-27.9	9	±.024
2	GS&EX	.2693 ±.0011	-.0163 ±.0050	0-27.9	9	±.014
3		.2705 ±.0017	-.0116 ±.0076	0-27.9	10	±.023
1	EX-GS	.3786 ±.0003		0-24.6	9	±.014
1	EX-GS	.1857 ±.0007		0-27.9	10	±.034
	EX=GS			0-20.0		

Table 32. HpC pattern centers and Zeeman splittings for DyES group J 1.0 mm single crystal at 20°K

Transition	M	Pattern centers C_0	10^3C_1 ($10^{12}C_3$)	10^8C_2 ($10^{16}C_4$)	N	σ
	11	25863.970 ±.066	.0634 ±.0108	.6650 ±.0373	10	±.080
	11	25853.624 ±.633	.2998 ±.0370		8	±.925
I -1,-2	212	25840.691 ±.089	-.0483 ±.0168	.2258 ±.0590	4	±.090
	11	25832.445 ±.569	.2748 ±.0347		8	±.932
	11	25830.407 ±.883	.1842 ±.0443		6	±.592
II -1,-2	43	25824.852 ±.048	.1076 ±.0252	-1.6464 ±.4138	10	±.049
			(.9068) (±.2401)	(-.1979) (±.0446)		
	11	25794.900 ±.694	.4956 ±.1144	-1.4977 ±.3938	10	±.850
I 0,3	11	25789.720 ±.081	.0340 ±.0051		10	±.137
I 1,2	212	25779.751 ±.142	-.0599 ±.0074		6	±.160
III 1,2	212	25757.481 ±.648			2	-
	11	25749.966 ±.054	.0233 ±.0034		10	±.092
	11	25744.192 ±.866	.0519 ±.1282		5	±.167

M	ID	Splittings $10^3 C_1$	Splittings $10^8 C_2$	Range kG	N	σ
				0-27.4		
				0-27.4		
1	GS	.4677 ±.0089	.2612 ±.0354	12.3-27.4	4	±.060
				0-27.4		
				12.3-27.4		
4	EX	.1349 -		27.4	2	-
8	GS	.2485 -		27.4	2	-
				0-27.4		
				0-27.4		
1	GS-EX	.1951 ±.0463	.8669 ±.1991	14.3-27.4	6	±.433
1	GS+EX	.8230 ±.1334		0-27.4	8	±.924
				0-27.4		
				8.2-20.0		

Table 32. (Continued)

Transition	M	Pattern centers C_0	10^3C_1 ($10^{12}C_3$)	10^8C_2 ($10^{16}C_4$)	N	σ
I -1,-2	313	25731.113 ±.058	-.0282 ±.0695	.1258 ±.0328	10	±.071
II -1,-2	414	25714.599 ±.059			3	±.102
I 1,2	212	25708.300 ±.039	-.0076 ±.0082	.1060 ±.0284	7	±.045
I 0,3	212	25701.612 ±.083	.0183 ±.0051		7	±.124
I -1,-2	11	25698.531 ±.066	-.0281 ±.0108	-.0456 ±.0372	10	±.080
III 1,2	423	25687.008 ±.041	.0062 ±.0062	.0623 ±.0214	8	±.045
II -1,-2	212	25682.153 ±.169	.0111 ±.0286		3	±.169
II 0,3	11	25683.910 ±.245	-.2020 ±.0139		8	±.277
I 0,3	212	25675.202 ±.315	.0649 ±.0863	-.4063 ±.4944	4	±.315
I 1,2	212	25666.079 ±.070	-.0274 ±.0110	.0523 ±.0373	7	±.077

M	ID	Splittings $10^3 C_1$	$10^8 C_2$	Range kG	N	σ
5	GS-EX	.4120 ±.0141	.1037 ±.0634	0-27.4	10	±.190
4	EX	.0857 -		0-8.2	2	-
8	GS	.2456 -		0-8.2	2	-
1	GS+EX	.6583 ±.0107	.1687 ±.0442	0-27.4	7	±.099
1	GS+EX	.7391 ±.0245	.1514 ±.1041	0-27.4	7	±.284
	GS≅EX			0-27.4		
1	EX	.2265 ±.0085	-.2388 ±.0352	0-27.4	7	±.090
5	GS	.6818 ±.0193	-.0973 ±.0776	0-27.4	5	±.158
				-		
				6.1-27.4		
				-		
1	GS-EX	.4384 ±.0024		0-27.4	7	±.091

Table 32. (Continued)

Transition	M	Pattern centers C_0	10^3C_1 ($10^{12}C_3$)	10^8C_2 ($10^{16}C_4$)	N	σ
II 0,3	212	25658.993 ±.070	.0450 ±.0196	.2074 ±.1193	5	±.070
III 0,3	11	25654.087 ±.068	-.3122 ±.0116		3	±.070
III 1,2	4A11	25644.888 ±.016	.0007 ±.0030	-.0514 ±.0117	9	±.019
II -1,-2	313	25632.488 .187	-.1079 ±.1043	1.7563 ±1.2646	4	±.187

M	ID	Splittings $10^3 C_1$	$10^8 C_2$	Range kG	N	σ
1	GS-EX	.1922 ±.0147	.1710 ±.1036	0-16.3	5	±.066
				0-8.2		
4	EX	.0717 ±.0032	.0309 ±.0163	0-24.6	9	±.037
8	GS	.6435 ±.0056	.0502 ±.0288	0-24.6	9	±.065
3		.5646 ±.0877	-1.5107 ±.4704	0-20.0	3	±.223
5	GS+EX	.7843 ±.0137		0-8.2	4	±.151

Table 33. HsC pattern centers and Zeeman splittings for DyES group_J 1.0 mm single crystal at 20°K
$\phi_m = \phi$

Transition	M	Pattern centers C_o	$10^3 C_1$	$10^8 C_2$	N	σ
	11	25863.952 ±.468	.1120 ±.0336		9	±.752
	11	25853.763 ±.256	.1313 ±.0283		5	±.332
I -1,-2	323	25838.430 ±1.763	.2969 ±.1883	-.5786 ±.4700	6	±.247
II -1,-2	212	25825.290 ±.182	-.0528 ±.0115		10	±.309
	313	25797.023 ±.339	-.0430 ±.0185		3	±.343
I 0,3	11	25789.689 ±.084	.0294 ±.0138		10	±.102
	11	25778.779 ±.111			7	±.294
	11	25777.464 ±.500			5	±.111
	212	25749.543 ±.656	.2416 ±.1056	-.7307 ±.3644	7	±.715
I -1,-2 IV 0,3	212	25731.064				
	11	25726.854 ±.291	-.0870 ±.0209		9	±.468

M	ID	Splittings 10^3C_1	Splittings 10^8C_2	Range kG	N	σ
				0-24.6		
				0-14.3		
1		.2183 ±.0361	-.5354 ±.1585	12.3-27.5	6	±.399
3	EX	.5426 ±.0616	-.7646 ±.2708	12.3-27.5	6	±.682
1	EX-GS	.0008 ±.0475	.2209 ±.2134	0-27.5	10	±.641
5		.5981 -	-1.0219 -	20.0-24.6	3	-
				0-27.5		
				0-16.3		
				12.3-24.6		
1		.5209 ±.0739	-1.8030 ±.3186	0-27.5	7	±.780
1		-.1012 ±.0240	.5388 ±.1081	0-27.5	10	±.325
				0-24.6		

Table 33. (Continued)

Transition	M	Pattern centers c_0	$10^3 c_1$	$10^8 c_2$	N	σ
II -1,-2	423	25714.860 ±.109	-.0421 ±.0069		10	±.186
III -1,-2	11	25709.558 ±.074			2	±.104
I 1,2	11	25707.436 ±.113			2	±.160
I 0,3	11	25701.752 ±.169	-.0010 ±.0278	.2968 ±.0956	10	±.207
I -1,-2	11	25698.409 ±.098	.0877 ±.0133		5	±.122
III 1,2	3123	25686.991 ±.151	-.0153 ±.0211	.2010 ±.0722	7	±.152
II -1,-2	2-	25682.180			1	
I 0,3	11	25675.144 ±.206	.0840 ±.0172		8	±.306
I 1,2	212	25665.835 ±.109	.0353 ±.0144	.1472 ±.0420	8	±.053
II 0,3	313	25659.066 ±.098	.0249 ±.0207	-.2979 ±.0987	7	±.103

M	ID	Splittings $10^3 c_1$	Splittings $10^8 c_2$	Range kG	N	σ
3	EX	.0382 ±.0038		0-27.5	9	±.219
7	GS	.4088 ±.0268	-.3964 ±.1259	0-27.5	9	±.419
				0-4.1		
				0-4.1		
				0-27.4		
				0-12.3		
2	GS&EX	.0925 ±.0046		0-27.5	7	±.224
4	GS&EX	.0909 ±.0052		0-27.5	10	±.364
				0		
				0-20.0		
1	GS+EX	.1854 ±.0081	.0806 ±.0004	6.2-27.5	8	±.105
1	EX	-.0543 ±.0292	.4571 ±.1785	6.2-20.0	6	±.233
3	GS	.3708 ±.0072		6.2-20.0		±.243

Table 33. (Continued)

Transition	M	Pattern centers C_o	$10^3 C_1$	$10^8 C_2$	N	σ
III 0,3	212	25654.152 ±.156	-.0269 ±.2456		3	±.070
I -1,-2	11	25649.082 ±.212	.0466 ±.0133		8	±.355
III 1,2	4A11	25644.941 .089	-.0297 ±.0128	-.0820 ±.0435	6	±.090
II -1,-2	323	25629.252 .012	.2746 ±.1285	-.8456 ±.3174	5	±.164
IV 0,3	11	25616.058 ±.265			5	±.593

M	ID	Splittings 10^3C_1	10^8C_2	Range kG	N	σ
1		.0644 ±.0022	-.1405 ±.0305	4.1-8.2	3	±.005
				0-27.5		
4	GS	.0165 ±.0147	.2462 .0630	0-27.5	6	±.156
8	EX	.1656 ±.0065	.0648 ±.0281	0-27.5	6	±.070
1	EX	.0320 ±.0249		12.3-20.0	4	±.797
3		.5861 ±.0581	-.7871 .2631	12.3-27.5	5	±.636
				0-12.3		

Table 34. HpC pattern centers and Zeeman splittings for DyES group J .098 mm single crystal at 20°K

Transition	M	Pattern centers C_o	10^3C_1	10^8C_2	N	σ
I -1,-2	212	25730.975 ±.048			5	±.107
II -1,-2	212	25714.745 ±.043	-.0051 ±.0095	.0524 ±.0492	5	±.043
I 1,2	212	25708.289 ±.018	.0011 ±.0029	.0460 ±.0102	10	±.021
I 0,3	212	25701.681 ±.028			5	±.062
I -1,-2	11	25698.529 ±.056	-.0504 ±.0168	.1545 ±.1116	5	±.056
III 1,2	423	25687.064 ±.069	.0144 ±.0040		8	±.092
II -1,-2	11	25682.224 ±.208	-.0973 ±.0482		3	±.215
I 0,3	212	25675.010 ±.029	-.0019 ±.0045	-.0608 ±.0156	9	±.032
I 1,2	212	25665.950 ±.024	-.0045 ±.0045	-.0212 ±.0174	8	±.029
II 0,3	212	25658.892 ±.077	-.0075 ±.0049		5	±.078
III 1,2	323	25644.896 ±.043	-.0043 ±.0072	-.0301 ±.0251	10	±.052

M	ID	Splittings $10^3 c_1$	Splittings $10^8 c_2$	Range kG	N	σ
1	GS-EX	.4350 ±.0100	.0484 ±.0481	12.6-24.6	5	±.080
1	GS-EX	.1779 ±.0171	.1603 ±.1006	12.6-20.0	5	±.092
1	GS+EX	.6768 ±.0044	.0518 ±.0201	0-26.9	10	±.058
1	GS+EX	.6304 ±.0242	1.1663 ±.1937	6.2-14.3	5	±.113
	GS≅EX			0-14.3		
1	EX	.1699 ±.0022		0-26.9	6	±.093
5	GS	.6628 ±.0056		0-26.9	7	±.236
				0-6.2		
1	GS-EX	.4468 ±.0071	.0902 ±.0323	0-26.9	9	±.091
1	GS-EX	.4130 ±.0019		0-24.6	8	±.070
1	GS-EX	.1965 ±.0091	.1540 ±.0449	0-24.6	5	±.080
1	EX	.0837 ±.0032		16.3-26.9	4	±.128
5	GS	.6576 ±.0056		16.3-26.9	4	±.222

Table 35. HsC pattern centers and Zeeman splittings for DyES group_J .098 mm single crystal at 20°K
$\phi_m = \bar{\phi}$

Transition	M	Pattern centers C_o	$10^3 C_1$ ($10^{12} C_3$)	$10^8 C_2$ ($10^{16} C_4$)	N	σ
I 0,3	11	25790.028 ±.079	.0029 ±.0132	.2459 ±.0460	10	±.096
	11	25752.768 ±3.367	-.8452 ±.7176	5.2173 ±3.4839	4	±.418
I -1,-2	11	25730.936 ±.086	.0005 ±.0144	.2309 ±.0502	10	±.105
II -1,-2	4A11	25714.803 ±.014	-.0194 ±.0046	-.1901 ±.0346	5	±.014
I 1,2	212	25708.336 ±.076	.0253 ±.0117	.3949 ±.0402	9	±.083
I 0,3	22	25701.748 ±.047	-.0186 ±.0153	.5314 ±.1373	10	±.049
			(-.0657) (±.0334)			
I -1,-2	11	25698.445 ±.151	.0679 ±.0188		4	±.195
III 1,2	313	25687.138 ±.200			1	±.200
I 0,3	11	25675.072 ±.017	-.0097 ±.0056	.7405 ±.0502	10	±.018
			(-.0658) (±.0122)			

M	ID	Splittings 10^3C_1 ($10^{12}C_3$)	Splittings 10^8C_2 ($10^{17}C_4$)	Range kG	N	σ
				0-26.9		
				6.2-14.3		
				0-26.9		
4	EX	.0207 ±.0074		0-12.6	5	±.124
8	GS	.3127 ±.0108	.3470 ±.1018	0-12.6	5	±.050
1	EX	.1262 ±.0111	.1463 ±.0503	0-26.9	9	±.141
				20.0-26.9		
				0-14.3		
5		.2864 ±.0593	-.5161 ±.3560	0-20.0	6	±.408
				0-26.9		

Table 35. (Continued)

Transition	M	Pattern Centers C_o	$10^3 C_1$ ($10^{12} C_3$)	$10^8 C_2$ ($10^{16} C_4$)	N	σ
I 1,2	4A11	25665.949 ±.112	.0081 ±.0135	.2188 ±.0371	7	±.033
II 0,3	212	25658.780 ±.081	.0277 ±.0125	-.2459 ±.0430	9	±.089
III 0,3	11	25652.862 ±.527	.0887 ±.0502	-.2099 ±.1160	4	±.027
III 1,2	423	25645.998 ±.128	-.0554 ±.0073		8	±.170

M	ID	Splittings $10^3 C_1$ ($10^{12} C_3$)	$10^8 C_2$ ($10^{17} C_4$)	Range kG	N	σ
4	GS	-.0079 ±.0042	.1213 ±.0190	8.3-26.9	7	±.050
8	EX	.2039 ±.0028	-.0696 ±.0128	8.3-26.9	7	±.034
1	GS	.3696 ±.0050		0-26.9	9	±.247
				16.3-26.9		
4	GS	.1198 -	-.6215 -	0-12.6	3	-
8	EX	.2796 -	-.8498 -	0-12.6	3	-
9	GS	.1444 ±.0276	-.1514 ±.1243	0-26.9	8	±.329
10	EX	.3995 -	-1.4713 -	0-12.6	3	-

Table 36. HpC pattern centers and Zeeman splittings for DyES group K 1.0 mm single crystal at 20°K

Transition	M	Pattern centers C_o	10^3C_1	10^8C_2	N	σ
	11	26432.995 ±1.568	.3704 ±.0995		9	±2.656
	11	26410.628 ±1.120	-.3045 ±.1845	1.1060 ±.6349	10	±1.371
	11	26383.480 ±.768	.1893 ±.1266	-1.1778 ±.4356	10	±.941
	11	26306.032 ±1.008	.1115 ±.0637		10	±1.713
	11	26285.851 ±1.175	.3695 ±.1936	-.8590 ±.6661	10	±1.439
	212	26266.507 ±.271			1	-
	212	26265.288 ±.081	-.0043 ±.0182	.0797 ±.0689	4	±.081
	11	26245.387 ±.325	.1563 ±.0563	.4635 ±.1924	9	±.392
	212	26244.235 ±.358	-.0881 ±.0525	.3166 ±.1857	6	±.359
	11	26214.029 ±.126	-.1331 ±.0082		9	±.214
	11	26201.224 ±.974	.2850 ±.1604	-2.0605 ±.5521	10	±1.192
	11	26199.490 ±.230	-.0436 ±.0145		10	±.391

M	ID	Splittings $10^3 c_1$	$10^8 c_2$	Range kG	N	σ
				0-27.4		
				0-27.4		
				0-27.4		
				0-27.4		
				0-27.4		
1		.2790 -		27.4	2	-
1		.2493 ±.0452	.1922 ±.1812	20.0-27.4	4	±.217
				0-27.4		
1		.7374 ±.1436	-.9682 ±.6172	14.3-27.4	6	±1.342
				0-27.4		
				0-27.4		
				0-27.4		

Table 36. (Continued)

Transition	M	Pattern centers C_0	$10^3 C_1$	$10^8 C_2$	N	σ
	11	26185.413 ±1.223	-.6332 ±.3752	3.1684 ±2.4447	6	±1.272
	11	26182.743 ±.858	.2804 ±.1413	-1.0390 ±.4864	10	±1.051
	11	26168.597 ±.931	.3033 ±.0668		9	±1.497
	11	26149.809 ±1.200	.1568 ±.0759		10	±2.039

M	ID	Splittings 10^3C_1	Splittings 10^8C_2	Range kG	N	σ
				0-14.3		
				0-27.4		
				0-24.6		
				0-27.4		

Table 37. HsC pattern centers and Zeeman splittings for DyES group K 1.0 mm single crystal at 20°K
$\phi_m = \bar{\phi}$

Transition	M	Pattern centers C_o	$10^3 C_1$	$10^8 C_2$	N	σ
	11	26439.634 ±.066	-.9646 ±.793	3.0298 ±2.1591	7	±2.055
	11	26386.117 ±.013	.3418 ±.0796		10	±2.142
	11	26309.695 ±.537			9	±1.612
	11	26288.062 ±.683	.3260 ±.0427		9	±1.148
	4A11	26265.826 ±.610	.1050 ±.0290		4	.624
	212	26245.836 ±.528	-.1235 ±.0472		7	±.780
	11	26214.095 ±.320	-.0728 ±.0527	.8962 ±.1811	10	±.392
	11	26199.390 ±.247	-.0918 ±.0156		10	±.419
	11	26202.125 ±.771	-.1674 ±.1269	-.6006 ±.4362	10	±.945
	11	26168.516 ±1.107	.2288 ±.1821	-.9925 ±.6261	10	±1.357
	11	26150.801 ±1.445	-.2504 ±.2376	1.3064 ±.8168	10	±1.770
	11	26082.819 ±1.300	-.6026 ±.2258	1.0794 ±.7772	9	±1.575

M	ID	Splittings $10^3 C_1$	$10^8 C_2$	Range kG	N	σ
				8.2-27.5		
				0-27.5		
				0-24.6		
				0-27.5		
5		.0527 ±.0200		20.0-27.5	4	±.839
6		.0888 ±.0235		20.0-27.5	4	±.989
1		.0949 ±.2461	1.9398 ±1.5150	0-20.0	7	±2.100
				0-27.5		
				0-27.5		
				0-27.5		
				0-27.5		
				0-27.5		
				0-27.5		

Table 38. HpC pattern centers and Zeeman splittings for DyES group L .096 mm single crystal at 20°K

Transition	M	Pattern centers C_o	10^3C_1	10^8C_2	N	σ
I -1,-2	212	27477.079 ±.015	-.0138 ±.0021	.0377 ±.0075	7	±.015
II -1,-2	212	27460.803 ±.025	-.0032 ±.0035	.0316 ±.0122	7	±.025
I 0,3	212	27457.454 ±.038	.0053 ±.0022		8	±.050
II 0,3	11	27441.400 ±.074	-.0214 ±.0123	.1036 ±.0429	10	±.090
III 0,3	212	27436.555 ±.088	-.0169 ±.0080		6	±.108
I 1,2	212	27416.408 ±.035	-.0026 ±.0053	.0197 ±.0191	6	±.035
III 1,2	11	27395.118 ±.054	.1239 ±.0029		7	±.064
I 0,3	212	27390.754 ±.057	.0404 ±.0082	-.1792 ±.0285	7	±.058
II 0,3	11	27374.900 ±.286	-.0905 ±.0663		3	±.295
III 0,3	212	27374.779 ±.278	-.5515 ±.0444	1.4553 ±.1772	6	±.279
I -1,-2	212	27354.421 ±.047	.0122 ±.0066	-.0507 ±.0231	7	±.047
II -1,-2	212	27338.199 ±.150	-.0572 ±.0213	.2208 ±.0743	7	±.151

M	ID	Splittings $10^3 c_1$	Splittings $10^8 c_2$	Range kG	N	σ
1	GS-EX	.4066 ±.0066	.0755 ±.0295	12.6-26.9	7	±.071
1	GS+EX	.3687 ±.0010		12.6-26.9	7	±.050
1	GS-EX	.2317 ±.0094	.1271 ±.0423	8.3-26.9	8	±.112
	GS≅EX			0-26.9		
1	GS-EX	.3820 ±.0046		0-16.3	6	±.125
1	GS-EX	.0845 ±.0031	.0792 ±.0136	14.3-26.9	6	±.028
	GS-EX			0-26.9		
1	GS-EX	.3219 ±.0118	-.1865 ±.0525	12.6-26.9	7	±.126
				0-6.2		
1	GS-EX	.4885 ±.0263	-.2169 ±.1304	0-24.6	6	±.231
1	GS-EX	.4080 ±.0169	.2011 ±.0753	12.6-26.9	7	±.181
1	GS-EX	.2914 ±.0276	-.3133 ±.1230	12.6-26.9	7	±.295

Table 39. HsC pattern centers and Zeeman splittings for DyES group_L .098 mm single crystal at 20°K
$\phi_m = \phi$

Transition	M	Pattern centers C_o	$10^3 C_1$ ($10^{12} C_3$)	$10^8 C_2$ ($10^{16} C_4$)	N	σ
I -1,-2	212	27477.037 ±.197	-.0072 ±.0281	.4366 ±.0979	7	±.199
II -1,-2	212	27460.874 ±.029	.1259 ±.0046	-.2869 ±.0160	5	±.029
I 0,3	11	27457.691 ±.203	.0068 ±.0338	.3053 ±.1179	10	±.246
III -1,-2	11	27455.711 ±.020	-.1937 ±.0036	1.0499 ±.0150	4	±.009
II 0,3	212	27441.350 ±.098	-.0251 ±.0101		5	±.115
III 0,3	11	27436.423 ±.129	.0732 ±.0215	-.5624 ±.0749	10	±.157
I 1,2	212	27416.618 ±.071	-.0441 ±.0186	.7788 ±.1354	9	±.022
			(-.0940) (±.0290)			
II 1,2	11	27398.730 ±1.781	.3188 ±.1816	-.5778 ±.4413	4	±.147
III 1,2	11	27395.307 ±.260			4	±.519
I 0,3	11	27391.124 ±.081	-.1450 ±.0174	.8110 ±.0607	4	±.091
II 0,3	212	27373.341 ±.727	.3429 ±.0793	-.6396 ±.2021	4	±.086

M	ID	Splittings $10^3 C_1$ ($10^{12} C_3$)	Splittings $10^8 C_2$ ($10^{17} C_4$)	Range kG	N	σ
1	EX	.2603 ±.0285	-.1915 ±.1268	12.6-26.9	7	±.304
		.3638 ±.0013		12.6-26.9	5	±.054
1	GS			24.6-26.9		
				4.2-20.0		
1	GS	.3498 ±.0134		0-14.3	5	±.290
				0-26.9		
1		.0003 ±.0005		4.2-26.9	9	±.024
				14.3-26.9		
				0-26.9		
				0-26.9		
1		-.0212 ±.0293	.1628 ±.1229	12.6-26.9	4	±.222

Table 39. (Continued)

Transition	M	Pattern centers c_0	$10^3 c_1$ ($10^{12} c_3$)	$10^8 c_2$ ($10^{16} c_4$)	N	σ
III 0,3	11	27369.723 ±.034	.0109 ±.0057	-.0491 ±.0198	10	±.041
I -1,-2	11	27354.467 ±.051	.0249 ±.0033		6	±.083
II -1,-2	3123	27338.253 ±.261	.0594 ±.0371	-.1403 ±.1293	7	±.263

M	ID	Splittings 10^3C_1 ($10^{12}C_3$)	10^8C_2 ($10^{17}C_4$)	Range kG	N	σ
				0-26.9		
				0-8.3		
1	EX	.2076 ±.0192	-.2279 ±.0856	12.6-26.9	7	±.206
3	GS	.2081 ±.0064		12.6-26.9	7	±.309
5	GS+EX	.3658 ±.0096		12.6-26.9	7	±.468

C is the center of gravity of the pattern under consideration in cm^{-1}, S is the splitting in cm^{-1}, and C_k in both cases is the coefficient of the k^{th} power of the external magnetic field strength in Gauss.

The criterion for choosing the "best" polynomial in each case was the standard deviation of its points from those observed in the experiment. If n is the number of observations, m the number of terms in the polynomial, and δx the difference between the observed and calculated points of C or S, the standard deviation is given by

$$s = \sqrt{\frac{\sum_n (\delta x)^2}{n - m}} \quad . \tag{96}$$

Because of the (n - m) factor in the denominator it was felt that this criterion always produced the lowest order polynomial which came closest to representing the "true" behavior of the centers of gravity or of the level splittings. Polynomials with inflection points in the region of experimental magnetic field strengths were rejected because the inflection points were almost always caused by random errors in the measurements and were not a true feature of the magnetic field dependence of the patterns or their splittings.

The first two columns of Tables 21 through 39 identify the initial and final states in the transitions responsible for each Zeeman pattern. As before, the three lowest lying

crystal field levels of the ground term are identified with the Roman numerals assigned by Gramberg, and the final levels are identified with the crystal quantum numbers of Murao, Spedding, and Good. The first digit of the numbers given in column three indicates how many absorption lines were resolved in each Zeeman pattern and the remaining digits tell which absorption lines were used in the determination of the center of gravity of the pattern. The lines in each pattern were labelled 1, 2, 3, 4 in order of decreasing energy, and the lines used in the determination of the center of gravity were carefully chosen to make best use of the experimental data for the pattern under consideration. Thus, if a pattern had four lines, for example, and lines 2 and 3 were not clearly resolved for applied magnetic fields below 15 kG, the lines used for determination of the center of gravity would be lines 1 and 4. Columns four through six give the coefficients of the type 94 polynomial which gave the best least squares fit of the experimental pattern centers as a function of the external magnetic field, column seven indicates the number of magnetic field strengths for which reliable experimental determinations of the center were made, and column eight gives the standard deviation of the centers calculated with the type 94 polynomial from those determined in the experiment.

The remaining columns of the tables have to do with the

Zeeman splittings. The numbers in column nine are code numbers to identify the method by which the Zeeman splittings of the crystal field levels were calculated from the experimental data. The code numbers and corresponding methods for calculation of the splittings of the levels are given in Table 40. The method or methods listed for each splitting were very carefully chosen to make best use of the experimental data for the pattern under consideration, and are thought to be the best methods available in each case. Column ten identifies the ground state or excited state crystal field levels whose Zeeman splittings, or sums or differences of Zeeman splittings, are described by the polynomial coefficients given in columns eleven and twelve. Column thirteen gives the range of magnetic field strengths and column fourteen gives the number of magnetic fields for which reliable determinations of the splittings were made. Column fifteen gives the standard deviation of the values of the splittings calculated from the type 95 polynomial and those determined in the experiment. The standard deviations of the coefficients in the polynomial expressions for the pattern centers and splittings were derived from the variance-covariance matrices used for determination of the coefficients. The method used was the same as that used earlier in this work for analysis of the HsC anisotropy parameters.

Table 40. Code numbers and corresponding methods for calculation of Zeeman splittings. The energies of the absorption lines are $E_1 \geq E_2 \geq E_3 \geq E_4$

Number of lines in the Zeeman pattern	Code number	Calculating method
3	1	(E_1-E_2)
	2	$(E_1-E_3)/2$
	3	(E_2-E_3)
	4	(E_1-E_2) and/or (E_2-E_3)
	5	(E_1-E_3)
4	1	(E_1-E_2)
	2	(E_3-E_4)
	3	(E_1-E_2) and/or (E_3-E_4)
	4	$[(E_1-E_4)-(E_2-E_3)]/2$
	5	(E_1-E_3)
	6	(E_2-E_4)
	7	(E_1-E_3) and/or (E_2-E_4)
	8	$[(E_1-E_4)+(E_2-E_3)]/2$
	9	(E_2-E_3)
	10	(E_1-E_4)

Two words of caution must be given concerning the information in Tables 21 through 39. The first is that all of group K and the high energy portions of most of the other line groups studied had very weak and diffuse absorption lines for which it was extremely difficult to identify the initial and final states. The Zeeman patterns arising from these lines were even more diffuse. The identifications for these patterns are tenuous if they are given at all, for it is not even certain that they arise from purely electronic transitions. Neither thicker crystals nor lower temperatures seemed to help in the measurement of these patterns, so the data given in the tables are probably as good as can be obtained with ordinary photographic techniques. The patterns in question may be recognized in the tables by the large standard deviations obtained for their centers and splittings.

The second word of caution has to do with the interpretation of one line patterns, i.e., absorption lines which do not appear to split under the influence of the applied magnetic field. The rule of thumb followed in this work was that if the polynomial expression for the energy of the one line pattern had a sizeable coefficient for the first power of the magnetic field strength, then it was probably the only allowed line in what was potentially a multiline Zeeman pattern. If the first order coefficient was small, the one line pattern was probably due to a completely unresolved

pattern. Except in the case of the spectra observed at 4.2°K, where parts of the patterns can be absent because of depopulation of the higher energy levels, the one line patterns are not to be relied on very much because of the uncertainty in knowing which type of one line pattern is being considered.

Determination of the Field Dependent Energy Level Scheme

The goal in this stage of the analysis was the determination of an energy level scheme such that the energy differences between the various initial and final Zeeman levels had the same magnetic field dependences as the corresponding absorption lines observed in the experiments. The problem is essentially the same as that encountered earlier in this work when the energy level scheme for the anisotropic HsC Zeeman effect was determined. The only difference is that this time it is the magnetic field dependence of the levels that we are interested in, not the angular dependence. Again only energy differences were observed in the experiments, not absolute energies, so again it was necessary to state side conditions in order to obtain unique solutions for the behavior of the energy levels.

Ordinarily the side conditions would have been specified by assuming that the center of gravity of the levels of an excited term which was energetically well isolated from all other excited terms was independent of the external magnetic

field in both the HsC and HpC cases. This is a good assumption as long as the Zeeman splittings are small compared to the energy between terms, because, according to perturbation theory, the levels of such a term are negligibly affected by magnetic interactions with other terms and its center of gravity is expected to be independent of the magnetic field. In the determination of the energy level scheme this assumption restricts the solutions for the magnetic field shifts of the levels so that the sum of the shifts for all the levels in the isolated term is equal to zero, and it allows the center of gravity of this term to be used as a constant energy reference for measurement of the energies and magnetic field shifts of all the other levels of the configuration.

The large uncertainties in the measured energies of the weak and diffuse absorption lines in the high energy portions of the line groups studied in the present work made it impossible to determine the center of gravity of any of the excited terms with sufficient precision to warrant its use in specifying side conditions. The side conditions were specified instead by assuming that the center of gravity of the two (-1,-2) final levels for the group G Zeeman patterns between 22005 and 22070 cm^{-1} was independent of the external magnetic field strength. The basis for this assumption is the same as in the case of an isolated excited term. The Hamiltonian for the HpC Zeeman effect commutes with the

operator of the C_{3h} point symmetry group, so the two (-1,-2) crystal field levels can only have magnetic interactions with other (-1,-2) levels. Since the nearest (-1,-2) level is some 110 cm^{-1} away and the Zeeman splittings are an order of magnitude smaller, perturbation theory tells us that the center of gravity of these two crystal field levels should be independent of the magnetic field. The situation is similar in the HsC case. The nearest level which can affect the center of gravity of the two (-1,-2) levels in this case is the (0,3) level nearly 60 cm^{-1} away. Again the Zeeman splittings are an order of magnitude smaller, so the center of gravity of the two (-1,-2) levels should be independent of the external magnetic field.

The advantage of using these particular final levels to specify the side conditions was that, since the absorption lines which resulted from transitions to them were quite sharp, their center of gravity could be measured with much better precision than the center of gravity of any of the excited terms. This increased the precision which could be obtained in the determination of the energy level scheme, and the solutions for the magnetic field shifts were restricted just as if the two (-1,-2) levels were a complete set of levels of an isolated excited term. The sum of their magnetic field shifts was restricted to zero for each orientation of the external magnetic field, and their center of

gravity was used as a constant energy reference for determination of the magnetic field shifts of the initial, i.e., ground term, energy levels in each orientation.

The field dependent energy level scheme for the four lowest crystal field levels of the "$^6H_{15/2}$" ground term of Dy^{+3} in DyES is given in Tables 41 and 42 for the HpC case, and in Tables 43 and 44 for the HsC case with $\phi_m = \bar{\phi}$. The zero of energy is the energy of the lowest crystal field level of the ground term in the absence of external magnetic fields, and the centers of gravity and Zeeman splittings as functions of the external magnetic field are summarized, as before, in terms of coefficients for the polynomial equation which gave the best least squares fit of the data. The energy of the $\begin{bmatrix}\text{high}\\\text{low}\end{bmatrix}$ energy branch of each of the levels for an applied magnetic field up to 27.5 kG is equal to the value of the level center polynomial at that field $\begin{bmatrix}\text{plus}\\\text{minus}\end{bmatrix}$ one half the value of the Zeeman splitting polynomial at the same field.

The results given in Tables 41 and 42 were obtained from the polynomial expressions for the centers and splittings of the Zeeman patterns in group G resulting from transitions to the two (-1,-2) levels at 22034.8 and 22063.0 cm^{-1}. These patterns were very sharp and were clearly the best patterns from which to determine the behavior of the ground term levels. In addition, the fact that magnetic dipole transitions contribute to the intensity of the lines in group G made it possible

Table 41. Polynomial expressions for the centers of gravity of the four lowest lying energy levels of the $^6H_{15/2}$ ground term of DyES as a function of the externally applied HpC magnetic field

Level	μ	C_o	10^3C_1	10^8C_2	$10^{12}C_3$	$10^{16}C_4$
I[a]	(0,3)	0	-.0029 ±.0031	+.0076 ±.0106		
II[a]	(1,2)	16.127 ±.033	+.0000 ±.0050	-.0061 ±.0240		
III[a]	(-1,-2)	21.118 ±.033	+.0057 ±.0055	-.3259 ±.0455	+.2804 ±.0277	-.0656 ±.0066
IV[a b]	(0,3)	58.461 ±.069				
I[c]	(0,3)	0				
II[c]	(1,2)	16.133 ±.012				
III[c]	(-1,-2)	21.118 ±.010				

[a]DyES at 20°K.

[b]Determined from group H measurements; field dependence was not measured.

[c]$(DyES)_{10}(YES)_{90}$ at 20°K; zero field measurements only.

Table 42. Polynomial expressions for the Zeeman splittings of the four lowest lying energy levels of the $^6H_{15/2}$ ground term of DyES as a function of the externally applied HpC magnetic field

Level	μ	10^3C_1	10^8C_2	$10^{12}C_3$	$10^{17}C_4$	Splitting for H = 27.5 kG
I[a]	(0,3)	.5149 ±.0005				14.16 cm^{-1}
II[a]	(1,2)	.2761 ±.0026	-.0215 ±.0117			7.43 cm^{-1}
III[a]	(-1,-2)	.6665 ±.0046	-.1623 ±.1280	+.0852 ±.0678	-.1682 ±.1193	17.91 cm^{-1}
IV[a]	(0,3)	.8199 ±.0239				22.55 cm^{-1}
I[b]	(0,3)	.5276 ±.0004				14.51 cm^{-1}
I[c]	(0,3)	.5130 ±.0014	+.0017 ±.0064			14.12 cm^{-1}
II[c]	(1,2)	.2702 ±.0012	-.0118 ±.0048			7.34 cm^{-1}
III[c]	(-1,-2)	.6501 ±.0015	-.0075 ±.0061			17.82 cm^{-1}

[a]DyES at 20°K.

[b]DyES at 4.2°K.

[c]$(DyES)_{10}(YES)_{90}$ at 20°K; determined in group I.

Table 43. Polynomial expressions for the centers of gravity of the four lowest lying energy levels of the $^6H_{15/2}$ ground term of DyES as a function of the externally applied HsC magnetic field $\phi_m = \overline{\phi}$

Level	μ	C_o	10^3C_1	10^8C_2	$10^{12}C_3$	$10^{16}C_4$
I[a]	(0,3)	0	+.0158 ±.0130	-.7809 ±.2283	+.2588 ±.1364	-.0475 ±.0255
II[a]	(1,2)	16.113 ±.036	-.0160 ±.0076	+.5749 ±.0640	-.1522 ±.0151	
III[a b]	(-1,-2)	20.979 ±.054	+.0366 ±.0224	-.2846 ±.2565	+.2588 ±.1364	-.0457 ±.0255
IV[a]	(0,3)	58.548 ±.082	-.0048 ±.0247	-.2219 ±.2843	+.1987 ±.1421	-.0475 ±.0255
I[c]	(0,3)	0	+.0351 ±.0102	-1.0349 ±.1576	+.3601 ±.0783	-.0585 ±.0126

[a]DyES at 20°K.

[b]The useful range of this polynomial is zero to 14.3 kG only.

[c]DyES at 4.2°K.

Table 44. Polynomial expressions for the Zeeman splittings of the four lowest lying energy levels of the $^6H_{15/12}$ ground term of DyES at 20°K as a function of the externally applied HsC magnetic field $\phi_m = \bar{\phi}$

Level	μ	10^3C_1	10^8C_2	$10^{12}C_3$	Splitting for H = 27.5 kG
I	(0,3)	-.0190 ±.0066	+.2303 ±.0695	-.0182 ±.0174	0.84 cm^{-1}
II	(1,2)	+.3609 ±.0050	+.2630 ±.0535	-.2109 ±.0138	7.528 cm^{-1}
III	(-1,-2)	+.0238 ±.0044	+.0409 ±.0195		0.96 cm^{-1}
IV	(0,3)	No splitting observed			

to obtain direct rather than indirect measurements of the Zeeman splittings of the levels involved. The latter fact is especially important because it completely eliminated the possibility of error in the identification of the splittings.

The results in Tables 43 and 44 for the HsC behavior of the I and II ground term levels were also derived from polynomial expressions for the centers and splittings of the group G Zeeman patterns resulting from transitions to the same two (-1,-2) levels. However, in the case of the II level, it was necessary to allow inflection points in the curves of energy versus magnetic field and splittings versus magnetic field in order to obtain polynomial expressions which gave reasonable fits of the experimental data. It was later determined theoretically, as will be shown in a later section, that inflection points should be expected for both the II and III levels in the HsC case, but the fit of the experimental data for the III level did not improve when inflection points were allowed. The results for the HsC behavior of the III level were derived from the polynomial expressions for the I to (0,3) and III to (0,3) Zeeman patterns at 24961.8 and 24982.8 cm^{-1} in group I because the latter pattern was the only really good example observed in this work of a transition originating from the III level.

Once the magnetic field dependence was known for the ground term energy levels and their splittings, it was a

simple matter to determine the field dependent energy level scheme for the main lines of the line groups studied in this work. Polynomial expressions for the Zeeman splittings of most of the crystal field levels were already known, or could be calculated, from the right hand sides of Tables 21 through 39, and expressions for the center of gravity of each of the final crystal field levels were obtained by adding the polynomial expression for the behavior of the appropriate crystal field level in the ground term to the polynomial expression for the behavior of the center of gravity of the Zeeman patterns given in the left hand sides of the tables.

In general several expressions were obtained for the magnetic field dependence of each of the final levels. However, rather than average the results, the field dependence reported was obtained from the sharpest and most accurately determined Zeeman pattern to which it contributed. Coefficients for the polynomial expressions for the centers of gravity and Zeeman splittings of the final levels for the main lines in groups G through L are listed in Tables 45 through 54. The format for these tables is similar to that used before. The only thing new is the plus or minus sign immediately following the μ values in the tables for the HpC Zeeman effect. As pointed out in the THEORY section, μ is still a good quantum number in the HpC case, and the plus

Table 45. HpC level centers and Zeeman splittings for DyES group G

	Level center					Zeeman splitting	
μ Value	C_o	10^3C_1	10^8C_2	$10^{12}C_3$	$10^{16}C_4$	10^3C_1	10^8C_2
(1,2)+	22238.046 ±.107	+.0971 ±.0197	-.4232 ±.0713			.1528 ±.0960	
(0,3)-	22175.434[a] ±.130					.1549 ±.0176	
(-1,-2)+	22158.730 ±.179	-.0091 ±.0248	+.1462 ±.0829			.0409 ±.0246	
(1,2)+	22122.615 ±.024	+.0032 ±.0034	-.0519 ±.0130			.1282 ±.0081	-.2424 ±.0742
(0,3)+	22106.292 ±.030	+.0124 ±.0055	-.0909 ±.0253			.3072 ±.0127	-.2327 ±.0746
(-1,-2)+	22062.955 ±.025	-.0074 ±.0035	+.1512 ±.0121			.4143 ±.0014	-.0611 ±.0084
(-1,-2)-	22034.803 ±.048	+.0073 ±.0068	-.1511 ±.0230			.5784 ±.0036	-.1595 ±.0164

[a]The field dependence of this level was not determined.

Table 46. HsC level centers and Zeeman splittings for DyES group G
$\emptyset_m = \overline{\emptyset}$

	Level center					Zeeman splitting	
μ Value	C_o	10^3C_1	10^8C_2	$10^{12}C_3$	$10^{16}C_4$	10^3C_1	10^8C_2
(1,2)	22237.004[a] ±1.327					-[b]	
(0,3)	22202.850[a] ±.155					-[b]	
(0,3)	22174.566 ±.063	+.0338 ±.0188	-.5891 ±.2335	+.2588 ±.1364	-.0475 ±.0255	.0220 ±.0263	+.3301 ±.1059
(-1,-2)	22158.624 ±.289	+.0183 ±.0191	-.0666 ±.0208			.3614 ±.0160	
(1,2)	22122.772 ±.077	+.0145 ±.0176	-.1848 ±.2341	+.2588 ±.1364	-.0475 ±.0255	.4441 ±.0152	-.1633 ±.0715
(0,3)	22106.275 ±.060	+.0241 ±.0155	-.6049 ±.2300	+.2588 ±.1364	-.0475 ±.0255	No splitting observed	
(-1,-2)	22062.954 ±.051	-.0256 ±.0289	+.4807 ±.5109	-.2587 ±.3050	+.0474 ±.0569	.1382 ±.0021	-.0324 ±.0101
(-1,-2)	22034.770 ±.037	+.0256 ±.0135	-.4807 ±.2285	+.2588 ±.1364	-.0475 ±.0255	.1634 ±.0014	-.0260 ±.0063

[a]The magnetic field dependence was not determined.

[b]No splitting was observed for these levels.

Table 47. HpC level centers and Zeeman splittings for DyES group H

	Level center					Zeeman splitting	
μ Value	C_o	10^3C_1	10^8C_2	$10^{12}C_3$	$10^{16}C_4$	10^3C_1	10^8C_2
(-1,-2)-	23485.042 ±.046	+.0179 ±.0053	-.0061 ±.0240			.0601 ±.0046	-.0426 ±.0202
(0,3)-	23467.512 ±.039	-.0060 ±.0078	+.0458 ±.0402			.2335 ±.0074	-.6604 ±.0425
(1,2)+	23461.776 ±.055	-.0070 ±.0084	+.1164 ±.0284			-.0057 ±.0040	+.0419 ±.0183
(0,3)+	23439.432[a] ±.038					.4531 ±.0040	
(1,2)+	23429.153 ±.030	-.0076 ±.0046	-.0646 ±.0158			.1187 ±.0010	
(-1,-2)+	23390.989 ±.053	-.0028 ±.0081	+.0288 ±.0324			.6438 ±.0037	-.0024 ±.0164

[a]The field dependence of this level was not determined.

Table 48. HsC level centers and Zeeman splittings for DyES group H
$\phi_m = \bar{\phi}$

μ Value	Level center					Zeeman splitting	
	C_o	$10^3 C_1$	$10^8 C_2$	$10^{12} C_3$	$10^{16} C_4$	$10^3 C_1$	$10^8 C_2$
(-1,-2)	23485.330 ±.132	-.0288 ±.0324	+.1425 ±.3035	+.1787 ±.1425	-.0475 ±.0255	.3455 ±.0045	-.2102 ±.0205
(0,3)	23467.282 ±.171	+.0719 ±.0132	-.0666 ±.0208			-[a]	
(1,2)	23461.914 ±.108	+.0010 ±.0196	-.6596 ±.2324	+.2588 ±.1364	-.0475 ±.0255	.3079 ±.0139	-.2951 ±.0626
(0,3)	23439.402 ±.063	+.0092 ±.0226	-.0719 ±.2814	+.1987 ±.1421	-.0475 ±.0255	-[b]	
(1,2)	23429.121 ±.068	+.0243 ±.0163	-.5578 ±.2307	+.2588 ±.1364	-.0475 ±.0255	.3035 ±.0105	-.2027 ±.0473
(-1,-2)	23390.983 ±.064	-.0237 ±.0226	-.1017 ±.2832	+.1994 ±.1425	-.0475 ±.0255	-[b]	

[a]The splitting polynomial for this level was not determined. The splitting is on the order of 2 cm^{-1} at 27.5 kG.

[b]No splitting was observed for these levels.

Table 49. HpC level centers and Zeeman splittings for DyES group I

μ Value	Level center					Zeeman splitting	
	C_o	10^3C_1	10^8C_2	$10^{12}C_3$	$10^{16}C_4$	10^3C_1	10^8C_2
(0,3)+	25156.879[a] ±.302					.0900 ±.0196	
(0,3)-	25143.331[a] ±.097					.0958 ±.0220	
(-1,-2)+	25137.974[a] ±.221					_[b]	
(0,3)+	25055.502[a] ±.214					+.0201 ±.0110	
(-1,-2)+	25052.490[a] ±.196					+.0037 ±.0238	+.2960 ±.1067
(-1,-2)-	24996.655 ±.065	-.0266 ±.0047	+.0076 ±.0106			+.2742 ±.0038	-.0366 ±.0167
(1,2)-	24986.599 ±.040	-.0020 ±.0064	-.3093 ±.0469	+.2804 ±.0277	-.0656 ±.0066	+.8138 ±.0191	+.0935 ±.0780
(0,3)-	24982.709 ±.042	+.0088 ±.0084	-.0737 ±.0464			+.6742 ±.0101	-.1686 ±.0713

[a]The field dependence of these levels was not determined.

[b]This splitting was not well resolved.

Table 50. HsC level centers and Zeeman splittings for DyES group I
$\phi_m = \overline{\phi}$

μValue	Level center					Zeeman splitting	
	C_o	10^3C_1	10^8C_2	$10^{12}C_3$	$10^{16}C_4$	10^3C_1	10^8C_2
(-1,-2)	24996.529 ±.073	+.0253 ±.0195	-.0857 ±.2470	+.2776 ±.1378	-.0475 ±.0255	+.5089 ±.0040	-.5043 ±.0191
(1,2)	24986.347 ±.062	+.1497 ±.0159	-.5628 ±.2302	+.2588 ±.1364	-.0475 ±.0255	+.4548 ±.0070	-.6507 ±.3080
(0,3)[a]	24982.781 ±.041	-.0088 ±.0163	-1.2054 ±.2375	+.2588 ±.1364	-.0475 ±.0255	+.0238 ±.0044	+.0409 ±.0195

[a]Interferences with other levels made it impossible to determine these polynomials for fields greater than 14.3 kG.

Table 51. HpC level centers and Zeeman splittings for DyES group J

μ Value	Level center					Zeeman splitting	
	C_o	10^3C_1	10^8C_2	$10^{12}C_3$	$10^{16}C_4$	10^3C_1	10^8C_2
	25863.970 ±.070	+.0605 ±.0112	+.6726 ±.0387				
	25853.624[a] ±.633						
(-1,-2)	25840.691 ±.092	-.0512 ±.0171	+.2334 ±.0599			-[b]	
(0,3)-	25789.720 ±.084	+.0311 ±.0060	+.0076 ±.0106			+.5149 -	
(1,2)	25779.481 ±.144	-.0628 ±.0080	+.0076 ±.0106			+.3198 ±.0463	-.8669 ±.1991
(-1,-2)-	25731.113 ±.062	-.0311 ±.0696	+.1334 ±.0345			+.1029 ±.0141	-.1037 ±.0634
(1,2)+	25708.300 ±.045	-.0105 ±.0088	+.1136 ±.0303			+.2265 ±.0085	-.2388 ±.0352

[a]The field dependence of this level was not determined.

[b]No splitting was observed for this level.

Table 51. (Continued)

μ Value	Level center					Zeeman splitting	
	C_o	10^3C_1	10^8C_2	$10^{12}C_3$	$10^{16}C_4$	10^3C_1	10^8C_2
(0,3)+	25701.612 ±.086	+.0154 ±.0060	+.0076 ±.0106			+.2242 ±.0245	+.1514 ±.1041
(-1,-2)-	25698.531 ±.070	-.0310 ±.0112	-.0380 ±.0387			+.5149 -	
(0,3)-	25675.120 ±.077	+.0450 ±.0202	+.2013 ±.1217			+.0839 ±.0149	-.1925 ±.1044
(1,2)-	25666.079 ±.073	-.0303 ±.0114	±.0599 ±.0387			+.0717 ±.0032	+.0309 ±.0163
(-1,-2)+	25648.615 ±.190	-.1079 ±.1044	±1.7502 ±1.2649			+.5141[c] ±.0150	

[c]This is an estimate. The splitting was not clearly resolved.

Table 52. HsC level centers and Zeeman splittings for DyES group J
$\emptyset_m = \overline{\emptyset}$

μ Value	Level center					Zeeman splitting	
	C_o	10^3C_1	10^8C_2	$10^{12}C_3$	$10^{16}C_4$	10^3C_1	10^8C_2
	25863.952 ±.470	+.1278 ±.0361	-.7809 ±.2283	+.2588 ±.1364	-.0475 ±.0255	-[b]	
	25853.763[a] ±.257					-[b]	
(-1,-2)	25838.430[a] ±1.765					+.5426 ±.0616	-.7646 ±.2708
	25797.023[a] ±.340					-[b]	
(0,3)	25789.689 ±.088	+.0452 ±.0189	-.7809 ±.2283	+.2588 ±.1364	-.0475 ±.0255	-[b]	
(1,2)	25778.779 ±.114	+.0158 ±.0130	-.7809 ±.2283	+.2588 ±.1364	-.0475 ±.0255	-[b]	
	25777.464[a] ±.500					-[b]	
	25749.543[a] ±.656					-[b]	

[a]The field dependence of these levels was not determined.

[b]No splitting was observed for these levels.

Table 52. (Continued)

	Level center					Zeeman splitting	
μ Value	C_o	10^3C_1	10^8C_2	$10^{12}C_3$	$10^{16}C_4$	10^3C_1	10^8C_2
(-1,-2)	25730.936 ±.090	±.0163 ±.0194	-.5500 ±.2337	+.2588 ±.1364	-.0475 ±.0255	+.0207[c] +.0074	
(1,2)	25708.336 ±.080	+.0411 ±.0175	-.3860 ±.2317	+.2588 ±.1364	-.0475 ±.0255	+.1262 ±.0111	+.1463 ±.0503
(0,3)	25701.748 ±.054	-.0028 ±.0201	-.2495 ±.2665	+.1931 ±.1404	-.0475 ±.0255	-[b]	
(-1,-2)	25698.409 ±.101	+.1035 ±.0184	-.7809 ±.2283	+.2588 ±.1364	-.0475 ±.0255	-[b]	
(0,3)	25675.072 ±.031	+.0061 ±.0141	-.0404 ±.2337	+.1930 ±.1371	-.0475 ±.0255	-[b]	
(1,2)	25665.949 ±.115	+.0239 ±.0187	-.5621 ±.2313	+.2588 ±.1364	-.0475 ±.0255	+.2039 ±.0028	-.0696 ±.0128
(-1,-2)	25649.082 ±.215	+.0624 ±.0188	-.7809 ±.2283	+.2588 ±.1364	-.0475 ±.0255	-[b]	

[c]This polynomial applies only for H = 12.6 kG.

Table 53. HpC level centers and Zeeman splittings for DyES group L

μ Value	Level center					Zeeman splitting	
	C_o	10^3C_1	10^8C_2	$10^{12}C_3$	$10^{16}C_4$	10^3C_1	10^8C_2
(-1,-2)-	27477.079 ±.027	-.0167 ±.0037	+.0453 ±.0130			+.0926 ±.0028	+.0215 ±.0117
(0,3)-	27457.454 ±.044	+.0024 ±.0038	+.0076 ±.0106			+.2832 ±.0094	-.1271 ±.0423
(1,2)-	27416.408 ±.041	-.0055 ±.0061	+.0273 ±.0218			+.4304 ±.0031	-.0792 ±.0136
(0,3)-	27390.754 ±.061	+.0375 ±.0088	-.1716 ±.0304			+.1930 ±.0118	+.1865 ±.0525
(-1,-2)-	27354.421 ±.052	+.0093 ±.0073	-.0431 ±.0254			+.1069 ±.0169	-.2011 ±.0753

Table 54. HsC level centers and Zeeman splittings for DyES group L
$\phi_m = \bar{\phi}$

μ Value	Level center					Zeeman splitting	
	C_o	$10^3 C_1$	$10^8 C_2$	$10^{12} C_3$	$10^{16} C_4$	$10^3 C_1$	$10^8 C_2$
(-1,-2)	27477.037 ±.199	+.0086 ±.0310	-.3443 ±.2484	+.2588 ±.1364	-.0475 ±.0255	±.2603 ±.0285	-.1915 ±.1268
(0,3)	27457.691 ±.205	+.0226 ±.0362	-.4756 ±.2569	+.2588 ±.1364	-.0475 ±.0255	-[b]	
(1,2)	27416.618 ±.076	-.0283 ±.0227	-.0021 ±.2655	+.1648 ±.1396	-.0475 ±.0255	-[b]	
(0,3)	27390.702 ±.064	+.0475 ±.0231	-.3337 ±.2573	+.2588 ±.1364	-.0475 ±.0255	-[b]	
(-1,-2)	27354.467[a] ±.057	+.0407 ±.0134	-.7809 ±.2283	+.2588 ±.1364	-.0475 ±.0255	+.2076 ±.0192	-.2279 ±.0856

[a]This polynomial applies only for H = 12.6 kG.

[b]No splitting was observed for these levels.

or minus sign tells whether the state with μ equal to 2, 3, or -2 increases or decreases in energy with increasing external magnetic field. The μ = 2, 3, and -2 states correspond to μ = +1/2, +3/2, and 5/2 states when Hellwege's crystal quantum numbers are used, so the signs used in the tables are consistent with the notation used by Gramberg (84).

No success was obtained in attempts to determine the field dependent energy level scheme for group K and for some of the very weak and diffuse absorption lines in the high energy portions of groups I, J, and L, because the rather large experimental uncertainties in the centers of gravity and Zeeman splittings of these lines made it impossible to confirm any of the many energy level schemes which were tried.

DISCUSSION

The Ground Term

The "$^6H_{15/2}$" ground term of DyES has been studied extensively in previous works.* Hill and Wheeler (108) studied the far infrared spectrum and Zeeman effect of transitions between levels of the ground term at 1.6°K and for magnetic fields up to 80 kG, Baker and Bleaney (109) determined the splitting factors and approximate energies of some of the low lying levels from paramagnetic resonance experiments, and Meyer and Smith (110) measured the magnetic specific heat between 2 and 20°K. Cooke et al. (111) measured both the magnetic specific heat and magnetic susceptibility in the neighborhood of liquid helium temperature, and the magnetic susceptibility from 14 to 20°K. Although the methods employed in these works have been useful in exploring various features of the ground term, none of them furnishes as much high precision data on the behavior of the ground term levels under various conditions as can be obtained from measurements of the visible absorption spectra. For this reason the previous work which is most pertinent to the present discussion is Gramberg's (84). He determined the zero field energies of the five lowest crystal field levels at 4.2 and 58°K from absorption spectra, and measured the HpC and HsC Zeeman splitting factors for the three lowest levels at 4.2°K. Even more precise and detailed information was obtained in the

present investigation.

Zero magnetic field

The energy levels of DyES at 4.2 and 58°K as determined by Gramberg are compared with the results of the present work for DyES and $(DyES)_{10}(YES)_{90}$ at 20°K in Table 55. The agreement is excellent, and although it appears that perhaps the energy of the II level decreases with increasing temperature, there is no strong evidence that the energies of the levels change with either temperature or dilution with yttrium ethylsulfate. No transitions were observed from the V level in the present work, but Hill and Wheeler place this level at approximately 70 cm^{-1} at 1.6°K.

HpC Zeeman splittings

It is clear from the last column of Table 42 that the HpC Zeeman splittings of the ground term crystal field levels depend to a small extent on both the temperature and the concentration of DyES in the sample for an external magnetic field of 27.5 kG. As has been pointed out by Gramberg, this is due to the fact that the magnetic field at a dysprosium ion site in a crystal is not the same as the external magnetic field. Thus if one wishes to compare the magnetic splittings of dysprosium ion energy levels at various temperatures and in different crystalline samples, it is important to compare splittings for the same value of the magnetic field at the

Table 55. Measured energies of some of the low lying crystal field levels of the $^6H_{15/2}$ ground term of DyES between 4.2 and 58°K

Level	μ	DyES[a]			$(DyES)_{10}(YES)_{90}$
		4.2°K	20°K	58°K	20°K
I	(0,3)	0	0	0	0
II	(1,2)	16.03 ±.05	16.127 ±.033	16.1 ±.2	16.133 ±.012
III	(-1,-2)	21.20 ±.10	21.118 ±.033	20.4 ±.2	21.118 ±.010
IV	(0,3)	-	58.461 ±.069	58.9 ±.2	-
V	(-1,-2)	-	-	68.1 ±.2	-

[a]The results listed for 4.2° and 58°K are from Gramberg (84).

dysprosium ion site.

The ordinary procedure for calculating the magnetic field within a crystal is to assume that the crystal lattice can be replaced by a homogeneous continuum with magnetization M, and that the crystal shape can be approximated by an ellipsoid. The internal magnetic field is then given by

$$H_{int} = H_{ext} - dM, \tag{97}$$

where H_{ext} is the external magnetic field, and d is a demagnetization factor which depends on the shape of the sample (112). The magnetization is

$$M = \chi H_{int}, \tag{98}$$

where χ is the magnetic susceptibility, so

$$H_{int} = H_{ext}/(1 + d\chi). \tag{99}$$

As pointed out by Lorentz (3), however, it is not accurate to replace the near neighbors of an ion in a lattice by a homogeneous continuum. Within some small sphere about each ion it is necessary to take into account the actual locations of the magnetic dipoles associated with the neighboring ions, while outside the sphere the ion is unable to distinguish between the effects of magnetic ions in the lattice and the effects of the assumed continuous medium. Using this approach Gramberg found that the magnetic field at the site of a

dysprosium ion in the ethylsulfate was given by

$$H_{ion} = H_{int}(1 + 0.65\ \chi) = H_{ext}(1 + 0.65\ \chi)/(1 + d\ \chi) \qquad (100)$$

in the HpC case, and by

$$H_{ion} = H_{int}(1 + 0.17\ \chi) = H_{ext}(1 + 0.17\ \chi)/(1 + d\ \chi) \qquad (101)$$

in the HsC case. Since the susceptibility depends on the magnetic field strength as well as on the temperature, a comparison of Zeeman splittings is normally done in the limit as the field approaches zero. The splittings are then given by

$$S = C_1' H_{ion}, \qquad (102)$$

where

$$C_1' = C_1(1 + d\ \chi)/(1 + 0.65\ \chi) \qquad (103)$$

in the HpC case, and

$$C_1' = C_1(1 + d\ )/(1 + 0.17\ ) \qquad (104)$$

in the HsC case. Here C_1 is the coefficient of the first power of the external magnetic field strength in the polynomial expressions for the Zeeman splittings as given in

Tables 21 through 39 and 41 through 54.

When the HpC Zeeman splittings of the ground term levels are expressed in terms of H_{ion} instead of H_{ext}, using the values of the magnetic susceptibility at 4.2 and 20°K as derived from reference (111), the results given in Table 56 are obtained. The result for the I level at 4.2°K is in

Table 56. HpC Zeeman splitting factors C_1' for some low lying levels of the $^6H_{15/2}$ ground term of DyES

Level	μ	$C_1' \times 10^3$		
		DyES 4.2°K	DyES 20°K	$(DyES)_{10}(YES)_{90}$ 20°K
I	(0,3)	.5064 ±.0004	.5106 ±.0005	.5126 ±.0014
		.5024[a] ±.0047		
		.5042[b] ±.0093		
II	(1,2)	.2615[a] ±.0093	.2738 ±.0026	.2700 ±.0012
				.2736[c] ±.0047
III	(-1,-2)	.5836[a] ±.0093	.6609 ±.0046	.6496 ±.0015
IV			.8130 ±.0237	

[a]Gramberg (84).

[b]Cooke et al. (111).

[c]Baker and Bleaney (109).

good agreement with the results of Gramberg and Cooke et al., and there seems to be a slight increase in the splitting factor for this level with increasing temperature and dilution. The values of the splitting factor for the II level in the concentrated and dilute crystal are in agreement with Baker and Bleaney's result, but are larger than Gramberg's result at 4.2°K. The results obtained for the splitting factor of the III level at 20°K are noticeably larger than the result obtained by Gramberg at 4.2°K. The probable reason for both of these discrepancies is that the absorption lines due to transitions from the II and III levels are very weak at 4.2° due to their small population. Gramberg's results for these levels are probably in error because of the larger errors encountered in measuring weak absorption lines.

HpC shifts of the crystal field level centers

The centers of gravity of the three lowest levels of the ground term were found to shift toward lower energies with increasing magnetic field. The shifts, calculated from Table 4 for H_{ext} = 27.5 kG, were -.022, -.046, and -.228 cm^{-1} for the I, II, and III levels, respectively. The result for the I level is in agreement with Gramberg, who observed no shift, and with the result of Cooke et al., who reported that there is no temperature independent contribution to the HpC magnetic susceptibility.

HsC Zeeman splittings

In the limit that the HsC magnetic field approaches zero, the ground term of DyES has no net magnetic moment and therefore no temperature dependent magnetic susceptibility. There is a temperature independent term which arises from the depression of the I level with increasing field, but, as shown by Gramberg and Cooke et al., it is much smaller than the HpC susceptibility. In addition, the demagnetization factors for the samples studied in this work were always near the value of .17 which appears in the numerator of Equation 101. The result is that the difference between the magnetic field at the dysprosium ion and the external magnetic field is negligible in the HsC case.

The HsC Zeeman splittings of the I and III ground term levels were much more difficult to determine than the HpC splittings because they were not well resolved below about 14 kG. The I level has $\mu = (0,3)$, so from reference (69) we know that its HsC splitting should be proportional to H^3. The observed splitting of 0.84 cm^{-1} for this level at 27.5 kG is in agreement with the observations of Gramberg, and it is in agreement with the results of Cooke et al., who mistakenly attributed its small contribution to the magnetic susceptibility below 3.3°K to misalignment of their sample.

The HsC splitting of the II level, in agreement with the results of Hill and Wheeler, is clearly not linear for fields above 10 kG. The depression of the II splitting is due to

the exchange of effective M values for the II and III states in the magnetic field region where the energies of these levels become comparable. The first order splitting factors for the II and III levels at 20°K are not in agreement with Gramberg's results at 4.2°, but the splitting factor for the II level is in fair agreement with Baker and Bleaney's result of $C_1 = .397 \pm .023$ for the dilute salt between 14 and 20°K. As has been pointed out earlier, Gramberg's results for the splittings of the II and III levels are questionable because, due to the small population of these levels at 4.2°K, absorption lines arising from transition from them are very faint. Powell and Orbach (113) have also noted that the ratio of Gramberg's HsC and HpC splitting factors for the II level is not consistent with the crystal symmetry. In the present work at 20°K the II and III levels were adequately populated, and the ratio of the HsC and HpC splitting factors obtained for the II level is consistent with the crystal symmetry. Powell and Orbach's attempt to determine crystal field parameters for DyES from Gramberg's crystal field and Zeeman splitting data at 4.2°K was probably not justified because the data on the II and III splittings were not very accurate.

The HsC Zeeman splittings and the shifts of the centers of gravity of the three lowest levels in the ground term have also been shown to depend on the angle ϕ_m between the x axis and the external magnetic field. This so called anisotropic

HsC Zeeman effect had not been observed in previous studies of DyES and, as far as is known, DyES is the first of the rare earth ethylsulfates in which this effect has been shown to be important for the levels of the ground term. Other facets of the anisotropic HsC Zeeman effect have been discussed at length in previous sections of this work.

Correlation with theory

The theoretical and experimental behavior of the five lowest levels of the ground term of DyES under the influence of HpC, HsC ($\phi_m = 0$), and HsC ($\phi_m = 30^\circ$) magnetic fields is summarized in Figure 18. The method used for calculating the theoretical behavior is the same as has already been described in considerable detail in reference (72), so it will not be described here. Hufner's (62) values for the crystal field parameters were used to calculate approximate crystal field wavefunctions for the case of no external magnetic field, and matrix elements of the Zeeman effect calculated with these wavefunctions were used to perturb the observed energies of the crystal field levels. Wybourne's (81) value for the g factor of the "$^6H_{15/2}$" in intermediate coupling was used in the calculation of the matrix elements of the Zeeman interaction.

As can be seen from Figure 18, the agreement between the observed and calculated HpC Zeeman effect is good except for the (0,3) level at 58.5 cm^{-1}. This discrepancy might have

Figure 18. Theoretical and experimental behavior of the five lowest levels of the ground term of DyES as a function of the external magnetic field

+ Experimental points for the magnetic field parallel to the c (HpC) or a axis (HsC $\phi_m = \bar{\phi}$)

X Experimental points for the magnetic field parallel to an x axis ($\phi_m = 0$)

Δ Experimental points for the magnetic field parallel to another x axis 30° away ($\phi_m = 30°$)

—— Calculated behavior for the HpC or HsC ($\phi_m = 0$) case. The x axis is chosen so that the off diagonal matrix elements of the crystal field potential are positive

--- Calculated behavior for the HsC ($\phi_m = 30°$) case

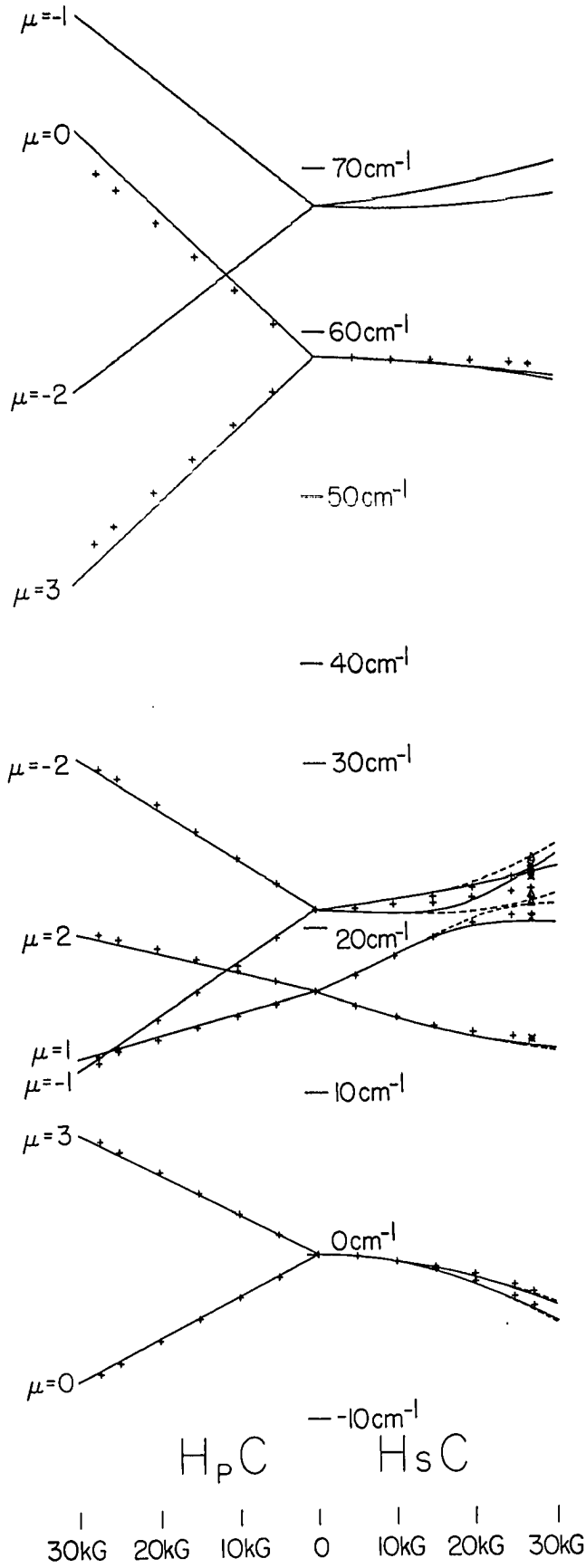
μ=-1
μ=0
μ=-2
μ=3
μ=-2
μ=2
μ=1
μ=-1
μ=3
μ=0
70cm⁻¹
60cm⁻¹
50cm⁻¹
40cm⁻¹
30cm⁻¹
20cm⁻¹
10cm⁻¹
0cm⁻¹
-10cm⁻¹
H_P C
H_S C
30kG
20kG
10kG
0
10kG
20kG
30kG

been expected, however, because the splitting of this level was determined indirectly from the single line IV to (0,3) Zeeman pattern at 23381 cm^{-1}. It is felt that the indirect determination gives a good first approximation to the splitting, but one should be careful not to attach too much significance to the result. The calculated shift of the center of gravity of the I level in the HpC case is in good agreement with the observed behavior, so it can be concluded that the assumption that the center of gravity of the two (-1,-2) levels at 22034.8 and 22063.0 cm^{-1} is independent of the external magnetic field is indeed correct for the HpC case. This is a very important conclusion since the energy level schemes for the HpC case were all based upon this assumption.

Comparison of the observed and calculated results in the HsC case is a little more difficult than in the HpC case because of the ϕ_m dependence of the energy levels. Below about 15 kG, where the ϕ_m dependence is very small, the agreement is excellent. At higher fields the splittings are also in good agreement, but the observed energies of the levels are consistently a few tenths of a wavenumber higher than the calculated energies. One might try to explain this discrepancy by saying that the assumption used to set the side conditions for the HsC energy level determination was incorrect. This is not a logical explanation, however, because the two

(-1,-2) levels chosen to set the side conditions are the two lowest energy levels of group G. Therefore if their center of gravity is not independent of the magnetic field, it must shift toward lower energies with increasing field. In this event the assumption that their center is independent of the field could only yield energies for the ground term levels which were too low, not too high.

A more plausible explanation is that while Hufner's values for the crystal field parameters give a good fit of the observed energies of the five lowest levels of the ground term, perhaps they give calculated energies for the three other levels expected for the ground term which are lower than the true values. If this were true, calculations of the Zeeman effect would yield erroneously depressed energies for the low lying levels. The error would be considerably larger for the HsC case than for the HpC case because matrix elements of the HsC Zeeman effect connect all states for values of the external magnetic field under consideration here. Those of the HpC Zeeman effect only connect states which have the same crystal quantum number. Unfortunately no experimental information is available on the three energy levels in question, so this explanation must be regarded as pure conjecture.

It is a curious fact that the theoretical results of the present work are in significantly better agreement with the observed energies of the levels than are the results of Hill

and Wheeler (108), who used a more sophisticated theoretical treatment.

Group G

This line group has been studied extensively in both $DyCl_3$ (85) and DyES (84), but the present work is the first in which Zeeman splittings are reported for the excited levels. The assignment of crystal quantum numbers and the energies of the levels at zero magnetic field as given in Tables 45 and 46 are in agreement with Gramberg (84), and in the HsC orientation the energy levels of group G were found to have very little dependence on the angle between the magnetic field and the x axis. Magnetic dipole transitions make considerable contribution to the intensities of the lines and, from the selection rule $\Delta J = 0 \pm 1$ for these transitions, it can be concluded that this group has a J value of 13/2, 15/2 or 17/2. Gramberg (84) and Singh (114) found that both DyES and $DyCl_3 \cdot 6H_2O$ had eight lines in this group at 4.2°K, so both the number of lines and the values of the crystal quantum numbers which were obtained for DyES indicate a J value of 15/2. This is also in agreement with Wybourne's interpretation that group G results from the free ion level having 53 percent $^4I_{15/2}$ character.

In group G, as in most of the other groups studied in this work, there is a large decrease in the intensity of the absorption lines, and an increase in their width, as one pro-

ceeds from the low energy portion of the group to the high energy part. See Figure 19. As a result thicker and thicker crystals are needed to observe the lines in the high energy part of the group and the Zeeman splitting of these lines are very difficult to measure. Many of the very broad and faint lines may not even be due to transitions between electronic energy levels, but may be arising from simultaneous excitation of the 4f electrons and a coupled oscillation of the crystal lattice or the rare earth ion--ligand complex. The result is that one cannot reliably determine J values for the line groups solely on the basis of the number of lines observed at 4.2°K. The point is illustrated quite well when we consider the results obtained by Sutherland (101) for group G. He observed thirteen lines in this group for a 3.2 mm crystal of DyES at 4.2°K. This number of lines, if they are all due to electronic transitions, is clearly not consistent with the J value of 13/2, 15/2 or 17/2 demanded by the fact that magnetic dipole transitions are observed, so it is clear that either many of the lines are not due to electronic transitions, or that more than one free ion level is involved in this group.

Attempts have also been made to determine the effective Lande' g factors for the various line groups, and to use these as a basis for confirming J value assignments (84). In theory this is a fine idea. If one knew which were the elec-

Figure 19. HsC spectra of DyES group G for a 1.0 mm crystal at 20°K

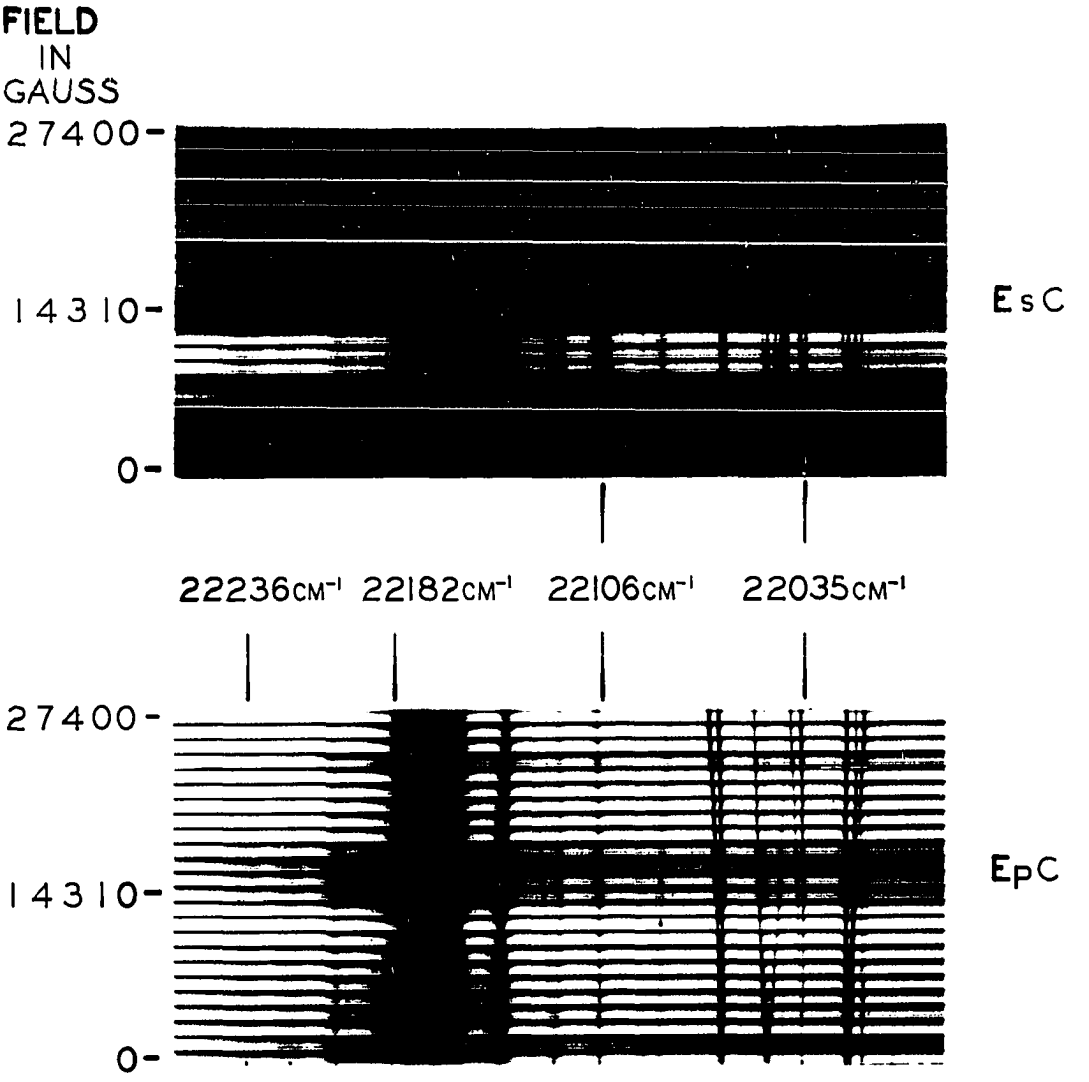
FIELD
IN
GAUSS
27400
14310
0
EsC
22236CM-1
22182CM-1
22106CM-1
22035CM-1
27400
14310
0
EpC

tronic transitions, if he knew that only one free ion level was present, and if he were able to measure the splitting factors of all of the electronic transitions with precision, this would certainly be a good way of confirming assignments. The fact is that for most of the line groups of DyES above 20000 cm^{-1} none of these conditions is fulfilled. In the case of group G, for example, Wybourne has attempted to confirm his assignment by comparing Gramberg's value of g = 1.02 $\pm$ .15, as determined from the (0,3) levels, with the calculated value of g = 1.067 for the intermediate coupling state with 53 percent $^4I_{15/2}$ character. He failed to mention that Gramberg had also determined the g factor for group G from the HpC splitting factors of the (-1,-2) levels, and that quite a different result (g = 0.84 $\pm$ .1) was obtained. When this is taken into consideration it is clear that, first, the experimental determination is not very reliable, probably because of difficulties in measuring the weak lines, and second, that the "confirmation" obtained by comparing observed and calculated g values, in this case at least, is quite questionable.

It seems that the most logical assignment for group G is J = 15/2, but this is certainly not conclusive. Before one can have any real confidence in the assignments for the line groups of DyES above 20000 cm^{-1} it will be necessary to find some way to clearly determine which lines are due to purely

electronic transitions, and calculations of the crystal field and magnetic splittings expected for the proposed free ion levels will have to be done. These calculations have been performed for some rather complex line groups of ErES (51) and HoES (72) and it was found that they can provide very conclusive confirmations of the proposed assignments.

Group H

The Zeeman effect of group H has been studied earlier by Gramberg for both the HpC and HsC orientations at 4.2°K. The results of the present work agree within experimental error with Gramberg's results for the number of levels, their energies at zero magnetic field, and for the first order terms in the HpC and HsC splitting factors of all but the (0,3) level at 23467.3 cm^{-1}. We are also in agreement for the values of the crystal quantum numbers assigned to the various levels. The discrepancy in the value of the HpC splitting factor for the (0,3) level arises from the fact that at 20°K the I to (0,3) transition is obscured by interference with the II to (-1,-2) transition. See Figure 20. At 4.2°K Gramberg was not bothered by this interference, so his result is probably correct. No anisotropy was observed for the energy levels of group H as a function of ϕ_m in the HsC orientation, and in view of the energy differences between the levels, none was expected.

The probable J value for the levels of group H is

Figure 20. HpC spectra for DyES group H for a 1.0 mm crystal at 20°K. The lines marked by the asterisk are from group I

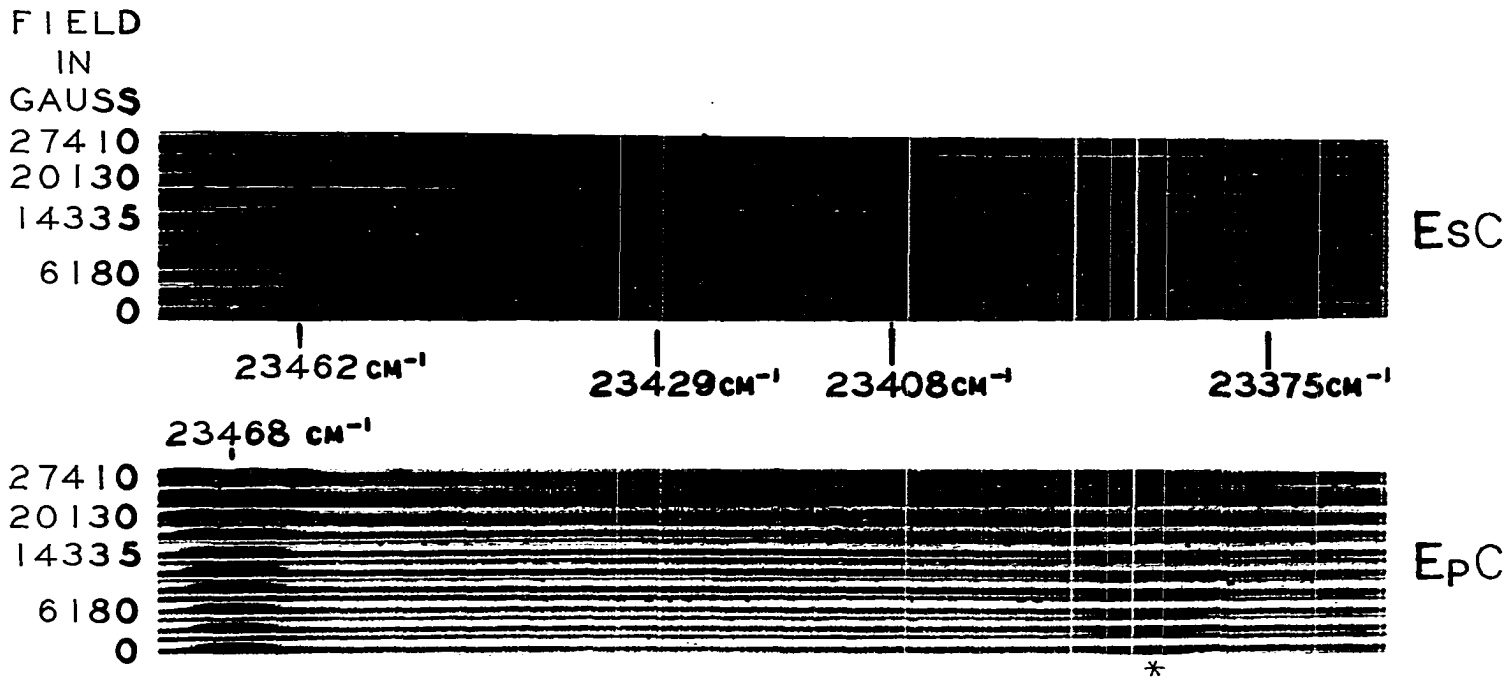
FIELD
IN
GAUSS
27410
20130
14335
6180
0
23462 cm⁻¹
23429cm⁻¹
23408cm⁻¹
23375cm⁻¹
EsC
23468 cm⁻¹
27410
20130
14335
6180
0
EpC
*

$J = 11/2$. There is no evidence of combination lines in this group, even with 4.4 mm crystals, so the fact that two (1,2), two (0,3), and two (-1,-2) levels are observed gives good indication that $J = 11/2$. The experimental values of the effective Lande g factor,

$g = 1.30 \pm .08$ from Gramberg, and

$g = 1.23 \pm .03$ from observations on the (1,2) and (-1,-2) levels in the present work,

are in reasonable agreement with the value of $g = 1.245$ obtained by Wybourne for the intermediate coupling state with 88% $^4G_{11/2}$ character. This also supports the assignment of $J = 11/2$.

Group I

The absorption lines in the high energy portion of group I were so weak and diffuse that it was very difficult to obtain good measurements. See Figures 9 and 21. The lines above 25000 cm^{-1} were measured from the second order spectrum obtained with the 600 line/mm grating, and those below were measured from the fifteenth order spectrum obtained with the 300 line/mm grating.

Group I has been studied earlier by Gramberg. He reported 8 lines in the ethylsulfate, 11 in the nitrate, and 9 intense lines in the hydrated chloride at zero magnetic field and 4.2°K. He obtained four (0,3), one (1,2), and three

Figure 21. HsC spectra of DyES group I for a 1.0 mm crystal at 20°K

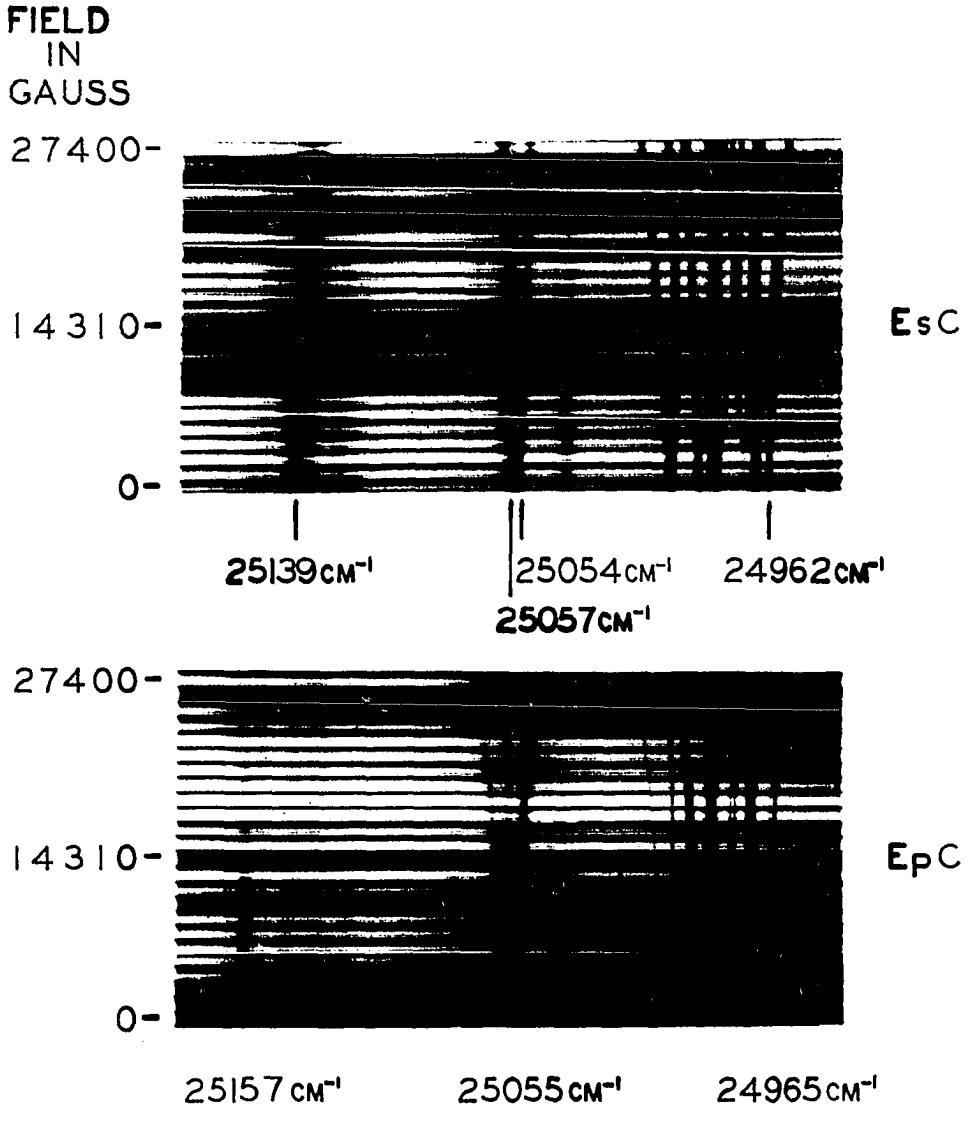
FIELD
IN
GAUSS
27400-
14310-
0-
EsC
25139cm⁻¹
25054cm⁻¹
24962cm⁻¹
25057cm⁻¹
27400-
14310-
0-
EpC
25157cm⁻¹
25055cm⁻¹
24965cm⁻¹

(-1,-2) levels in the ethylsulfate and suggested a probable J value of 21/2 to account for the four (0,3) levels. No Zeeman data was reported.

In the present work an additional (0,3) level was definitely identified at 25143.3 cm^{-1} (See Table 49.), and there is good evidence for an additional (1,2) level very close to the previously identified (-1,-2) and (0,3) levels at 25052.5 and 25055.5 cm^{-1}. The EsC spectrum in the latter region has two very closely spaced lines at 4.2°K, and the EpC spectrum one line. Also, the Zeeman patterns which are observed for these lines are more complicated than those expected for transitions to the (-1,-2) and (0,3) levels only, and the HsC spectrum in this region resulting from transitions from the I level in the ground term has large energy variations as a function of ϕ_m. Since the energy variations are not expected in the excited state unless three levels with different values of the crystal quantum numbers are present, it was concluded that there is a (1,2) level within a few wavenumbers of the (0,3) and (-1,-2) levels.

There was also reasonable evidence, although the lines involved were so weak that they had to be measured from high contrast prints of the second order spectrum, for an additional (-1,-2) level at 25132.7 cm^{-1}. At 4.2°K there is an EsC line at 25132.7 cm^{-1}, and at 20°K there is another EsC line at 25116.7 cm^{-1}. These were attributed to I to (-1,-2)

and II to (-1,-2) transitions.

Group I therefore has a total of five (0,3), two (1,2), and four (-1,-2) levels. The maximum value of J for the free ion levels of Dy^{+3} is 23/2, with four (0,3) levels, so it is clear that more than one free ion level must be contributing to the excited levels for group I. Wybourne (81) has suggested that perhaps the J = 13/2 and J = 7/2 levels calculated to occur at 24296 and 24720 cm^{-1}, respectively, are contributing, but these do not yield the proper number of (0,3) levels. It seems unwise to speculate further until the intermediate coupling calculation is refined, or until better measurements of the very weak and diffuse absorption lines can be obtained. It is suggested that if long slits and fine grain photographic plates were used to obtain photographs of the first or second order spectrum at 4.2°K or lower, considerably better measurements could be obtained for these lines.

Group J

The absorption spectrum and Zeeman effect of group J and higher energy groups of DyES have not been reported before. In the present work four (-1,-2), three (1,2), and three (0,3) levels were measured and clearly identified. There were a number of absorption lines with energies greater than 25745 cm^{-1}, however, whose initial and final states were not identified. In addition, the 4.2°K spectrum showed a

large number of absorption lines between groups J and K which were so diffuse that it was impossible to measure them on the recording microphotometer. See Figure 22. These lines are almost certainly combination lines because they have no Zeeman splittings, and because they become even more diffuse with increasing temperature. This behavior is similar to that observed for known combination lines in the spectrum of thulium ethylsulfate.

The fact that four (-1,-2) levels were observed would seem to indicate J = 23/2. However, according to Wybourne's intermediate coupling calculation, and J = 23/2 level is not expected below 40000 cm^{-1}. This led to the conclusion that there must be more than one free ion level contributing to the spectrum of group J. It is not profitable to speculate on which free ion levels are involved, however, until more complete data is obtained for the very weak lines, and until more refined intermediate coupling and crystal field calculations are performed.

Group K

As noted earlier, the absorption lines of group K were so weak that they were not observable in the high order photographs of the spectrum. The measurements given in Tables 36 and 37 were therefore obtained in the second order with the 600 line/mm grating. It was not possible to construct a reliable energy level scheme or to determine the

Figure 22. HsC spectra of DyES groups K and J for a 1.0 mm crystal at $4.2^{\circ}K$

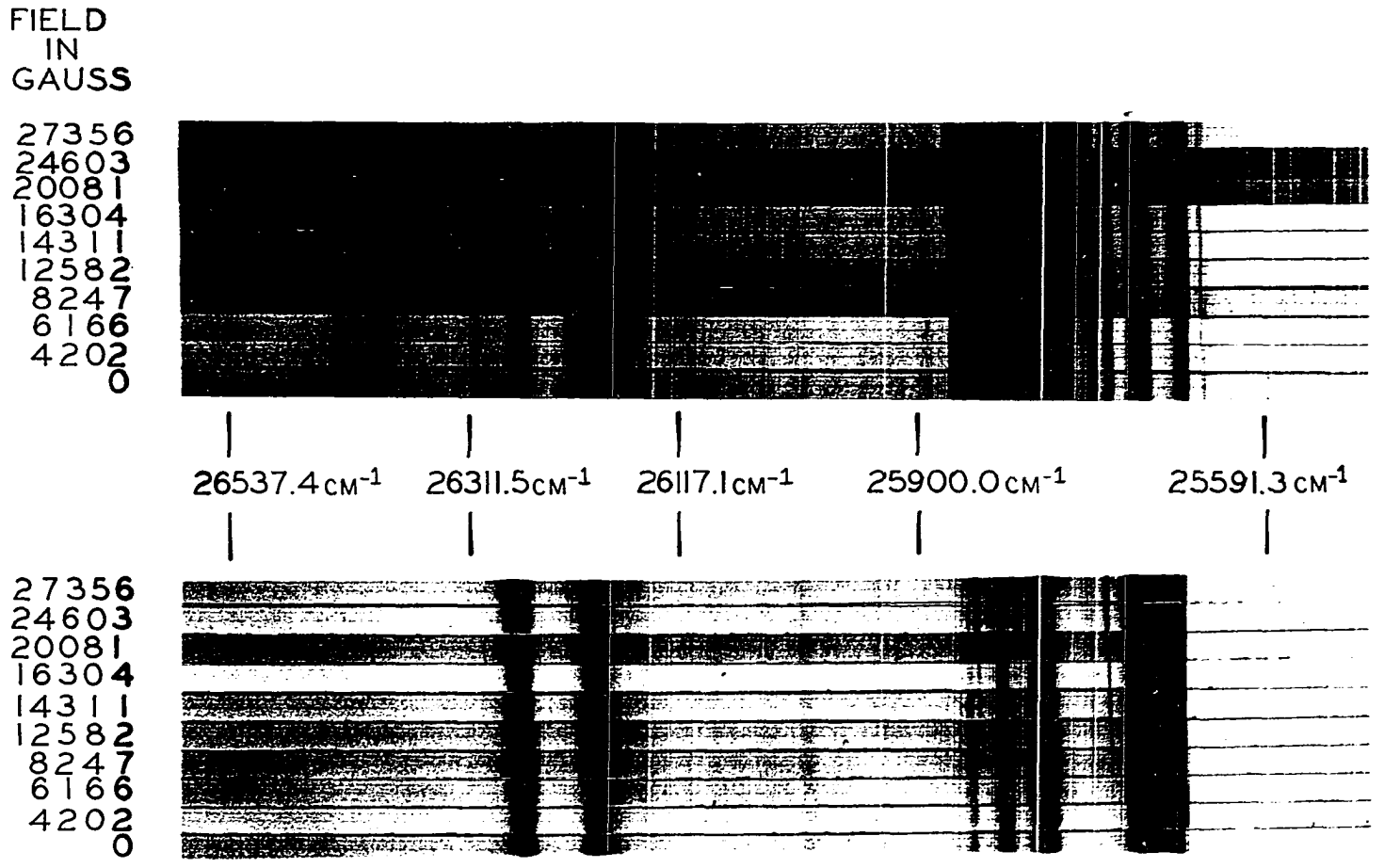
FIELD IN GAUSS
27356
24603
20081
16304
14311
12582
8247
6166
4202
0
EsC
26537.4 cm-1
26311.5 cm-1
26117.1 cm-1
25900.0 cm-1
25591.3 cm-1
27356
24603
20081
16304
14311
12582
8247
6166
4202
0
EpC

values of the crystal quantum numbers for the levels of group K because the Zeeman splittings were not resolved, and because the energies of the absorption lines could not be measured with sufficient precision even in the second order. All that can be said is that at 4.2°K there are seven lines in the EsC polarization and only two lines in the EpC polarization. At 20°K several other lines are present, but because the measurements are not very precise, it is not possible to state with certainty in any case whether the additional absorption line results from a transition from the II or III level in the ground state. The spectra shown in Figures 22 and 10 for 4.2 and 20°K seem to indicate that all the observed lines are due to purely electronic transitions because the lines are quite sharply polarized. Therefore, if the selection rules for electric dipole transitions are being obeyed, group K has two (0,3) levels, a total of seven (-1,-2) and (1,2) levels, and a probable J value of 17/2.

Future work on this group should employ long slits, very fine grain photographic emulsions, and measurements at 2°K or lower in an attempt to improve the precision of the measurements. It should be a fairly simple matter to derive the energy level scheme and fix the J value for this group once precise measurements become available.

Group L

Two (-1,-2), one (1,2), and two (0,3) levels have been clearly identified in group L. The lines resulting from transitions from the three lowest levels in the ground state to these levels were quite sharp and very intense. The measurements reported in Tables 38 and 39 and the energy level schemes given in Tables 53 and 54 are from photographs of the high order spectrum. There are a large number of much weaker absorption lines between 27480 and 27870 cm^{-1} on the high energy end of the group. See Figure 11. These weak lines were visible only in the second order spectrum and were not measured in this work. The 20°K spectrum had no more lines between 27480 and 27870 cm^{-1} than the 4.2°K spectrum, so it was concluded that the lines observed in this region were probably combination lines. If this assumption is justified the J value for group L is 11/2 or greater because two (-1,-2) levels are observed. J values of 11/2 and 13/2 can be excluded, however, because the data yield negative g factors for free ion levels with these J values. It was concluded therefore that at least some of the weak lines are due to electronic transitions, and that the J value for group L is 15/2 or greater. A J value of 15/2 cannot be ruled out, even though there is no evidence for magnetic dipole transitions, because, as Wybourne's calculations have shown, the 15/2 level expected in this region has very little $^4I_{15/2}$ or $^6H_{15/2}$ character. Thus the contribution of mag-

netic dipole transitions would be expected to be very small even if the J value were 15/2.

Group M

As will be seen below, the probable J value for group M is J = 11/2. This line group has six extremely sharp lines at 4.2°K, two in the EpC polarization and four in the EsC polarization. In addition, there are five very weak and diffuse lines between 28100 and 28350 cm^{-1} on the high energy end of the group. The latter are present at 4.2°, but are very much weaker at 20°K. They are probably combination lines. Figure 23 gives the energy level scheme and HpC splitting factors for the sharp lines of group M as derived from measurements of the second order spectra at 20°K. Two (0,3), two (1,2), and two (-1,-2) levels were clearly identified, and both the total number of levels and the number in each μ class suggest J = 11/2.

The experimental values of the Lande g factor for group M were:

g = 0.95 from the (0,3) levels,

g = 1.05 from the (1,2) levels, and

g = 0.83 from the (-1,-2) levels.

The variation in the g factors obtained from the splittings of levels with different crystal quantum numbers is appreciably larger than the experimental error, but this is probably due to interaction of the levels of group M with those of

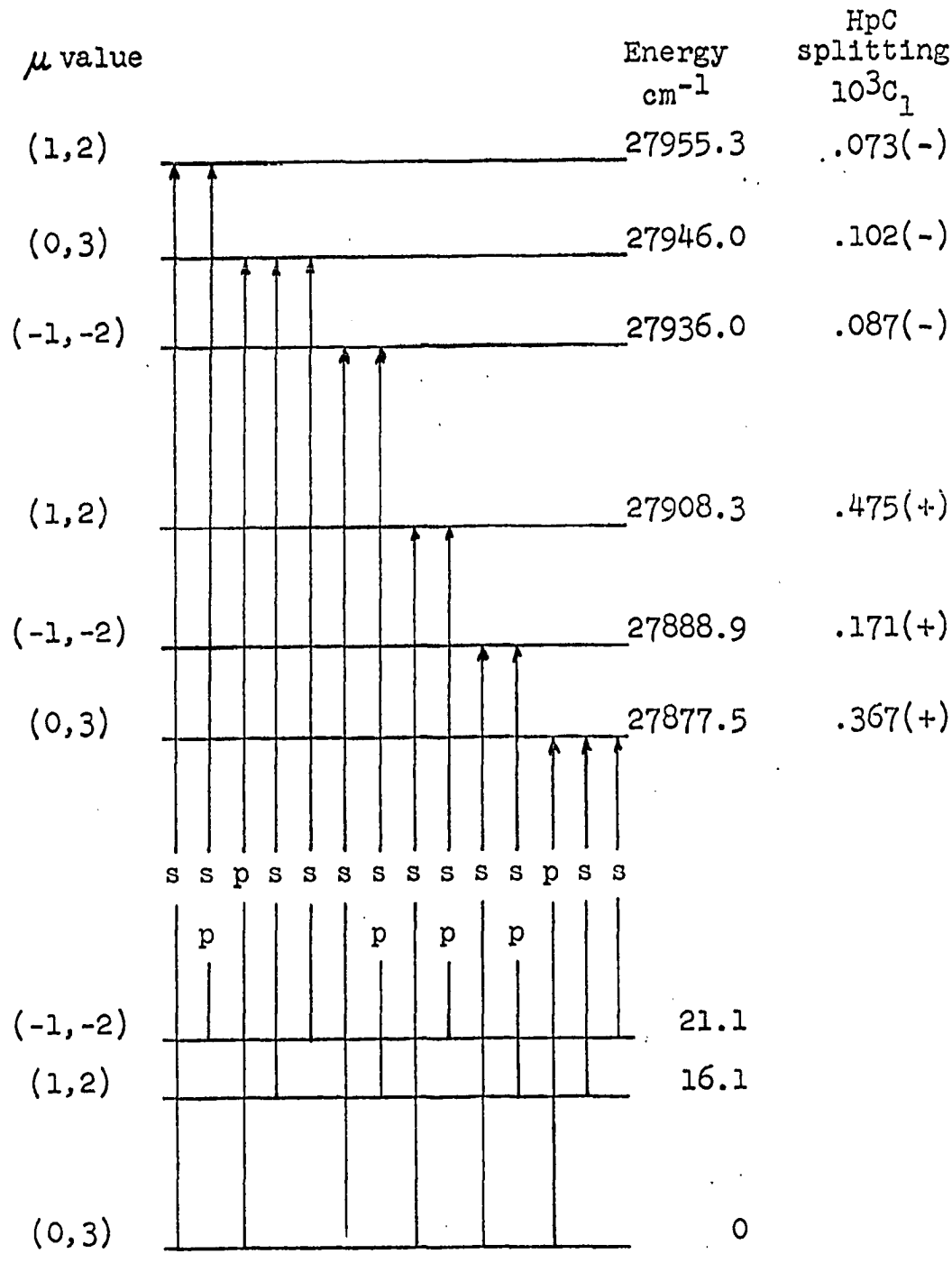

Figure 23. Energy level diagram and HpC splitting factors for DyES group M

groups L and N, whose centers are only 500 and 600 cm^{-1} away, respectively. The mean experimental value of the g factor, g = 0.94, compares favorably with the value of g = 0.93 which was calculated for the free ion level which Wybourne's intermediate coupling calculation places at 26224 cm^{-1}. This level, according to the calculation, has 76% $^4I_{11/2}$ character.

SUMMARY AND CONCLUSIONS

The energies and/or intensities of many absorption lines in the HsC Zeeman patterns of single crystals of DyES have been found to have 60° periodic anisotropy with respect to the angle ϕ_m between the x axis of the crystal and the direction of the external magnetic field. The energy of every line, if it had a measurable variation, reached its maximum or minimum at a common angle, but the intensities of the lines attained their maximum or minimum values at various angles. The observations were in qualitative agreement with recent works (69, 73) on the theory of the Zeeman effect for rare earth ions in crystal fields with C_{3h} symmetry.

Detailed measurements of the energy variations of the absorption lines of groups G and I of DyES in an external magnetic field of 28 kG showed that most of the energy variations resulted from changes in the energies of the low lying HsC Zeeman levels of the ground term. Since these levels are the initial levels in the absorption transitions responsible for all the line groups, the fact that their energies depend on ϕ_m explains why so many of the absorption lines observed throughout the spectrum have energy variations as a function of ϕ_m. The present work is the first in which the anisotropic HsC Zeeman effect has been observed in DyES, and DyES is the first of the rare earth ethylsulfates for which this effect has been shown to be important for the levels of the ground

term.

In the HsC Zeeman effect the C_{3h} point symmetry at the rare earth ion imposes the requirement that the energy of every absorption line, if it varies at all, must reach its maximum or minimum when the magnetic field is parallel to an x axis of the crystal. This fact was used to determine the angle $\bar{\phi}$ between the x axis and the a translation axis of single crystals of DyES, $(DyES)_{10}(YES)_{90}$, and $(DyES)_v(ErES)_{100-v}$ with v equal to 10, 50, and 90. It was found that $\bar{\phi}$ was the same, to within a few tenths of a degree, for Dy^{+3} and Er^{+3} in each of the mixed crystals, but comparison of the results for different crystalline samples was not very fruitful because of a rather large uncertainty in the absolute values of $\bar{\phi}$. This uncertainty was primarily due to difficulties in determining the a axis direction while the samples were in place in the dewar. Methods were suggested to drastically improve the a axis determination in future measurements, but all that could be said from the present experiments was that the average value of $\bar{\phi}$ for both Er^{+3} and Dy^{+3} in all the samples studied was 6.5 ± 1.4^{o}.

The HpC and HsC Zeeman effects of line groups G through L (22000 to 27870 cm^{-1}) were also studied as a function of external magnetic field, up to 28 kG, and field dependent energy level schemes were derived for the low lying levels of the ground term and for the excited levels of all but group K. The energy level scheme for the excited levels of

group M (27919 cm^{-1}) was also determined, but only for the HpC case, since this was sufficient to determine the J value of the excited levels. The results for the ground term, including the HsC anisotropy at 28 kG, were in good agreement with calculations performed in this work in which the crystal field and Zeeman interactions were treated as comparable perturbations on the free ion ground level.

The experimental results for the excited levels of many of the line groups did not permit a definitive identification of the free ion levels involved because the interpretation of the spectrum was hampered by the large number of very weak and diffuse absorption lines in the high energy portions of the line groups. These will be discussed further in the next paragraph. The wealth of high precision data obtained in this work, however, will be extremely useful in later work in which the results of intermediate coupling calculations performed specifically for DyES and calculations of the crystal field and Zeeman splittings to be expected for the various free ion levels are used to obtain conclusive identifications.

Identifications obtained in this way will also be helpful for the interpretation of the weak and diffuse lines. These are extremely difficult to measure and one can be sure, from the fact that most of them become even weaker with increasing temperature, that many of these lines do not arise from purely electronic transitions between energy levels of

the $4f^n$ configuration. Other possibilities are: 1) that they result from the absorption of light and simultaneous excitation of the 4f electrons and a coupled oscillation of the crystal lattice or the rare earth ion-ligand complex, and 2) that they arise from $4f^n$ to $4f^n$ transitions, but that the final states in these particular transitions have very short lifetimes because the rare earth ion immediately gives up part of its energy to excite oscillational modes of the lattice or rare earth ion-ligand complex, and decays to a lower energy electronic state. Both of these mechanisms are consistent with the fact that the weak and diffuse lines usually occur only in the high energy portion of the line groups and become weaker with increasing temperature, and it seems that further work on these lines could yield valuable information on the interaction of the rare earth ion with its surroundings in a crystal lattice.

Precision data should also be obtained for the many line groups beyond 28000 cm^{-1}. This data should ultimately be included in calculations of the electrostatic and spin-orbit parameters for DyES, and in calculations of the effects of configuration interaction. This is extremely important because the calculations performed so far, by Wybourne, are hardly more than calculations of the spin-orbit splittings of the ^6H and ^6F terms. Until more experimental data is included in these calculations, they will continue to provide

only very primitive estimates of the energies of the free ion levels. It should be clear that while much is known about the spectrum of DyES, there is a great deal more to be learned.

LITERATURE CITED

1. Kayser, H. Handbuch der Spektroskopie. Vol. 3. Leipzig, S. Hirzel. 1905.

2. Zeeman, P., Phil. Mag. 5, 43 (1897).

3. Lorentz, H. A. The Theory of Electrons. Liepzig, Teubner Verlagsgesellschaft. 1916.

4. Becquerel, J., Radium 5, 5 (1908).

5. Becquerel, J. and Onnes, H. K., Proc. Acad. Amsterdam 10, 592 (1908).

6. Becquerel, J., Onnes, H. K., and de Haas, W. J., Proc. Acad. Amsterdam 29, 264 (1926).

7. Hund, F., Z. Physik 33, 855 (1925).

8. Van Vleck, J. H. and Frank, A., Phys. Rev. 34, 1494 (1929).

9. Spedding, F. H., Phys. Rev. 46, 308 (1934).

10. Freed, S., Phys. Rev. 38, 2122 (1931).

11. Ewald, H., Ann. Physik 34, 209 (1939).

12. Merz, A., Ann. Physik 28, 569 (1937).

13. Gobrecht, H., Z. Physik 37, 851 (1936).

14. Spedding, F. H. and Bear, R. S., Phys. Rev. 42, 58 (1932).

15. Becquerel, J. Notice sur les Travaux Scientifiques, Paris, 1934., Supplement, Paris, 1943. Original not available; cited in Hellwege, K. H. Spectroscopy of Crystalline Rare Earth Compounds: Quantum Electronics Proceedings, 1963. p. 623. New York, Columbia University Press. 1964.

16. Brunetti, R., Physikal. Z. 29, 571 (1928).

17. Brunetti, R. and Ollano, Z., Nuovo Cimento 6, 345 (1929).

18. Freed, S. and Spedding, F. H., Nature 123, 525 (1929).

19. Bethe, H., Z. Physik 53, 133 (1929).

20. Kramers, M. H. A., Proc. Acad. Amsterdam 32, 1176 (1929).

21. Kramers, M. H. A., Proc. Acad. Amsterdam 33, 959 (1930).

22. Slater, J. C., Phys. Rev. 34, 1293 (1929).

23. Condon, E. U. and Shortley, G. H. The Theory of Atomic Spectra. London, Cambridge University Press. 1959.

24. White, H. E. Introduction to Atomic Structure. New York, McGraw-Hill Book Co., Inc. 1934.

25. Herzberg, G. Atomic Spectra and Atomic Structure. 2nd ed. New York, Dover Publications, Inc. 1944.

26. Van Vleck, J. H., J. Phys. Chem. 41, 67 (1937).

27. Bethe, H. and Spedding, F. H., Phys. Rev. 52, 454 (1937).

28. Spedding, F. H., Phys. Rev. 58, 255 (1940).

29. Broer, L. J. F., Gorter, G. J., and Hoogschagen, J., Physica 11, 231 (1945).

30. Racah, G., Phys. Rev. 61, 186 (1942).

31. Racah, G., Phys. Rev. 62, 438 (1942).

32. Racah, G., Phys. Rev. 63, 367 (1943).

33. Racah, G., Phys. Rev. 76, 1352 (1949).

34. Judd, B. R. Operator Techniques in Atomic Spectroscopy. New York, McGraw-Hill Book Co., Inc. 1963.

35. Wybourne, B. G. Spectroscopic Properties of Rare Earths. New York, John Wiley and Sons, Inc. 1965.

36. Fano, U. and Racah, G. Irreducible Tensorial Sets. New York, Academic Press, Inc. 1959.

37. Bleaney, B. and Stevens, K. W. H., Repts. Prog. in Phys. 16, 108 (1953).

38. Elliott, R. J. and Stevens, K. W. H., Proc. Roy. Soc. (London) 219A, 387 (1953).

39. Alberg, J. E., Blanchard, E. R., and Lundberg, W. O., J. Chem. Phys. 5, 552 (1937).

40. Penney, W. G. and Schlapp, R., Phys. Rev. 41, 194 (1932).

41. Schlapp, R. and Penney, W. G., Phys. Rev. 42, 666 (1932).

42. Hellwege, K. H., Ann. Physik (6) 4, 95 (1948).

43. Hellwege, K. H., Ann. Physik (6) 4, 127 (1948).

44. Hellwege, K. H., Ann. Physik (6) 4, 136 (1948).

45. Hellwege, K. H., Ann. Physik (6) 4, 143 (1948).

46. Hellwege, K. H., Ann. Physik (6) 4, 150 (1948).

47. Hellwege, K. H., Ann. Physik (6) 4, 357 (1949).

48. Dieke, G. H. and Leopold, L., J. Opt. Soc. Am. 47, 944 (1957).

49. Dieke, G. H., Crosswhite, H. M. and Dunn, B., J. Opt. Soc. Am. 51, 820 (1961).

50. Crosswhite, H. M., Dieke, G. H. and Carter, W. J., J. Chem. Phys. 43, 2047 (1965).

51. Spedding, F. H., Haas, W. J., Sutherland, W. L. and Eckroth, C. A., J. Chem. Phys. 42, 981 (1965).

52. Ketelaar, J. A. A., Physica 4, 619 (1937).

53. Fitzwater, D. R. And Rundle, R. E., Z. Krist. 112, 362 (1959).

54. Gruber, J. B. and Conway, J. G., J. Chem. Phys. 32, 1178, 1532 (1960).

55. Wong, E. Y. and Richman, I., J. Chem. Phys. 34, 1182 (1961).

56. Wybourne, B. G., J. Chem. Phys. 32, 639 (1960).

57. Wong, E. Y., J. Chem. Phys. 35, 544 (1961).

58. Varsanyi, F. and Dieke, G. H., J. Chem. Phys. 36, 2951 (1962).

59. Eisenstein, J. C., J. Chem. Phys. 39, 2128 (1963).

60. Kahle, H. G., Z. Physik 161, 486 (1961).

61. Erath, E. H., J. Chem. Phys. 34, 1985 (1961).

62. Hufner, S., Z. Physik 169, 417 (1962).

63. Margolis, J. S. The Energy Levels of Pr^{+3} in $PrCl_3$. Unpublished Ph.D. thesis. Los Angeles, California, Library, University of California. 1960.

64. Rajnak, K. and Wybourne, B. G., Phys. Rev. 132, 280 (1963).

65. Wong, E. Y., J. Chem. Phys. 38, 976 (1963).

66. Rajnak, K. and Wybourne, B. G., Phys. Rev. 134, A596 (1964).

67. Watson, R. E. and Freeman, A. J., Phys. Rev. 133, A1571 (1964).

68. Jorgensen, C. K., Pappalardo, R. and Schmidtke, H., J. Chem. Phys. 39, 1422 (1963).

69. Murao, T., Spedding, F. H. and Good, R. H., J. Chem. Phys. 42, 993 (1965).

70. Hamm, F. S., Ludwig, G. W., Watkins, G. D. and Woodbury, H. H., Phys. Rev. Letters 5, 468 (1960).

71. Bartel, L. C. and Spedding, F. H. Nature of the Energy Levels in Hydrated Thulium Ethylsulfate: IS-968 [Iowa State University of Science and Technology, Ames. Institute for Atomic Research]. Washington, D.C., Office of Technical Services, U.S. Dept. of Commerce. 1964.

72. Spedding, F. H., Rothwell, M. T., Haas, W. J. and Sutherland, W. L. (To be published in J. Chem. Phys. ca. 1968.)

73. Murao, T., Haas, W. J., Syme, R. W. G., Spedding, F. H. and Good, R. H., J. Chem. Phys. 17, 1572 (1967).

74. Syme, R. W. G., Haas, W. J., Spedding, F. H. and Good, R. H. (To be published in J. Chem. Phys. ca. 1968.)

75. Wigner, E. P. Group Theory. New York, Academic Press. 1959.

76. Haas, W. J. Anisotropic HsC Zeeman Effect in Erbium Ethylsulfate. Unpublished M.S. thesis. Ames, Iowa, Library, Iowa State University. 1964.

77. Edmonds, A. R. Angular Momentum in Quantum Mechanics. Princeton, N.J., Princeton University Press. 1957.

78. Wybourne, B. G., J. Chem. Phys. 35, 334 (1961).

79. Wybourne, B. G., J. Chem. Phys. 35, 340 (1961).

80. Wybourne, B. G., Energy Matrices of the f^5 Electron Configuration: UCRL-10448 [University of California, Lawrence Radiation Laboratory, Berkeley, California]. Office of Technical Services, U.S. Dept. of Commerce. Washington, D.C. 1962.

81. Wybourne, B. G., J. Chem. Phys. 36, 2301 (1962).

82. Rosa, A., Ann. Physik 43, 161 (1943).

83. Dieke, G. H. and Singh, S., J. Opt. Soc. Am. 46, 495 (1956).

84. Gramberg, G., Z. Physik 159, 125 (1960).

85. Crosswhite, H. M. and Dieke, G. H., J. Chem. Phys. 35, 1535 (1961).

86. Rotenberg, M., Bivins, R., Metropolis, N. and Wooten, J. K., Jr. The 3-j and 6-j Symbols. Cambridge, Mass., Technology Press. 1959.

87. Tinkham, M., Group Theory and Quantum Mechanics. New York, McGraw-Hill Book Co., Inc. 1964.

88. Koster, G. F. and Statz, H., Phys. Rev. 113, 445 (1959).

89. Statz, H. and Koster, G. F., Phys. Rev. 115, 1568 (1959).

90. Schiff, L. I. Quantum Mechanics. 2nd ed. New York, McGraw-Hill Book Co., Inc. 1955.

91. Fastie, W. G., J. Optical Soc. of Am. 42, 641 (1952).

92. Fastie, W. G., J. Optical Soc. of Am. 42, 647 (1952).

93. Fastie, W. G., Crosswhite, H. M., and Gloersen, P., J. Optical Soc. of Am. 48, 106 (1958).

94. Jarrell-Ash Company. Instruction manual for 3.4 meter Ebert spectrograph Mark IV. Newtonville, Mass., author 1961.

95. Crosswhite, H. M., Dieke, G. H., and Legagneur, C. S., J. Optical Soc. of Am. 45, 270 (1955).

96. Herzberg, G., Trans. Int. Astron. Union 11A, 97 (1961).

97. Jenkins, F. A. and White, H. E. Fundamentals of Optics, 3rd ed. New York, McGraw-Hill Book Co., Inc. 1957.

98. Dieke, G. H. and Singh, S., J. Chem. Phys. 35, 555 (1961).

99. Hellwege, K. H., Hufner, S., and Kahle, H. G., Z. Physik 160, 149 (1960).

100. Coleman, C. D., Bozman, W. R., and Meggers, W. F., U.S. Dept. of Commerce, National Bureau of Standards Monograph 3, 1 (1960).

101. Sutherland, W. L. Absorption Spectrum of Dysprosium Ethylsulfate. Unpublished manuscript. Ames, Iowa, Institute for Atomic Research, Ames Laboratory. 1967.

102. Hellwege, K. H., Horstik, G., Hufner, S., and Lammermann, H., Z. Physik 165, 253 (1961).

103. Wong, E. Y., Stafsudd, O. M., and Johnston, D. R., J. Chem. Phys. 39, 786 (1963).

104. Jorgensen, C. K. Orbitals in Atoms and Molecules. New York, Academic Press. 1962.

105. McLaughlin, R. D., and Conway, J. G., J. Chem. Phys. 38, 1037 (1963).

106. Rumanova, I. M., Volodina, G. F., and Belov, N. V., Soviet Physics-Crystallography 9, 545 (1965).

107. Deming, W. E. Statistical Adjustment of Data. New York, John Wiley and Sons, Inc. 1943.

108. Hill, J. C. and Wheeler, R. G., Phys. Rev. 152, 482 (1966).

109. Baker, J. M. and Bleaney, B., Proc. Roy. Soc. (London) 245A, 156 (1958).

110. Meyer, J. H. M. and Smith, P. L., J. Phys. Chem. Solids 9, 285 (1959).

111. Cooke, A. H., Edmonds, D. T., McKim, F. R. and Wolf, W. P., Proc. Roy. Soc. (London) 252A, 246 (1959).

112. Bozorth, R. M. Ferromagnetism. New York, D. Van Nostrand Co., Inc. 1951.

113. Powell, M. J. D. and Orbach, R., Proc. Phys. Soc. (London) 78, 753 (1961).

114. Singh, S. Absorption, Fluorescence and Zeeman Effects of Dysprosium, Terbium, Holmium and Uranyl Compounds, at Low Temperatures. Unpublished Ph.D. thesis. Baltimore, Maryland, Library, Johns Hopkins University. 1957.

ACKNOWLEDGEMENTS

The author wishes to express his gratitude to Professor F. H. Spedding for his direction and encouragement in this investigation. Special thanks are also extended to Mr. W. L. Sutherland, who obtained all the photographs of the spectrum studied here, to Mr. H. O. Weber, who prepared the single crystals, and to Mrs. P. A. Croy for her assistance in handling the data.